MODIFICATION OF NON-METALLIC INCLUSIONS TO IMPROVE THE FATIGUE PROPERTIES OF NITRIDING STEELS

A thesis
submitted in fulfilment
of the requirements for the degree
of
Master of Engineering (Mechanical)
in the
University of Canterbury
by

HAIPO ZHOU

Department of Mechanical Engineering
University of Canterbury

October 1993

ENGINEERING
LIBRARY
THESIS

ABSTRACT

Nitriding processes are widely used to improve the fatigue properties of steel. Fatigue failures in nitriding steels initiate from sub-surface non-metallic inclusions, which are usually oxide inclusions. It is known that duplex oxysulphide inclusions are less harmful to the fatigue properties of steel than oxide inclusions alone, since the sulphide outer phase acts as a buffer to the oxide in the core, and thus reduces the fatigue-initiating stress influence of oxide inclusions.

Twelve nitriding steel melts were produced, and non-metallic inclusions, modified by adding CaSi cored wire, were investigated. Since calcium has a high vapour pressure and a low solubility in molten steel, it is difficult to effectively modify non-metallic inclusions by the addition of CaSi cored wire in small furnaces. However, it was found that the addition of CaSi cored wire at a lower temperature was favourable to higher calcium injection yield in a small furnace, and it was also observed that the reaction with liquid steel was less violent, resulting in the effective modification of non-metallic inclusions.

Analysis by a scanning electron microscope with energy dispersive X-ray technique showed a proportion of duplex oxysulphide inclusions formed in ingots from 11A, with the remainder being predominantly globular calcium aluminate inclusions.

Specimens for direct stress fatigue testing were produced from steels containing both modified and unmodified inclusions, and the fatigue properties were compared.

It was found that calcium aluminate inclusions had a more deleterious effect on the fatigue properties of steel than alumina inclusions. In calcium modified steels, at lifetimes of more than 5×10^5 cycles, fatigue cracks always initiated from calcium aluminate inclusions, which were partly or completely debonded from the matrix. The fatigue properties of the calcium modified steel was found to be

inferior to those of the unmodified steel.

No duplex oxysulphide inclusions were found among those inclusions which produced fatigue crack initiations, and this indicated that when they were present calcium aluminate inclusions governed the fatigue properties of steel whether or not duplex oxysulphide inclusions were present in the steel.

It is inferred that the fatigue properties of steel can be improved if all large calcium aluminate inclusions are modified to duplex oxysulphide inclusions.

ACKNOWLEDGEMENTS

I would like to express my sincere gratitude to my supervisor Dr. J.M.Cowling for the help and guidance he has always so freely given.

My appreciation is given also to the many technicians in the Department of Mechanical Engineering, University of Canterbury, who assisted me with the experiments and in particular, Messrs M.J.Flaws, D.K.Healy and O.Bolt.

My grateful thanks to all those who gave so willingly of their time, in particular, Mr. D.Pepperle.

TABLE OF CONTENTS

LIST OF FIGURES

LIST OF PHOTOS

LIST OF TABLES

LIST OF SYMBOLS

a: activity.

A_o: constant.

C_s': sulphide capacity.

c/c^s: degree of supersaturation.

I: rate of homogeneous nucleation.

ΔG^*_{hom}: activation energy required for the formation of nuclei at the rate I.

ΔG: difference in Gibbs free energy between the matrix and the new phase in massive form.

g: acceleration of gravity.

K: equilibrium constant.

ΔK: the alternating stress intensity.

K_{IC}: fracture toughness of the material.

L: sulphur partition coefficients.

M: molecular weight of oxide.

N: number of cycles.

r: radius.

S: stress.

T: absolute temperature.

α: thermal expansion coefficient.

η: viscosity of molten steel.

ν: molar volume of the new phase.

ρ: density.

υ: floating velocity.

σ: interfacial tension between the matrix and the new phase.

σ_C: circumferential stress.

σ_R: radial stress.

σ_T: tessellated stress.

CHAPTER 1

Introduction

Nitriding is a process for case hardening of an alloy steel in an atmosphere consisting of a mixture of ammonia gas and dissociated ammonia in a specific ratio. The absorption of nitrogen by steel when the latter is heated in a medium which supplies the gas in the nascent or monatomic form has been known for many years. About 1921 Fry[1] reported on an extensive investigation into the nitriding of plain carbon and alloy steels based on previous works and determined the nitriding treatment temperature range in which nitriding brittle layers can be avoided. Fry[2] also showed that by the addition of certain alloying elements, such as aluminium, chromium and manganese, the surface hardness can be increased considerably without introducing brittleness. Since the original work of Fry the industrial development of the nitriding process and steel suitable for nitriding has been rapid.

Nitrided steels have high surface hardness, increased wear resistance and anti-galling properties, improved fatigue strength and corrosion resistance, and have a good high temperature performance. Therefore this surface hardening treatment can extend the uses of some steels and some steel products due to the suitable combination of high surface hardness and tough supporting core. Nitriding, therefore, is currently an important surface hardening method, which is in widespread use in industry.

One of the advantages of nitriding is to improve the fatigue resistance of nitrided components. It is known that the fatigue strength of steel is improved in two ways by nitriding. First, the material of the case may, because of its high hardness and different composition produced by the nitriding, develop a higher fatigue resistance than that of the core. Second the change of case volume is

different from that of the core, due to precipitation of very small particles of alloy nitride in the surface layers during nitriding. This results in residual compressive stresses in the surface layers after nitriding, and this greatly improves the fatigue strength of the steel.

During bending the residual compressive stress in the case counters the applied tensile stress acting at the surface(the most vulnerable area), thus the tendency to fatigue-failure initiated in the surface layer decreases greatly. But in contrast with the surface situation, the core stress state is more severe due to the existence of core residual tensile stresses cause by nitriding.

Some studies[3][4] showed that, in axial fatigue tests corresponding to long lives, nitrided specimens always failed by nucleation of fatigue cracks in the specimen core and that at lives $> 10^4$ cycles, fatigue failure is controlled by cracks which propagate from non-metallic subsurface inclusions within the specimen core. This indicates that the fatigue strength after suitable nitriding would be expected to depend principally on the core properties and core stress conditions. Since non-metallic inclusions originating from the steelmaking process have an associated residual stress field, it is very important to control and modify these inclusions in nitriding steels.

Non-metallic inclusions in steel are often detrimental to the mechanical properties of steel, and the fatigue properties of materials are intimately linked to the presence of inclusions[33]. Since it is impossible to produce steel without non-metallic inclusions (due to the metallurgical steelmaking practice), it is essential, in modern steelmaking practice, to reduce the number and size of non-metallic inclusions as far as possible. They should be modified and controlled in shape and distribution in order to reduce their detrimental effect on the fatigue properties of the steel.

The method often employed in current steelmaking practice is to add elements and compounds which have the ability to modify the inclusions, and to control their shape and distribution in the liquid steel. Calcium is often adopted as the modifier in modern steelmaking practice because of its very strong affinity for

both oxygen and sulphur.

Many works[3,4,6,10,11] show that oxide inclusions, especially Al_2O_3 and SiO_2, are very harmful to the fatigue properties of steel. Fatigue cracks often initiate at the larger oxide inclusions, since most of them are very hard, non-deformable and of lower thermal expansion coefficient than the steel matrix. In addition, even though sulphides, the most common being MnS, are relatively less harmful to fatigue strength, they decrease the mechanical properties in the through-thickness direction. Therefore the existence of both types of inclusions is detrimental to steel properties.

Some works[5,7,8,9] concerning the role of calcium in the production of inclusion-controlled steel show that both types of inclusions can be modified by calcium addition to form duplex oxysulphide inclusions. That is, the calcium aluminate or calcium aluminium silicate, which is harder and of lower thermal expansion coefficient, is enveloped by the (Ca.Mn)S, or CaS phase, which has a higher thermal expansion coefficient. These duplex inclusions are probably less harmful, or even harmless to fatigue properties in steel.

The influence of non-metallic inclusions on the fatigue properties of steel has been studied for a long time. At present, it is still not possible to give a full theoretical treatment of the subject, because the influence of inclusions on fatigue failure is very complex. One difficulty when discussing the influence of inclusions on fatigue is that the fatigue life of a material is a statistical concept, which has to be defined in a manner consistent with the wide dispersion generally observed in the fatigue life of individual test pieces. For the above reasons some experimental results are conflicting.

The aims of this thesis are as follows:

(1) To investigate how to desulphurize and modify non-metallic inclusions by adding calcium, and to analyze the factors which influence calcium-retention and the transformation of non-metallic inclusions in liquid steel.

(2) To produce a nitriding steel in which the non-metallic inclusions have been modified by adding calcium;

(3) To compare the fatigue properties of nitrided steels containing modified and unmodified non-metallic inclusions; and to determine experimentally whether the fatigue strength of nitrided steel can be further improved when non-metallic inclusions are modified to duplex oxysulphide inclusions.

(4) To analyze the reasons for fatigue crack initiation, and the role of non-metallic inclusions in fatigue failure, in both of types of nitrided steels.

CHAPTER 2

Kinetics of Formation and Elimination of Non-metallic Inclusions in Liquid Steel

2.1 General

The deoxidation reaction in molten steel is one of the most important in steelmaking and is directly related to the number, size and distribution of non-metallic inclusions in commercial steels[32,36].

Deoxidation comprises both the lowering of oxygen activity in the liquid steel and the decrease of the total oxygen content of the steel. The most common method of achieving this in modern steelmaking is to add some element having great affinity for oxygen into the liquid steel. Because deoxidizers react with oxygen to precipitate deoxidation products in the melt, a small amount of reaction product may remain as non-metallic inclusions in the steel, although most of them are removed in the slag.

Many studies[34,35,37,38,39,40,41,44,46,47,50,51] summarize the kinetics of molten-steel-deoxidation, and investigate the mechanism of the formation, growth and elimination of deoxidation products. They also try to ascertain which mechanism most determines the deoxidation rate in order to obtain clean steel, and to distribute the remaining non-metallic inclusions as evenly as possible.

According to work by Turkdogan[37,51] there are three consecutive steps involved in the deoxidation reaction. These are nucleation, growth and flotation or elimination of oxides in liquid steel.

2.2 Formation of Critical Nuclei in the Deoxidation Products in Liquid Steel.

Most researchers[37,38,39,50] assume that deoxidizers dissolve uniformly in the liquid metal when they are added and some works[41,50] also show that the dissolved oxygen content decreases very sharply, within 0.5-1 min after the addition of silicon and aluminium elements. This means that deoxidizers dissolve very quickly after addition. However Turkdogan suggested[37] that uneven mixing of added deoxidizers in liquid steel is not an uncommon occurrence, and cites aluminium with which the formation of an impervious oxide layer surrounding the undissolved droplets may lead to inefficient deoxidation.

The critical radius of the nucleus is very important in the study of the kinetics of deoxidation of steel[38][41], because only spherical nuclei having a radius equal to, or larger than the critical radius can be stable and grow in the liquid steel. In the classical nucleation theory[27], the work to form a spherical nuclei is

$$\omega = 4\pi r^2\sigma + (4/3)\pi r^3(\Delta G/v) \qquad (2\text{-}1)$$

where σ is the interfacial tension between the matrix and the new phase; r is the particle radius, ΔG is the difference in Gibbs free energy between the matrix and the new phase in massive form, and v is the molar volume of the new phase.

The critical radius r^* is derived by differentiating Eq.2-1 and putting the differential equal to zero

$$\partial\omega/\partial r = 8\pi r^*\sigma + 4\pi r^{*2}(\Delta G/v) = 0 \qquad (2\text{-}2)$$

The critical radius r^* is then given by

$$r^* = -(2\sigma v)/(\Delta G) = (2\sigma M)/[\rho RT \cdot \ln(c/c^s)] \qquad (2\text{-}3)$$

where ρ: density of oxide.

M: molecular weight of oxide.

T: absolute temperature.

c/c^s: degree of supersaturation.

Then the minimum work required to form the critical nuclei homogeneously from the melt is

$$\omega^* = (16\pi\sigma^3 v^2)/3(\Delta G)^2$$
$$= (16\pi\sigma^3 M^2)/\{3\rho^2 \cdot R^2T^2[\ln(c/c^*)]^2\} \qquad (2\text{-}4)$$

The rate of homogeneous nucleation may be approximately estimated as follows[43]:

$$I = A_o e^{-\Delta G^*_{hom}/kT} \qquad (2\text{-}5)$$

where A_o is a constant and ΔG^*_{hom} ($=\omega^*$) is the activation energy required for the formation of nuclei at the rate I, nuclei/cm^3·s.

Turpin and Elliott[38] estimated approximately the rate of homogeneous nucleation using the above formula, and show "I" varies extremely rapidly with supersaturation, so that it may be considered to be discontinuous with temperature. Some works[41,50] show that nucleation appears to occur within a very short time and nucleation rates are so large that this step could not be a rate-determining one for deoxidation.

Turpin and Elliot[38] suggested that because of the very high energy barrier which must be overcome for homogeneous nucleation, and because of the high probability of the presence of particles in the liquid steel that can serve as substrate for the formation of the new phase, heterogeneous nucleation is the more likely occurrence. Senda reported[44], that when deoxidant is added to the molten steel, only an oxide dissolved as a monomolecule was produced, unable to grow into oxide particles. Oxide particles only form at the surface of the crucible when dissolved monomolecular oxides diffuse to the boundary between the melt and the crucible. According to Koojima et al[45] heterogeneous nucleation occurs when weak deoxidizers, such as Cr and Mn, are added into the molten steel.

2.3 Growth of Oxide Inclusions in Liquid Steel

When oxide nuclei equal to or larger than the critical size exist in the liquid steel, growth follows. It is very important to know whether these nuclei can grow or not, and how long they need for growth. Although the growth mechanism is not as yet clear, some models have been established.

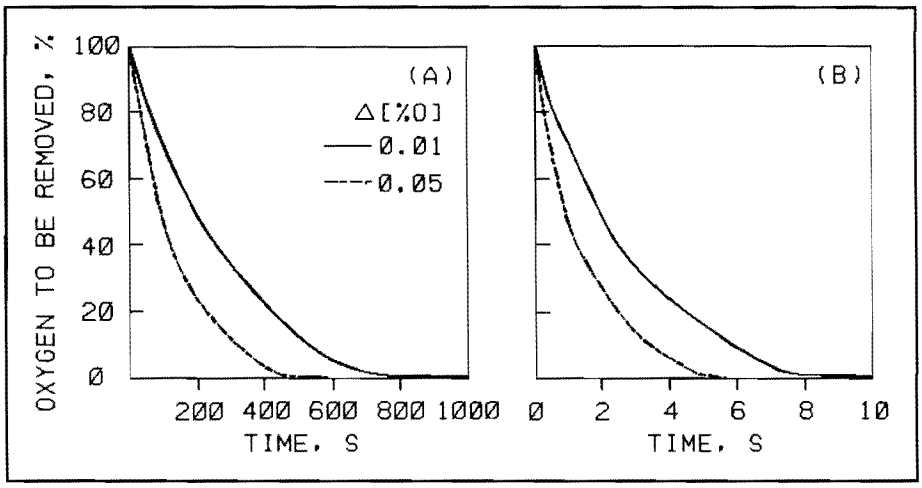

Figure 2.1 Percentage of oxygen to be removed as a function of time for (a): $Z=10^3/cm^3$ or $r_0=6.2\times10^{-2}cm$, (b): $Z=10^6/cm^3$ or $r_0=6.2\times10^{-3}cm$ (particles are considered to be stationary in the melt). Δ[%O] is difference between initial and final equilibrium oxygen contents, e.g. $\Delta[\%O]=[\%O]_0-[\%O]_i$

2.3.1 Growth by Diffusion

The rapid growth of nuclei to inclusion size has been described by diffusion models[37,39,40,41]

The mechanism of growth according to Turkdogan[37], is the diffusion of reactants to the surface of the inclusions. He assumed that when deoxidizers are added, they are quickly and homogeneously dissolved in the liquid steel, and a state of equilibrium is reached at the interface between inclusions and the liquid iron. This interfacial equilibrium will be taken to be that ultimately reached between bulk liquid metal, and the deoxidation products. He also assumed that there are a fixed number of growing inclusions in liquid steel, each inclusion having its own spherical diffusion zone, which is tangential to adjacent spherical diffusion zones. Thus the extent of deoxidation, as a function of time, is

dependent on the number of nuclei, Z, assumed to be present in a unit volume of the liquid at the start of the reaction; (or the radius r_o of the spherical diffusion zone) and the difference between the initial and final equilibrium oxygen concentrations, i.e. Δ[%O]. The results of computations based on these assumptions are given in figure 2.1[37]. Collins et al and Kahlweit[28,29] showed that the number of nuclei formed apparently spontaneously in supersaturated solutions, Z, is within the range 10^5-$10^6/cm^3$ in aqueous solutions.

2.3.2 Coalescence by Brownian Movement

Brownian movement, is very important to coalesce very fine, colloidal particles and some models for growth by Brownian movement collision have been established[40,41,51]. It is assumed that the particles are too small to float out of the melt, and initially there are a certain number of nuclei with a uniform size in the melt.

Sano et al[41] calculated that, after 100 sec, silica particles can grow to 0.5μm according to theory of Brownian movement. However this is significantly different from the size of the particles, actually observed this being 30μm. It probably means that the growth of particles in the molten steel is not dominated by this mechanism of growth.

2.3.3 Coagulating Growth During Flotation of Particles

This mechanism is based on the different rising velocities among different sizes of particles under the action of buoyancy and it is assumed[40,41] that the velocity of floating particle obeys Stokes' law:

$$\upsilon = [2gr^2(\rho_m - \rho_s)]/(9\eta) = Kr^2 \qquad (2\text{-}7)$$

where υ: floating velocity.

g: acceleration of gravity.

ρ_m and ρ_s: density of liquid metal and particle respectively.

η: viscosity of molten steel.

The volume passed by a floating particle with radius, r, within Δt is

$$\pi r^2 \upsilon \Delta t$$

and it is assumed, the volume of particles present in a unit volume of the liquid

is α, therefore, the volume of particles absorbed during floating is

$$\pi r^2 \upsilon \Delta t \cdot \alpha$$

Thus the increment of a particles volume is

$$(4/3)\pi(r+\Delta r)^3-(4/3)\pi r^3=\pi r^2 \upsilon \Delta t \cdot \alpha \qquad (2\text{-}8)$$

the terms with (Δ^2) and higher order are ignored, and Eq.(2-8) become

$$4\Delta r=\upsilon\alpha\Delta t$$

$$\frac{dr}{dt}=\lim_{\Delta t\to 0}\frac{\Delta r}{\Delta t}=\frac{\nu\alpha}{4}=\frac{k\alpha}{4}r^2 \qquad (2\text{-}9)$$

integrating Eq.(2-9) with initial conditions

$$r=r_o^* \qquad at\ t=0$$

$$r=\frac{r_o^*}{1-cr_o^*t}=\frac{r_o^*}{1-\dfrac{g\alpha(\rho_m-\rho_s)r_o^*t}{18\eta_m}} \qquad (2\text{-}10)$$

During steelmaking, Stokes' collisions occur very often, because of the different velocities of the particles and inclusions suspended in the liquid. Injected and/or dispersed particles, either solid, liquid or gaseous, are usually larger than the non-metallic inclusions, so that the particles are accelerated more slowly and/or rise faster under the action of buoyancy than the inclusions. Thus both can approach each other and coagulate.

Because the growth of small particles is very complex during steelmaking, it is probable that the three growth processes described above occur simultaneously and independently[40,41].

Kawawa et.al[40] gave the calculated performances of these three models for silicon deoxidation with C_0-C_{eg}=0.1%O, as represented in fig.2.2, in which growths of SiO_2 inclusion are calculated by the three models and by a combined model of Stokes' model with the other two models. and the results agree well with experimental results. But Sano[41] considered that since these three models are

not enough to explain all the observed behaviour, the growth of oxide inclusions in liquid steel must be much more complex than these models.

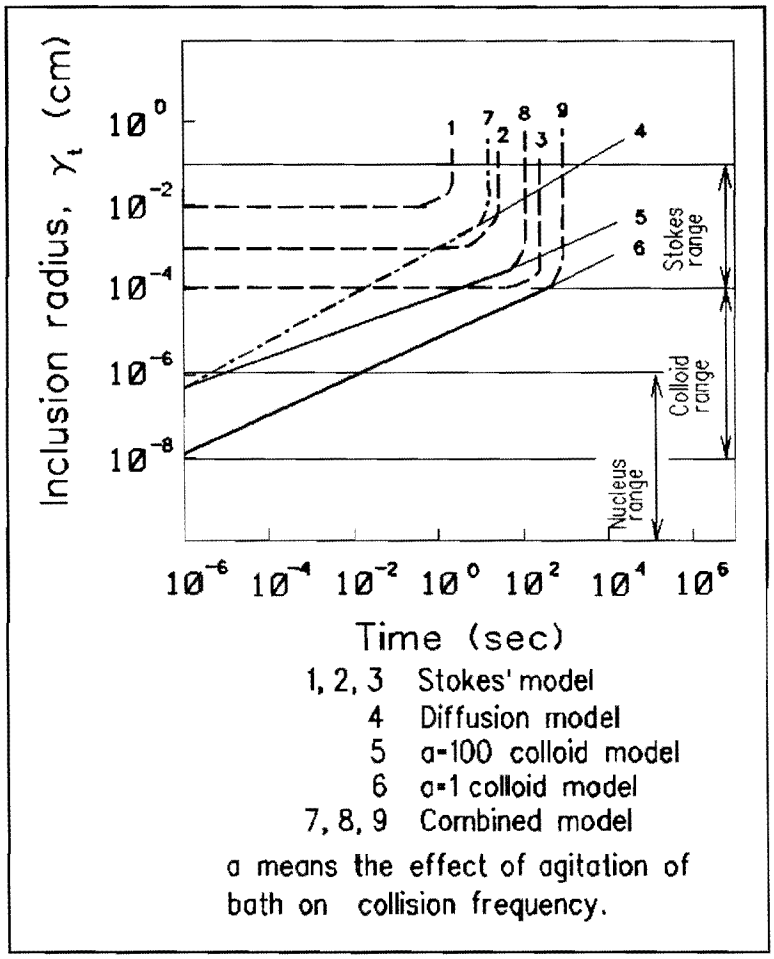

Figure 2.2 Growths of inclusions according to three typical models and combined model.

2.4 Elimination of Inclusions

The final aim in the study of the kinetics of steel deoxidation is to eliminate inclusions as far as possible. Many factors such as the velocity of rising particles, the characteristics of slag and refractory, and the stirring of the bath etc. can

affect the elimination of inclusions.

A faster velocity of floating particles is expected in liquid steel. In the classical theory, their velocity obeys Stokes' law as described in the last section. Because the velocity of rising spherical particles is proportional to the radius squared, r^2, some metallurgists think an efficient method of elimination of inclusions is to increase their radius. Since inclusions in the liquid state coalesce easily, deoxidation products should be more removable in the liquid state. Sano's work[41] showed that large spherical liquid silicates separated from the melt very quickly using silica-manganese as a deoxidizer. Miyashita et.al.[39] concluded that the floating velocity of silica inclusions in a tranquil iron bath is in agreement with Stokes' law.

However, since in practice baths are usually stirred by gas or induction, the velocity of rising particles may not obey Stokes' law[48].

Stirring by induction is beneficial to the floating-up rate of inclusions and their floating-up rate becomes lower as the degree of agitation becomes smaller, according to the result of Kamama's[40] experiment.

Gas stirring is a very efficient method for the removal of non-metallic inclusions[41,95]. The inclusions adhere to the bubble caused by gas stirring because of favourable surface forces, and are then carried upwards, driven by the buoyancy force.

Iyengar and Philbeook[48] also studied the rate of removal of inclusions in a bath stirred by natural convection, and it was observed that a boundary layer effect, and the presence of a thin liquid metal film, prevented rapid removal of inclusions from the stirred metal. Meanwhile they also found some large inclusions present in the ingot, which should not exist in steel according to Stokes' law, perhaps because Stokes' law neglects the effect of fluid motion.

The aim of deoxidation is that the rising oxides enter finally into slag phase, or are adsorbed by the crucible wall. So the nature of both slag and inclusions is very important. Low interfacial tension between inclusions and receiving slag will promote coagulation of inclusions with a top slag[65] and with increasing liquid metal/inclusion wetting angle, solid inclusions are more deeply immersed in the

slag and less deeply immersed in the liquid steel.

Several studies show[35,48,51] that many inclusions can be assimilated by the crucible wall rather than rising to the surface of the liquid steel. So refractory material also appears to play a very important role during deoxidation. Care should be given to the composition of refractory material.

For many authors the stage of elimination alone determines the success of deoxidation.

CHAPTER 3

The Role of Calcium In the Steelmaking Process

3.1 General

In the past two decades calcium-treatment of steels has been greatly developed, since calcium is very effective in desulphurisation, deoxidation, improving cleanliness, and modification of non-metallic inclusions present in steels.

Many workers have investigated the behaviour of calcium in the steelmaking process and the methods of calcium-treatment in modern steelmaking, and great progress in the field has been made. However, because there is little thermodynamic data available on the high-temperature behaviour of calcium, and calcium has a very low solubility and high vapour pressure in the melt, some experimental thermodynamic data on the deoxidation and desulphurisation reactions with calcium are still conflicting.

3.2 Desulphurisation and Deoxidation by Calcium

3.2.1 Mechanism of Desulphurisation

Sulphur exist in a gaseous state at steelmaking temperatures since the boiling point of sulphur is 718 K. However sulphur can dissolve in the liquid steel and slag, if the liquid metal is exposed to gases which contain sulphur.

There are many methods available for desulphurisation in iron and steelmaking processes, but they can be classified into two types according to the different

mechanisms involved. These are, desulphurisation by exchange reactions, and by precipitation reactions.

(a) Desulphurisation by exchange reactions

It is well known that basic slags are effective in desulphurising steel and desulphurisation occurs at the interface between liquid steel and slag. Most workers[30,31,52] think that desulphurisation by the top slag is responsible for the reaction at the boundary with the basic slag, and the transfer of sulphur from the metal to the slag is by an electrochemical exchange reaction:

$$[S] + (O^{-2}) = (S^{-2}) + [O] \qquad (3\text{-}2\text{-}1)$$

The above equation shows that sulphur exchanges two electrons with oxygen bringing one oxygen ion from the slag to the metal as atomic oxygen and atomic sulphur transfers from the metal to the slag. Because a prerequisite for this mechanism is the presence of some oxygen ions which act as electron donors in the slag, only basic slags are suitable, since no oxygen ions are present in acid slag.

CaO (lime) is the main desulphurizer in basic slag and desulphurisation with calcium oxide alone is expressed by the reaction:

$$(CaO) + [S] = (CaS) + [O] \qquad (3\text{-}2\text{-}2)$$

The sulphide capacity, C_s', of a slag is commonly expressed as[31]:

$$C_s' = a_{[o]}(\%S)/[\%S] \qquad (3\text{-}2\text{-}3)$$

where $a_{[o]}$ is activity of oxygen in liquid steel.

Hassall et. al[53] showed that, for desulphurisation treatment, higher sulphur partition coefficients, $L = (\%S)/[\%S]$, were achieved for slags with higher basicities $[(CaO)/(SiO_2) > 5]$ and with low (FeO) contents ($< 1.5\%$) according to the various compositions of top slag. In addition, from equation (3-2-3), it is clear that, for a given sulphide capacity, the sulphur partition coefficient is critically dependent on the level of deoxidation of the liquid steel. Figure 3.1 shows sulphide capacities in the $CaO\text{-}Al_2O_3\text{-}SiO_2$ system[31].

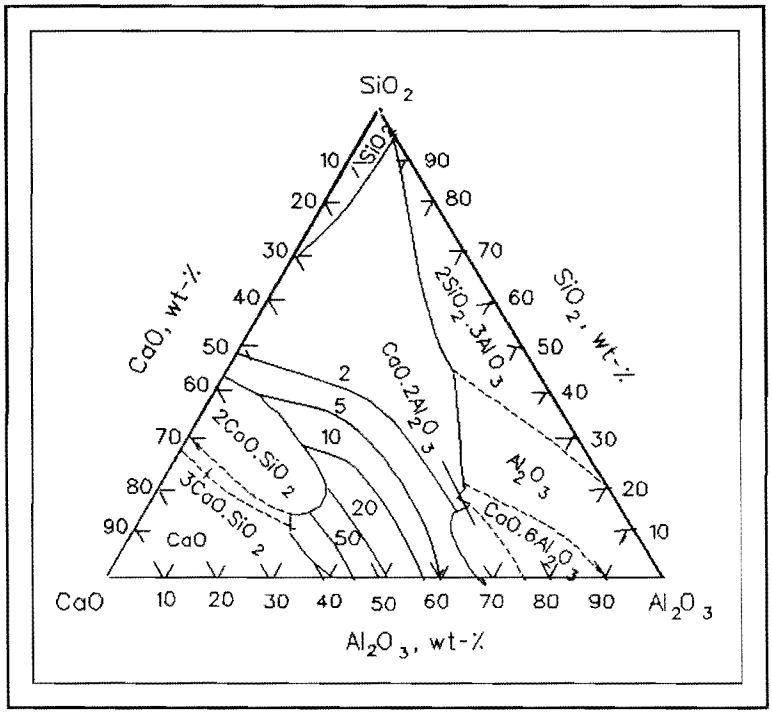

Figure 3.1 Sulphide-capacity C_s' contours in Al_2O_3-CaO-SiO_2 system at 1600°C; C_s' values in 10^{-3}wt-%.

(b) Desulphurisation by precipitation reactions

Like the method of deoxidation, some elements which have high affinities for sulphur are added into the melt and the reaction occurs between sulphur and a desulphurising element, both of which are dissolved the liquid steel. Sulphides will be precipitated and subsequently removed from the steel. Calcium is one of the most common desulphurisers, since the equilibrium constant, K_{CaS}, is very low ($1.3*10^{-9}$)[65].

In modern metallurgical processes, calcium-desulphurisation by precipitation reaction can be effected in two ways: (1) powder injection with a carrier-gas using a submersed lance, (2) injection into the melt of a metal wire with a core of powdered calcium alloy. Both techniques are usually used for final desulphurisation in the steelmaking process, and produce fully-modified non-metallic inclusions.

The injection of calcium-bearing powder with carrier-gas for desulphurisation has been adopted widely in iron and steelmaking[15,22,23,57]. In addition to alloys such as CaSi and CaC_2, mixture powders containing CaO and CaF_2 have also been used. Research by Kaneko et. al[61] showed that the minimum sulphur concentrations attained were as low as 0.0007% by CaO-CaF_2 injection with carrier gas in molten steel.

Adding calcium alloy powder to liquid steel by using a cored-wire technique began in the early eighties and developed very quickly since cored-wire injection causes less agitation and pollution of steel, much better injection efficiency, less heat loss, more complete modification of non-metallic inclusions, and lower investment and operating costs compared with powder injection with carrier-gas[22,59]. Wire injection also allows the treatment practice to be simplified.

Some workers[54,55,56] have investigated calcium absorption and elimination rates to discover the main form in which calcium is retained in liquid steel when calcium alloy is added into the melt, and also to measure the efficiency of calcium usage and retention, and its influence on steel properties.

Calcium-content in molten steel usually increases rapidly when calcium is first added, but levels off after a short time, even though calcium is still being fed[56].

In full-scale practice, calcium alloy is usually injected deeply into the liquid steel, so that the boiling of calcium can be suppressed by ferrostatic pressure in order to achieve higher injection yield. Turkdogan[54] reported that the CaSi injection should be at a certain rate to ensure that the core wire melts deep in the melt, e.g. = 1.5m below the melt surface, since the vapour pressure of calcium at 1600°C is 1.86 bar. The calcium at this depth can become liquid, therefore, the reaction between the liquid calcium and steel is very efficient. The other benefit of deep injection is to retain calcium in liquid steel for a longer time in order to provide longer reaction time with sulphur and oxygen.

Calcium solubility in the liquid steel is only about 160 ppm[60] at 1 atm pressure of calcium vapour. However the addition of silicon, carbon, aluminium and nickel can increase the solubility of calcium and its suitability is fully realised in combination with these elements. Calcium injection yields of 20% with the

cored wire process can be obtained by using CaSi (Si 60%, Ca 30%) and the method of deep injection[55].

When calcium alloy is added into the melt, the bath will be stirred by calcium vaporisation, and the bubble-stirring is beneficial to the elimination of inclusions. Lu et al[56] showed that, after injection, the total calcium content in steel reduced quite rapidly, apparently following first order kinetics:

$$\frac{d(\%Ca)}{dt} = -K(\%Ca) \qquad (3\text{-}2\text{-}4)$$

where K is the rate constant for elimination of calcium.

If the calcium compound is deeply injected into the liquid steel, liquification occurs. Calcium particles in the liquid state react with oxygen and sulphur as they rise in the steel, and any unreacted particles vaporize as the ferrostatic pressure decreases. So any excess calcium then reaches the surface and reacts with the top slag or burns in the air. Therefore it is a generally accepted view that the calcium retained in liquid steel is almost all in non-metallic inclusions, and as Turkdogan[54] reported, it is primarily in the form of calcium aluminate inclusions, and to a lesser extent as calcium sulphide inclusions dispersed in the melt.

3.2.2 Deoxidation by Calcium

Although a major role of calcium in steelmaking is to desulphurise and control non-metallic inclusion morphology, deoxidation by calcium is unavoidable due to its very high affinity with oxygen. The equilibrium constant for K_{CaO} is reported to lie between 10^{-11} and 10^{-7}, depending on the literature source[62,63,64].

Because dissolved oxygen competes with sulphur for calcium and impedes the removal of sulphur, oxygen activity has to be lowered before adding calcium. In fact, desulphurisation and deoxidation occur simultaneously when calcium alloy is injected into the melt. Therefore oxygen activity in the molten steel can be further lowered and cleaner steel can be obtained even though some calcium is consumed in deoxidation.

3.3 The Improvement of Non-metallic Inclusions Morphology by Calcium

3.3.1 The Modification of Sulphide Inclusion by Calcium

The attraction of calcium lies in its ability to modify non-metallic inclusions in steel.

Sulphides are very important and often highly detrimental in steel, and MnS inclusions are the main sulphides present in steel. Usually these MnS inclusions are classified into three types I, II, III, according to their different shapes and distribution, and these types form as the result of different steel deoxidation practices. Type I sulphides form as isolated globular particles, they may be pure MnS, also MnS containing FeO, MnO and SiO_2, and are usually formed in rimmed or semi-killed steels where the oxygen content of the liquid steel is high. Type II form as chains or fans of small rod shapes and appear as eutectic distributed in grain boundaries. They occur in steel which has been fairly heavily deoxidised by aluminium. Type III which have angular or octahedral shapes are precipitated as solid particles from the melt and occur in steel which has been very heavily deoxidised. In general, they usually are mono-phased with little or no oxide associated with them[12,14,18]. Thus type II and III MnS always exist in Al-killed steel, especially type II. Because they form films which precipitate between grains late in the solidification, they can cause hot-shortness during rolling at elevated temperature. On the other hand, since MnS is plastic, these inclusions are deformed during rolling to produce long stringers of sulphides which lead to a reduction in mechanical properties transverse to the rolling direction, and are detrimental to toughness and bend formability.

Normally sulphur is dissolved in molten steel and the manganese content is not sufficient to form sulphides at higher temperature. However during solidification, impurity levels in the residual melt rise, as the temperature falls, and manganese and sulphur can react to form manganese sulphide. Therefore these sulphide phases, especially type-II MnS, precipitate late in the part of the steel

ingot which solidifies last.

It is well known that the addition of calcium can prevent the precipitation of MnS. Many workers[19,42,56,66,67,68,69,70,71] have investigated the behaviour of CaS or (Ca,Mn)S in the molten steel and the suppression mechanism of MnS precipitation by calcium addition.

Since CaS can be precipitated by reaction (3-3-1) even in the molten steel according to the thermodynamic data for calcium, the dissolved sulphur content decreases greatly in the residual liquid near the end of solidification.

$$[Ca] + [S] = (CaS) \qquad (3\text{-}3\text{-}1)$$

With decreasing temperature, the above reaction can continue. If there is more sulphur in the melt, residual sulphur reacts with manganese to form manganese sulphide during solidification, which can diffuse to the CaS inclusions to form (Ca,Mn)S inclusions[56]. Investigation by Kitamura et.al[66] showed, calcium-aluminate can directly contribute to the desulphurisation reaction (3-3-2) during solidification.

$$CaO.mAl_2O_3 + [S] = CaS + mAl_2O_3 + [O] \qquad (3\text{-}3\text{-}2)$$

He considered that it is possible to increase its ability to desulphurise as solute segregation in the residual liquid increases during solidification. However, Ozhun and Turkdogan[71] considered this reaction does not have a large effect on desulphurisation in the molten steel.

CaS inclusions are harder and less deformable than MnS. Some papers[65,72] show that a small amount of calcium in manganese sulphide inclusions can change their morphology and decrease their deformability during rolling. For Al-killed steels, complete transformation of sulphide into globular inclusions can be obtained when the calcium left from deoxidation is sufficient to react with more than 40% of dissolved sulphur at the start of solidification[72]. Because they resist change of form into long stringers and remain globular during the rolling process, their influence on properties both parallel and perpendicular to the rolling direction are similar. Consequently by the modification of the lenticular MnS to spheroidal CaS, (Ca,Mn)S or RE_2O_2S and RE_2S_3, the isotropy of properties can be greatly increased[74]. Sulphides of a globular type also enhance bendability[17,42].

3.3.2 The Change of Oxide Inclusion Morphology by Adding Calcium

Al_2O_3 is the most common oxide inclusion in aluminium killed steel. Because the inclusions have very high melting point, are hard, and can form as Al_2O_3-clusters, they are usually responsible for nozzle blockage during continuous casting, and degradation of the mechanical properties of steels due to the formation of elongated discontinuous stringers during rolling.

Calcium can reduce aluminium in alumina inclusions and change Al_2O_3-clusters to spherical calcium aluminate in Al-killed steel by the following precipitation reaction[65,73].

$$xCa+y(Al_2O_3)incl.=[xCaO*(y-\frac{x}{3})Al_2O_3]incl.+\frac{2}{3}xAl \qquad (3-3-3)$$

Fig.3.2 depicts the $CaO-Al_2O_3$ binary system[65] which shows the mechanism of calcium-addition to an aluminium-deoxidized melt. Six intermediate phases have been reported to exist in the system depending on the Ca/Al ratio in the liquid steel[25]. It is very important that the composition of calcium aluminate inclusions is controlled to avoid the formation of high melting point types, e.g. $CaO.6Al_2O_3$ which can cause nozzle blockage during continuous casting. When the Ca/Al ratio in the steel exceeds 0.08, the alumina and $CaO.6Al_2O_3$ (CA_6-type) inclusions are totally converted to low melting point calcium aluminates, type $CaO.Al_2O_3$ and $12CaO.7Al_2O_3$[75].

Fig.3.3 shows total calcium contents needed to obtain liquid inclusions in liquid Al-killed steels[72].

3.3.3 The Formation Mechanisms of Duplex Oxy-sulphide Inclusions Formed by Adding Calcium

Although CaS or (Ca,Mn)S inclusions can exist as a single phase inclusion, they often occur surrounding calcium aluminate to form duplex oxy-sulphide

inclusions in calcium-treated steel[15,21,31,33,58,65,66,67,68]. Because this type of inclusion probably alleviates the detrimental effects of oxide inclusions on steel properties, especially fatigue properties[66,67], many workers have investigated its formation.

Since large oxide inclusions surrounded by calcium sulphide were identified as of primary origin, Saxena[15] considered that the primary inclusions, CaO-Al_2O_3 act as nuclei for the precipitation of calcium sulphide, with the result that the calcium sulphide phase is confined to the outer surface.

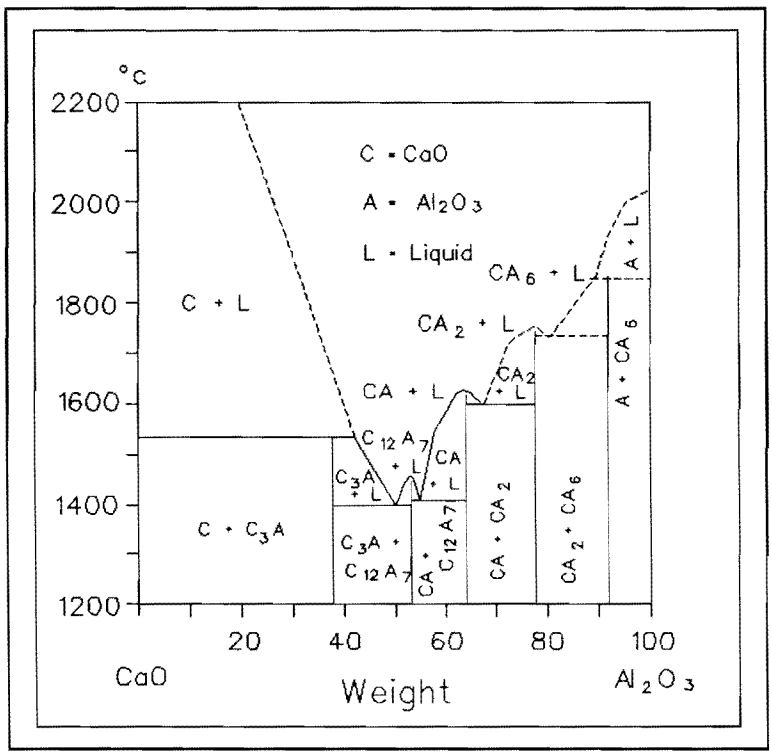

Figure 3.2 The equilibrium diagram for the CaO-Al_2O_3 binary system.

Salter el.al[21] considered that since the calcium silicide when added is more likely to form oxides than sulphides, the CaS probably originates from the pre-existing silicates which were picked up from the slag, or produced by calcium silicide deoxidation. When reaction occurs between calcium silicate and aluminium, the sulphur combines with calcium in the reacting silicate due to the greater stability of CaS.

As the amount of silicate decreases and becomes no longer able to hold the sulphur in solution, all the sulphur is eventually precipitated within the calcium aluminate or as a peripheral phase around it.

Some workers[21,68] report the oxide inclusions surrounded by CaS being formed during the solidification process of steel. Since calcium sulphide is distributed relatively uniformly on the outer surface of calcium aluminate in steel, the workers assumed that CaS deposited on the surface of oxide inclusions is probably formed by precipitation from within the CaS-containing inclusions. Takenouchi el.al[68] investigated the solubility of CaS in $CaO\text{-}Al_2O_3$, shown in fig.3-4, and reported that the formation mechanism of peripheral CaS on the oxide surface is one of precipitation of CaS from the $CaO\text{-}Al_2O_3$ inclusions (containing CaS uniformly distributed) due to the solubility drop as the temperature decreases.

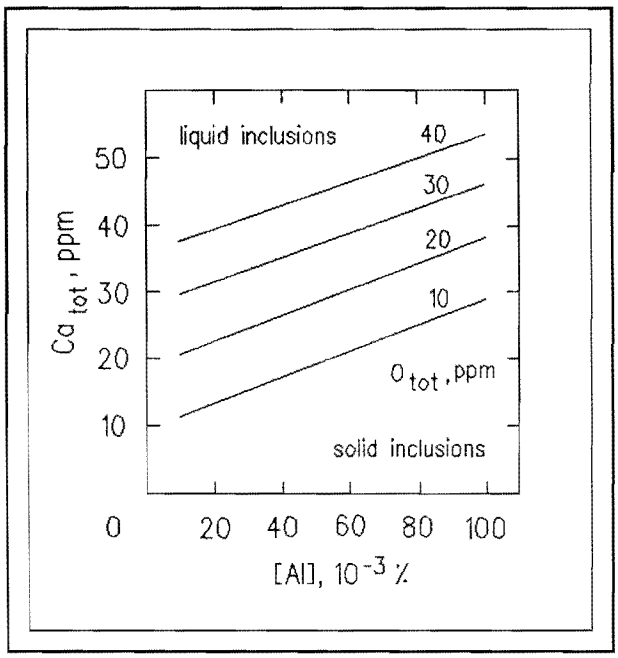

Figure 3.3 Possibilities of transformation of alumina clusters by calcium in Al-killed steel.

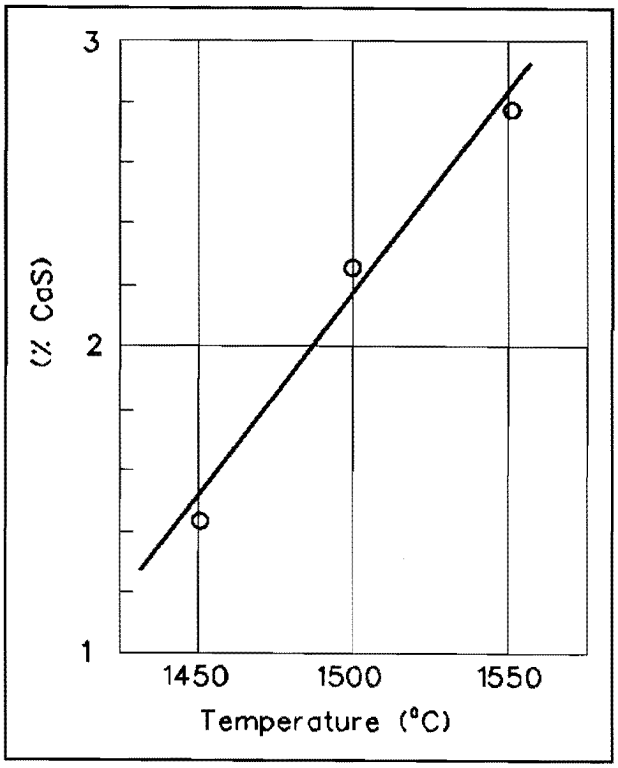

Figure 3.4 Solubility of CaS in 50% $CaO\text{-}Al_2O_3$ slag.

CHAPTER 4

The Influence of Non-metallic Inclusions on Fatigue Strength of Steels

4.1 General

Fatigue failures can be regarded as the progressive failure of parts under repeated loading. The fatigue strength of a material is usually expressed by the S-N curve which shows a relation obtained between the fluctuating loads or stresses, S, and the number of cycles to fracture, N.

Three ranges can seen in the S-N diagram for steels (fig.4.1), a large-amplitude or H range where life increases with decreasing amplitude; a small-amplitude, or F range, where life further increases with decreasing amplitude, and a fail-safe or S range, at still smaller amplitudes, where life becomes infinitely long[78].

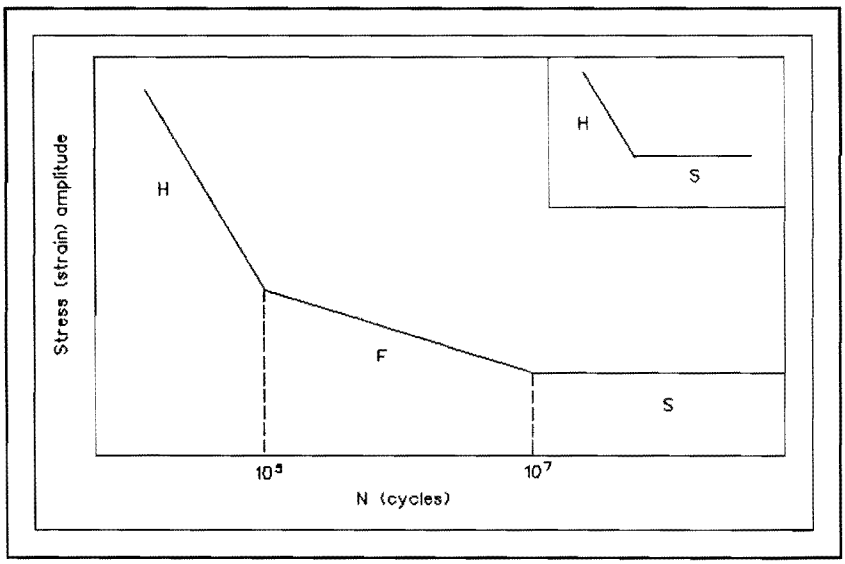

figure 4.1 Idealised S-N curve for steels.

The development of fatigue cracks usually is divided into two stages: initiation and growth (propagation) of fatigue cracks. Since the initiation of fatigue cracks starts at the beginning of component service, the process of component fatigue failure is one of initiation and growth of a fatigue crack or cracks. The ratio of cycles for initiation to cycles for growth varies over the three regions in the S-N curve. In the low-cycle region, the fatigue life of steels is dominated by crack growth, that is, crack growth occupies the largest proportion of fatigue life. However, crack initiation governs the fatigue life in the high-cycle region. Eid and Thomason[82] showed that the nucleation phase in low-alloy steels under high-cycle fatigue condition may occupy well in excess of 95% of the total fatigue life. Also the proportion of the fatigue life occupied by each stage is different for various materials.

Some researchers[80,102] have shown that fatigue crack initiation in many high strength steels occurs primarily at non-metallic inclusions, whereas fatigue crack initiation in soft steels often occurs in slip bands.

4.2 Influence of Non-metallic Inclusions on the Nucleation of Fatigue Cracks

The important role played by non-metallic inclusions as initiation sites for fatigue cracks in high strength steels has been investigated extensively[79,80,81,82,83,84]. It is thought that the nature, size, shape and distribution of non-metallic inclusions and the stress state around non-metallic inclusions greatly influence the nucleation of fatigue cracks.

4.2.1 Tessellated Stresses

Since non-metallic inclusions and the steel matrix have different thermal expansion coefficients, microstresses will exist at the interface between particles and matrix following heat treatment, and these are called "Tessellated Stresses" (or Structural Tessellated Stresses). The tessellated stress σ_T caused by different thermal expansions are of the general form[20,76]

$$\sigma_T = \Phi(\alpha_2 - \alpha_1)T \qquad (4\text{-}1)$$

where Φ is a function of the elastic moduli of inclusion and matrix, and also of the inclusion size, shape and distribution; α_1 and α_2 are the thermal expansion coefficients of the inclusion and matrix respectively, and T is the temperature change. Brooksbank el.al[20,76,77,86,87,88] comprehensively investigated the thermal expansion properties of some typical types of inclusions and calculated their nature and magnitude. Brooksbank et. al[87] considered that the stress level at the interface between inclusions and matrix is determined principally by the term $(\alpha_2-\alpha_1)$. The relative expansion coefficients are summarized in fig.4.2.

Because Al_2O_3 and calcium aluminate have lower thermal expansion coefficients than the matrix, these oxide inclusions are shown to give rise to high tensile matrix-stresses which are very detrimental to fatigue properties. In fact, the stress in the matrix around each inclusion is the sum of the tessellated and applied stresses and, if the total stress exceeds the matrix yield point, plastic deformation of the matrix around non-metallic inclusions occurs, and fatigue cracks will probably be initiated from these boundaries.

Since, in contrast with Al_2O_3, manganese sulphides have a larger thermal expansion coefficient than the matrix, that is, $\alpha_1 > \alpha_2$, see fig.4.2, microvoids could form around inclusions during cooling. The result of the formation of microvoids is that adverse stresses will not develop at the interface, even though there is still a stress concentration in the void.

Many metallurgists are very interested in duplex oxysulphide inclusions in the calcium-treated steels, that is, calcium aluminates enveloped by peripheral CaS or (Ca,Mn)S. Analysis of this type of inclusions according to the tessellated stresses shows that the interface stress between the inclusion and the matrix is reduced[20,76]. The inclusion core, of calcium aluminate, would give matrix tensile stresses, whereas the (Ca,Mn)S outer shell might leave a void, so the process of encapsulation would reduce, or even eliminate the tensile stresses caused by Al_2O_3 or $CaO\text{-}Al_2O_3$, which are very deleterious to fatigue properties if the oxide was present by itself.

Several investigations show that calcium aluminates, alumina, spinel, silicates and titanium nitride inclusions are the most detrimental to fatigue life[4,20,21,86,87,89].

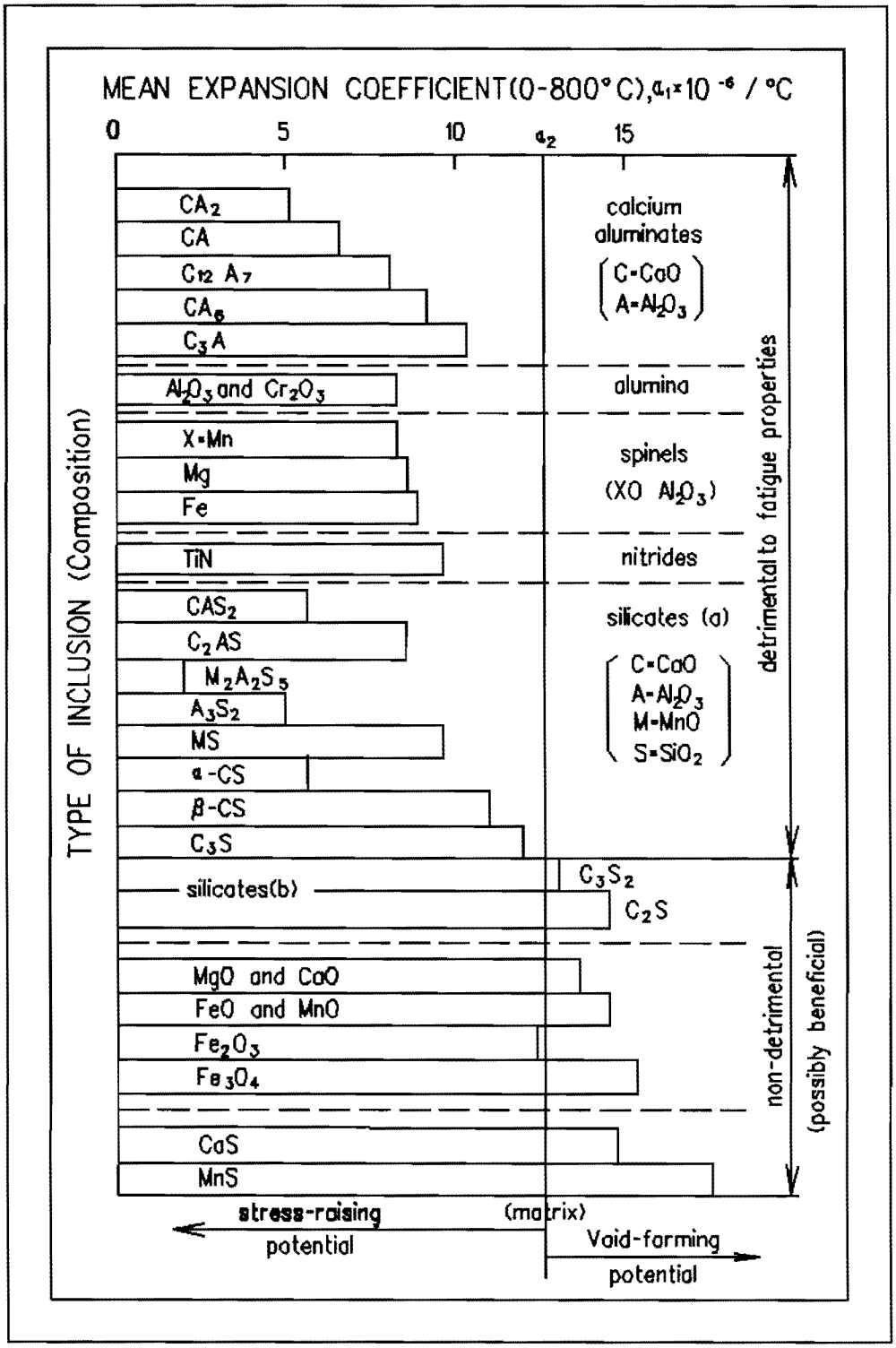

Figure 4.2 Stress-raising properties of inclusions in 1%C-Cr bearing steels.

4.2.2 Influence of Size and Position of Inclusions on Fatigue Crack Initiation

It is well known that the size of non-metallic inclusions affects the fatigue properties of steel and some researchers[10,90] have shown that larger inclusions in steels are more detrimental to fatigue strength than small ones.

Brooksbank and Andrew[20,85] calculated tessellated stresses around inclusions and showed that tessellated stresses increase with increasing size of inclusions, if the thermal expansion coefficient of the inclusions is less than that of matrix.

The position of non-metallic inclusions in steels also greatly effects the initiation of fatigue cracks. Usually fatigue cracks will be more easily initiated by inclusions in the near surface than by those further from the surface. Harkegard[91] classified the position of the crack-initiation defects in his fatigue specimens and showed surface and sub-surface defects occupied 65% and 17% respectively of all fatigue crack initiation defects.

The effect of both the size and depth of inclusions has been studied by some workers[10,102]. The critical inclusion size was found to depend on the distance beneath the steel surface and increased from 10 μm just below the surface to 30 μm about 100 μm below the surface when Al_2O_3 inclusions in steel were studied[10].

If near-surface inclusions are below the critical size, they will not effect the fatigue strength. So one of the methods for improving the fatigue properties of steels is to eliminate steel inclusions, which are larger than the critical size, as far as possible.

Fatigue cracks are also initiated by hard undeformable inclusions which, during hot-working, form end-cavities between inclusions and matrix causing an increase of inclusion-matrix decohesion. Rudnik[92] showed that as the index of deformability decreases, the inclusions, particularly large ones, do not elongate uniformly during rolling of steel, and a conical gap will form at the interface of inclusion and matrix. This may lead to cracking due to high local stress concentration.

4.2.3 Mechanism of Fatigue-crack Initiation by Inclusions

The reasons for fatigue-crack initiation in different cycle ranges may vary. In the low cycle range ($<10^4$ cycles) fatigue cracks usually initiate at intense slip-bands due to the large cyclic-plastic strains, and propagate rapidly by ductile tearing between the main crack front and voids produced by inclusions and second-phase particles[79] ahead of the crack front. In the intermediate-cycle range (10^4-10^6 cycles) crack-initiation usually takes place adjacent to both bonded and debonded non-metallic inclusions[80], and for the upper end of this range, all cyclic-plastic strains are confined to small regions of local stress-intensification at the site of inclusions[81]. Fatigue-crack nucleation always occurs at debonded or damaged non-metallic inclusions in the high cycle range ($>10^6$ cycle), and because the intensity of the stress field is quite low, localized cyclic-plasticity in the adjacent matrix does not occur during crack-initiation[82].

Several models for fatigue nucleation have been established to explain the mechanisms of fatigue crack initiation from inclusions. An investigation of the initiation of fatigue cracks in 4340 steel by Lankford[81] showed that some non-metallic inclusions at the free surface, which initiated fatigue cracks, were all debonded or partially debonded from the matrix, and debonding between the inclusions and the surrounding matrix always occurred first at the poles (where the tension axis intersects the inclusions). The model of fatigue crack initiation, based on debonding of surface inclusions prior to microvoid nucleation within the metal matrix, is shown in figure 4.3[81]. Eid and Thomason[82] further researched fatigue crack initiation under high-cycle conditions and reported that fatigue crack nucleation often initiated from debonded, and damaged inclusions which led to the formation of holes at the specimen surface in high-cycle conditions. Although the applied stress is very low under high-cycle conditions, the stress is greatly intensified at the equatorial point on the boundary of a hole caused by debonding. Local fatigue of alumina inclusions and cyclic-plastic zones will develop at the equatorial surfaces of holes. Eid[82] considered that the prerequisite for initiating fatigue cracks under high-cycle conditions is hole-formation caused by either progressive debonding, or local fatigue damage of inclusions.

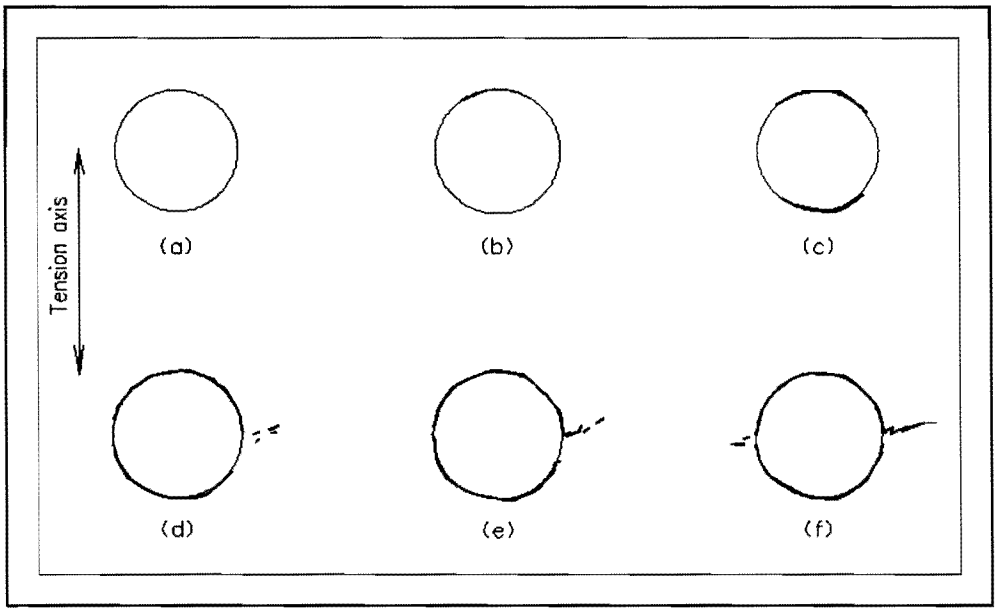

Figure 4.3 Proposed model of fatigue crack initiation based on debonding of surface inclusions prior to microvoid nucleation within metal matrix. (a) Bonded inclusion. (b) Initial debond at one pole. (c) Growth of initial debond seam; nucleation of debond at opposite pole. (d) Further debond seam growth accompanied by point surface defect nucleation within matrix. (e) Defect growth and coalescence to form fatigue microcrack. (f) Growth of microcrack, and nucleation of surface defects at opposite side of inclusion.

If the inclusions and the interface are strong enough not to break under the initial loading and the cyclic stress is high, plastic flow is accumulated in the matrix after some repetitions of cyclic loading. Because slip bands in the matrix will be blocked by inclusions and inclusions are impinged by the accumulation of dislocations, debonding or cracking of inclusions will occur, and fatigue cracks will be initiated[84,93,94,95].

4.3 Propagation of Fatigue Cracks

Fatigue cracks are able to grow under cyclic loads after initiation. In many materials the crack propagation phase occupies a major fraction of the useful

fatigue life.

Most studies have confirmed that the crack-growth increment per cycle (da/dN) is principally a function of the alternating stress intensity, ΔK, according to the Paris' relationship:

$$da/dN = C(\Delta K)^n \qquad (4\text{-}2)$$

where C and n are experimentally-determined constants which may depend on material, microstructure and environment, etc., and ΔK is given by the difference between the maximum and minimum stress intensities for each cycle.

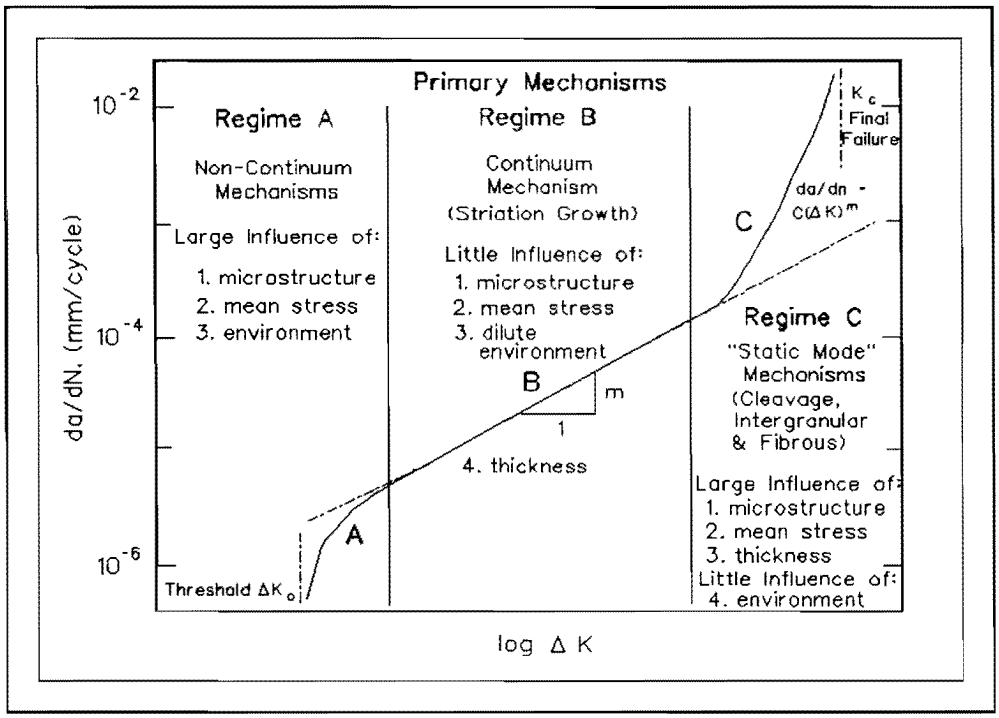

Figure 4.4 Typical fatigue crack growth curve.

The typical curve of crack growth rate is illustrated in figure 4.4[24,96], which shows three distinct regions. In stage I, crack growth is very slow since the value of ΔK is near the threshold for fatigue crack growth, ΔK_{th}, and is strongly affected by microstructure, mean stress and nature of the environment. In the intermediate ΔK range, log da/dN is almost linearly related to log ΔK according to the power-equation (4-2) proposed by Paris. During stage II, rates of crack growth are usually largely independent of the tensile strength and composition of the

material, but anything that significantly modifies crack tip profiles will affect crack growth rates. The region labelled III shows very rapid fatigue crack growth rate, because the applied K_{max} approaches the fracture toughness, K_{IC}, of the material, and fatigue crack growth rate in this region is known to be sensitive to microstructure, and stress ratio.

CHAPTER 5

The Influence of Nitriding on the Fatigue Properties of Steels

5.1 Principle of Nitriding

Nitriding is a thermochemical surface-hardening heat treatment, that introduces nitrogen into the steel surface, by holding the metal at a suitable temperature in contact with a nitrogenous gas, usually ammonia. The temperature range of nitriding is 500-590°C, and no phase transformation occurs on cooling to room temperature. Thus distortion caused by nitriding is the smallest of all the surface heat treatments.

For gas nitriding, the ammonia dissociates near the surface due to the reaction

$$2NH_3 \rightarrow 2N + 3H_2 \qquad (5\text{-}1)$$

At the instant of dissociation, nitrogen occurs in the atomic form which can be absorbed at the steel surface. Several phases may form according to the temperature and the concentration of nitrogen which diffuses into the ferrite during nitriding.

The iron-nitrogen equilibrium diagram is shown in Figure 5.1[26]. Since the maximum solubility of nitrogen in pure iron at 590°C is only 0.1 percent, the solubility limit is soon reached at the surface of the steel and γ'-nitride (Fe_4N) will form. If the nitrogen concentration increases continuously and exceeds 6%, the γ'-nitride starts to change into ϵ-nitride.

It is well known that the soft and brittle "white layer" will form if the nitrogen potential is too high during nitriding. The whiter layer consists of ϵ and γ'-nitride which form up to 0.05 mm thick on the surface of nitrided parts. Some alloying elements, such as Al,Ti,V,Cr,Mo etc. can form stable nitrides and increase case hardness during nitriding[2]. The results obtained from some investigations are

shown in Figure 5.2[25], from which it can be seen that very high hardness results from alloying a steel with aluminium or titanium in amounts of about 1.5%. Meanwhile, the hardenability of steel containing these alloying elements can be greatly increased, so that the strength and toughness of nitrided steels can be improved.

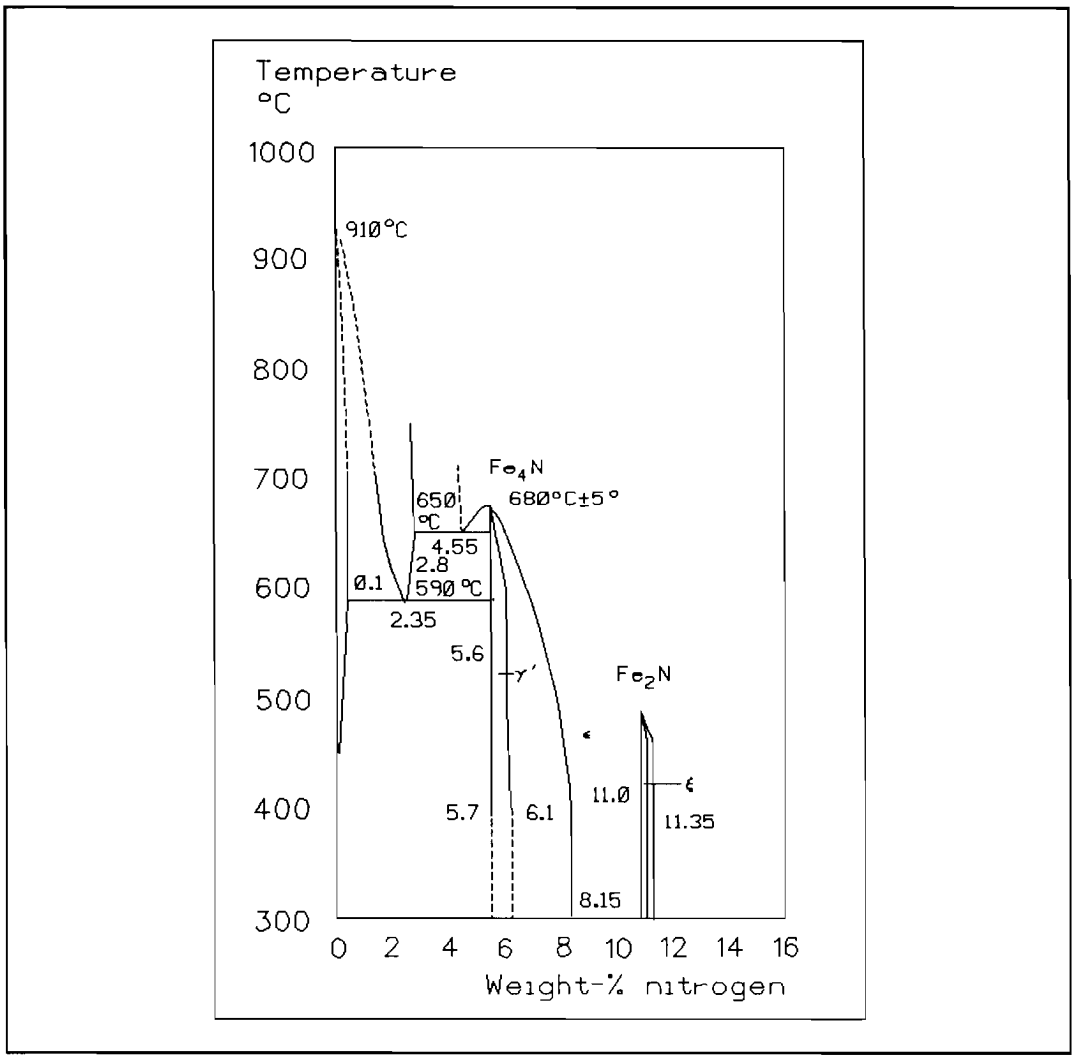

Figure 5.1 Equilibrium diagram for iron-nitrogen.

In addition to gas nitriding, some other nitriding methods, such as salt-bath nitriding and plasma nitriding (ion-nitriding), are widely used in industry, and each

method has its own advantages. In specific cases, one particular process may be preferable.

5.2 Fatigue Properties Improved by Nitriding

The fatigue properties of steels may be improved by nitriding in two ways: (1) the increase in surface hardness resulting from the formation of stable nitrides; (2) the development of compressive residual stresses in the case, which counter applied tensile stresses.

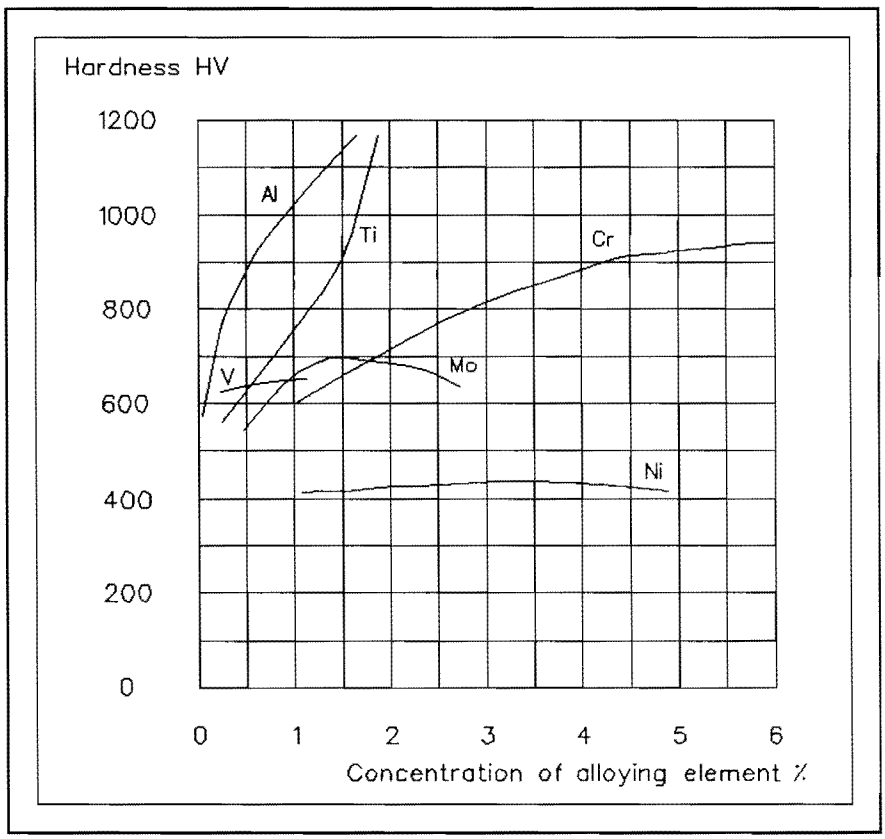

Figure 5.2 Effect of alloying element additions on hardness after nitriding. Base composition: 0.25%C, 0.30%Si, 0.70%Mn.

The development of compressive residual stresses is primarily because of volume differences between alloy nitrides which form in the case during the nitriding process and the alloying elements which are in solution in the steel in the

core. Since alloy nitrides occupy a greater volume than the alloying elements in solution in steel, they thus tend to expand the surface layer. On the other hand, the non-nitrided core will prevent the surface layers from obtaining their free growth size. The result is that expansion of the surface layers is restrained by the core.

In steels which are not surface hardened fatigue failure usually originates at a surface location under applied tensile stress during bending and direct stress testing. However, if residual compressive stresses are present in the case, the tendency for fatigue failure to initiate in the surface layer will decrease greatly. Figure 5.3 shows the resultant stress distribution in tension-compression fatigue testing of a nitrided cylindrical specimen.

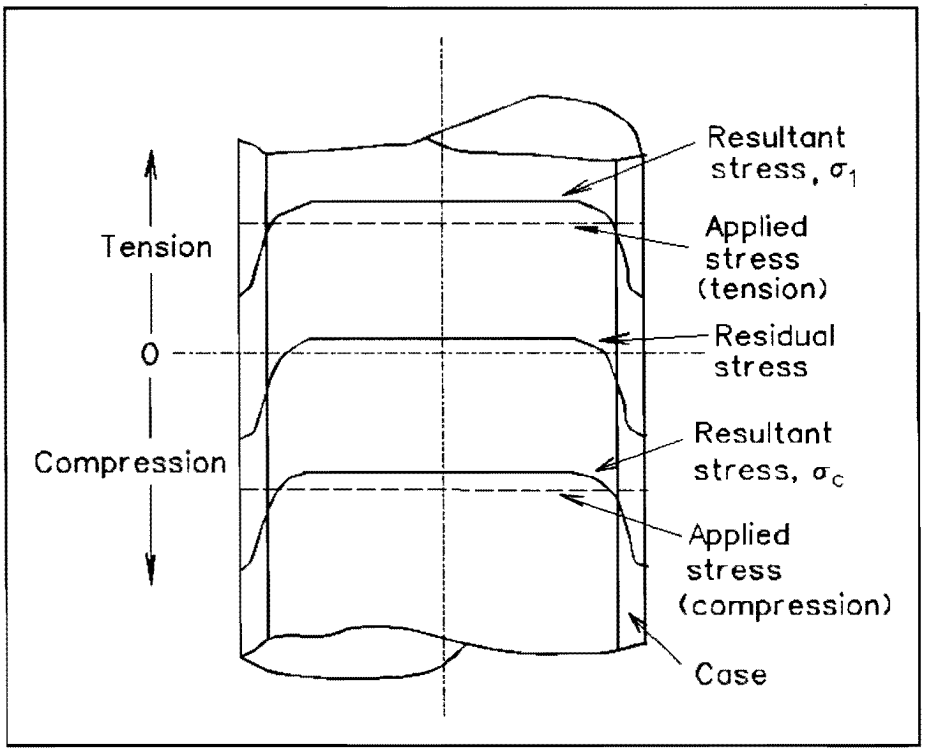

Figure 5.3 Addition of residual stresses to applied stress system in tension-compression fatigue of nitrided cylindrical specimen[89].

Fatigue crack initiation is often associated with non-metallic inclusions in nitrided steels. Some researchers[3,4] show that, at longer lives, failure is normally from a single sub-surface nucleated crack which is nucleated at an

alumina inclusion.

It should be noted that the non-metallic inclusions which initiate fatigue cracks in nitrided steels are mainly well below the surface. This is not so for non-nitrided steel where cracks are initiated mainly in the surface. This phenomenon is the result of compressive residual stresses in the case.

CHAPTER 6

Production of Experimental Steels

6.1 Introduction

The first phase of experimental work was to produce a nitriding steel in which non-metallic inclusions were modified by calcium additions to the melt. It was hoped that the modified inclusions would consist of oxides encapsulated by sulphides.

Since calcium has very low solubility in liquid steel, a high vapour pressure at steelmaking temperature, and it tends to float due to its low density, the yield of calcium addition are in general low. In full-scale practice, because the furnace or ladle is very large, it is usual to increase the efficiency of calcium usage by increasing the depth of cored wire injection. However, in a small furnace most of the calcium added is lost by vaporization, rather than contributing desulphurization and modification of non-metallic inclusions.

Since desulphurization and modification of non-metallic inclusions in the experiments are dominated by calcium, it was necessary to investigate which process of adding CaSi can increase calcium yield in a small furnace.

6.2 Materials and Equipment

The experiments were carried out in the Mechanical Engineering Department's Coreless High Frequency Induction Furnace. The induction furnace has a 14kg capacity, a maximum power of 40 kw, and a frequency of 3000 HZ. The crucible had a basic refractory lining. Grade 300 reinforcing bar was used as the starting material and its typical chemical composition is shown in table 6.1. 12 melts were produced, and modification of non-metallic inclusions by adding CaSi cored wire was investigated. The charge and alloying elements which were added to each melt in order to achieve the desired composition are shown in table 6.2.

Table 6.1 Typical Composition Of Grade 300

Elements	C	Mn	Si	Ni	Cr	S	P	Ti	Cu
Content(%)	0.19	0.48	0.15	0.09	0.06	.019	.007	.003	0.21

Table 6.2 Charge And Alloying Elements Added For Every Melt Unit kg

Melts No.	Stock(Grade 300)	C	Al	FeMn 75%Mn	FeCr 65%Cr	FeMo 75%Mo	Si
No.1	10	0.031	0.15	0.01	0.26	0.03	-
No.2	11	0.029		0.073	0.19	0.032*	-
No.3	8.5	0.024		0.06	0.15	0.028	-
No.4	8.5	0.04	0.014**	0.06	0.145	0.028	-
No.5	14	-		-	-	-	-
No.6	10.22*	0.045		0.091	0.182	0.032	-
No.7	14	-		-	-	-	-
No.9	10.5	0.034		0.087	0.173	0.028	0.021
No.10	10.556	0.029	0.01**	0.073	0.166	0.028	0.021
No.11	11.067	0.032		0.077	0.178	0.029	-
No.12	10.09*	0.027		0.095	0.161	0.027	-

* Remelt

** Deoxidizer

6.3 Experimental Process

No.1 melt

No.1 melt was intended to produce the nitriding steel, 905.M39 with non-metallic inclusions modified by adding CaSi. The chemical composition for 905 M39 is shown in table 6.3. 10kg of Grade 300 reinforcing bar was melted under normal atmospheric pressure without slag additions and the amounts of alloying elements added are shown in table 6.2.

Table 6.3 The Chemical Composition For 905 M39

Elements	C	Si	Mn	Cr	Mo	Al	S	P
Content(%)	0.35-0.43	0.10-0,45	0.40-0.65	1.40-1.80	0.15-0.25	0.90-1.30	Max 0.025	Max 0.025

Cored wire was used to add CaSi. A metal tube, 5 mm in diameter and 0.5mm wall thickness, from a vehicle hydraulic breakpipe, was cut into ten, 1 meter lengths. The tubes were filled with CaSi powder (60% Si, 30%Ca and the rest of content is Fe, C and Al). The mean CaSi weight in each tube was 12.1 gram. Each length of cored wire was compacted by cold rolling.

All elements and alloys were added directly to the molten feedstock in the furnace at 1650°C in order of increasing reactivity, i.e. the most easily oxidised elements were added last. CaSi cored wire was added at 1630-1650°C before teeming, and the method of adding CaSi is shown in table 6.4 and will also be described below.

Four tubes of CaSi (12.1×4 gram) cored wire were added into the melt and the liquid steel was poured into a 2.5 kg mould with hot top for first ingot, named 1A; A further three tubes of CaSi cored wire (12.1×3 gram) were injected into the melt for the second ingot, named 1B; Two more tubes of CaSi cored wire were injected into the melt for the third ingot, named 1C and the final tube of CaSi cored wire was added for fourth ingot, named 1D.

No.2 Melt

For No.2 melt and all subsequent melts the steel produced was 708 M40, nitriding steel. This is because 905 M39 nitriding steel contains 0.90-1.30% Al, and the amount of calcium needed increases with increasing aluminium content[101], if calcium is used to modify non-metallic inclusions. So more calcium would be needed in this case, and this is really difficult to realize in a small furnace.

CaSi powder was fed into a tube of 9 mm diameter and 1.5 mm wall thickness, in order to the maintain the CaSi cored wire longer in the liquid steel prior to the sheath melting in the experiment. Thicker cored wire sheath affects favourably the yield of binary alloys rich in calcium in liquid steel[55].

The experimental process was similar to No.1 melt and elements and alloys added are shown in table 6.2. The chemical composition for 708 M40 steel is given in the table 6.5. Some aluminium was added as a deoxidizer into the melt before injection of CaSi cored wire. For the method of addition, and amount of CaSi cored wire see table 6.6.

Table 6.4 Method of Addition And Amount of CaSi Cored Wire in No.1 Melt

Melt No.	Addition	Addition	Addition	Addition	Casting
No.1 Melt 10 kg	CaSi 48.4 gram	----	----	----	1A
		CaSi 36.3 gram	----	----	1B
			CaSi 24.2 g	----	1C
				CaSi 12.1g	1D

Table 6.5 The Chemical Composition For 708 M40 Steel

Element	C	Si	Mn	P	S	Cr	Mo
Content(%)	0.36-0.44	0.10-0.40	0.70-1.00	Max. 0.035	Max. 0.04	0.9-1.20	0.15-0.25

Table 6.6 Method of Addition And Amount of CaSi Cored Wire in No.2 Melt

Melt No.	Addition	Addition	Addition	Addition	Casting
No.2 Melt 11 kg	Al* 22 gram	----	----	----	2A
		CaSi 33 gram	----	----	2B
			CaSi 10.5 gram	----	2C
				CaSi 17 g	2D

* Deoxidizer.

No.3 and No.4 Melts

Desulphurization by adding basic slag into the induction furnace was investigated. The purpose of the basic slag was to obtain a lower sulphur content in the melt before adding the CaSi cored wire. Since the calcium yield in the steelmaking process is very low, especially in a small furnace, sulphur should be lower in the liquid steel before adding CaSi, so that most of the (small) amount of calcium taken up by the melt modifies the non-metallic inclusions.

Basic slag was chosen because this slag system is very effective in desulphurization[30,31].

8.5 kg of Grade 300 reinforcing bar and low carbon steel pellets were melted in the induction furnace, and aluminium was added into the melt to lower the [O] activity at 1550°C. Powder mixtures of lime (CaO), alumina (Al_2O_3), SiO_2 and MgO were added to form a slag and the amount of each compound is shown in table 6.7.

The temperature of liquid steel was kept at 1650°C for 20 minutes so that the liquid slag could react with and desulphurize the liquid steel. Before adding CaSi cored wire , the slag was removed from the furnace, and 0.011 kg of aluminium was added into the melt to further deoxidize. The process of adding CaSi was similar to that of No.2 melt, which is shown in table 6.8, and the size of cored wire was the same as for the second melt.

Table 6.7 The Amount of Each Compound Used as Slag

Melt No.	CaO	Al_2O_3	SiO_2	MgO
No.3	110 gram	34 gram	36 gram	20 gram
No.4	300 gram	75 gram	75 gram	50 gram

Table 6.8 Method of Addition and Amount of CaSI Cored Wire in No.3 Melt

Melt No.	Addition	Addition	Addition	Casting
No.3 Melt 8.5 kg	Aluminium* 18 gram	----	----	3A
		CaSi 30 gram	----	3B
			CaSi 20 gram	3C

* Deoxidizer.

Since the bath was stirred very strongly the amount of slag added could not cover the agitating liquid steel surface. This resulted in the liquid steel being almost totally exposed to air for about 20 minutes.

The metallurgical process of the fourth melt was similar to that of No.3 melt. However a larger amount of slag was added. The slag composition, elements and alloys added, and the process of adding CaSi cored wire are shown in tables 6.7, 6.2 and 6.9 respectively.

Since the materials used to produce the slag were powder, except the lumplime used in No.4 melt, some powder floated on the liquid steel surface because of its lower density and did not melt. It was intended to use lumplime, alumina, quartz sand, and magnesite to further investigate desulphurization by basic slag. However, some materials were not available, and desulphurization by

basic slag first followed by adding CaSi cored wire was only investigated in these two melts.

Table 6.9 Method of Addition And Amount of CaSi Cored Wire in No.4 Melt

Melt No.	Addition	Addition	Addition	Casting
No.4 Melt 8.5 kg	Aluminium* 9 gram	----	----	4A
		CaSi 30 gram	----	4B
			CaSi 21 g	4C

* Deoxidizer.

No.5 and No.6 Melts

Since the CaSi used contains of 30%Ca and 60%Si and silicon is very easy to dissolve in the liquid steel, most of the silicon dissolved in the melt, whereas most of calcium evaporated from the melt. The result was that the silicon content was higher in the steel after adding CaSi and the silicon content exceeded the specification of 708 M40.

An ingot-remelting method was employed. That is, first the stock was melted, desulphurized by adding CaSi, and ingots with low sulphur content were obtained as No.5 melt. Second the ingots from No.5 melt were remelted to produce No.6 melt and only a small amount of CaSi was injected to further modify the non-metallic inclusions. Meanwhile silicon was expected to be lost by oxidation during remelting.

The charge, elements and alloys, and CaSi cored wire added for No.5 melt are shown in table 6.2 and 6.10 respectively.

Desulphurised ingots totalling 10.2 kg were obtained. Splashing generated by adding CaSi cored wire, and excessive spillage in the process of pouring into ingot moulds accounted for the loss of weight.

Table 6.10 Amount of Aluminium And CaSi Cored Wire in No.5 Melt

Melt No.	Addition	Addition	Casting
No.5 Melt 14 kg	Al* (21 gram)	CaSi (126 gram)	5A

* Al was added as deoxidizer.

Since in previous melts (No.1-5), some liquid steel was lost due to calcium vaporisation and a very violent reaction, a lid made of a refractory material, with a 20 mm diameter hole in the centre, covered the furnace in the experiment when CaSi cored wire was injected for No.6 melt. Also the effect of temperature on CaSi yield was investigated in this experiment.

Table 6.11 Method of Addition And Amount of CaSi Cored Wire in No.6 Melt

Melt No.	Addition	Addition	Addition	Addition	Casting
No.6 Melt 10.2 kg	Al* (23 gram)	CaSi (40 gram)	----	----	6A
			CaSi (40 gram)	----	6B
				CaSi(40g)	6C

* Aluminium was added as deoxidizer.

The 10.2 kg of ingots from melt No.5 was remelted and certain amounts of elements and alloys, shown in table 6.2, were added into the melt at 1630°C, followed by adding 29 gram of aluminium to lower [O] activity. CaSi cored wire was injected at 1550°C, the process being described in table 6.11. It was observed that the violence of the reaction cause by adding CaSi decreased greatly compared to previous melts where the CaSi was added at about 1630-1650°C.

No.7 and No.12 Melts

The metallurgical processes of both these melts were similar to those of No.5 and No.6 melts. The addition of CaSi at lower temperature was further investigated, and CaSi cored wire with a higher calcium content, and lower silicon content was employed in No.12 melt.

To produce melt No.7, 14 kg of Grade 300 reinforcing bar and low carbon steel pellets were melted, and 28 gram of aluminium was added at 1620°C. Cored wire with 226 gram CaSi was injected at 1550°C into the furnace with lid to desulphurize and modify non-metallic inclusions. The melt was reheated to 1600°C and cast into 3.5 kg moulds with hot top.

10.9 kg of pre-desulphurized melt No.7 was remelted to produce melt No.12 and elements and alloys were added as shown in table 6.2. CaSi cored wire containing a higher calcium and lower silicon content was adopted in this experiment, and obtained from Odermath of Germany. CaSi composition and cored wire size are given in table 6.12. 47 gram of this CaSi was injected into the melt at 1550°C, and the melt was reheated to 1600°C and ingots for 12A were cast.

Table 6.12 Composition of CaSi64

Composition (%) of CaSi64					Size	
Al	C	Ca	Mg	Si	Wire diameter (mm)	9
<2.0	<0.5	64	<1.0	30	Casing (mm)	0.4

No.11 Melt

Injection of CaSi cored wire with 64%Ca and 30%Si into the melt was further investigated. Charge, elements and alloys added are shown in table 6.2. Cored wire with 140 gram of CaSi was injected into the liquid steel. The injection temperature was about 1550°C. It was observed that the reaction of the CaSi with

steel was violent due to the higher calcium content of this wire. Ingots for 11A were cast.

No.9 and 10 Melts

The purpose of these two melts was to produce 708 M40 nitriding steel without adding any CaSi so that steel with unmodified inclusions was obtained, in order to compare the fatigue properties of this steel with a similar steel containing modified non-metallic inclusions

Charge, elements and alloys added are shown in table 6.2.

Ingots from these melts were named to 9A and 10A respectively.

CHAPTER 7

Analysis of Experimental Steels and Examination of Non-Metallic Inclusions

7.1 Chemical Analysis

All samples from the eleven experimental melts were sent to Pacific Steel Limited for analysis of chemical composition by optical emission spectrometer and the average compositions are shown in table 7.1. Because Pacific Steel had no standard for high aluminium steel in their spectrometer, the aluminium content in ingots 1A-1D, from No.1 melt, was given as "more than 0.11%". In fact the aluminium content should be 0.9-1.10% based on the amount of aluminium added.

The calcium content was not shown in the chemical composition of any samples, even though a larger amount of CaSi cored wire was added in some melts. This is because of the absence of a calcium standard in the spectrometer.

In No.3 melt, only sample 3C was sent for analysis, since the other two ingots were too spongy (Because No.3 melt was exposed to air for about 20 min at 1650°C without a slag cover, a large amount of gas entered the liquid steel and caused ingot porosity. However, when a certain amount of CaSi was added into the melt, the gas was probably removed from the liquid steel by the very violent reaction with liquid steel caused by the rapid vaporisation of the calcium, and a solid ingot, sample 3C, was obtained).

7.2 Analysis of Non-Metallic Inclusions

7.2.1 Experimental Procedure

Samples for analysis of non-metallic inclusions were cut from every ingot,

mounted in conductive bakelite, ground and finally polished to a 1 micron finish. Non-metallic inclusions were analyzed by the scanning electron microscope.

Table 7.1 Average composition for every sample

No.	C	Mn	Si	S	P	Al	Ni	Cr	Mo	Cu	Sn
1A	.45	.99	.45	.024	.024	.11*	.09	1.6	.24	.28	.042
1B	.44	1.05	.73	.026	.026	.11*	.08	1.5	.024	.34	.06
1C	.44	1.10	.86	.017	.025	.11*	.08	1.5	.24	.36	.067
1D	.45	1.11	1.04	.013	.026	.11*	.08	1.5	.23	.43	.08
2A	.36	.70	.05	.028	.022	-	.09	.94	.208	.22	.021
2B	.35	.71	.15	.025	.022	-	.09	.94	.197	.21	.02
2C	.35	.76	.22	.03	.023	-	.08	.94	.216	.21	.02
2D	.35	.75	.42	.022	.022	-	.08	.91	.201	.21	.02
3C	.24	.74	.33	.025	.02	.014	.08	1.0	.25	.27	.051
4A	.50	.89	.02	.02	.016	.02	.07	1.2	.26	.18	.018
4B	.47	.90	.16	.016	.017	.013	.08	1.19	.255	.19	.019
4C	.45	.91	.47	.012	.017	.02	.08	1.14	.251	.09	.018
5A	.08	.43	.29	.023	.02	-	.10	.06	.012	.021	.021
6A	.43	.66	.27	.024	.025	.079	.08	1.16	.26	.23	.022
6B	.41	.72	.57	.019	.026	.068	.08	1.12	.25	.23	.022
6C	.40	.72	.95	.008	.025	.063	.08	1.04	.238	.22	.021
7A	.22	.35	.95	.007	.019	.11	.08	.06	.013	.21	.018

* Al content is more than 0.11.

Table 7.1 (continue)

No.	C	Mn	Si	S	P	Al	Ni	Cr	Mo	Cu	Sn
9A	.46	1.01	.29	.026	.025	.059	.07	1.18	.224	.20	.02
10A	.39	.87	.19	.024	.026	.017	0.1	1.13	.212	.23	.022
11A	.37	1.07	.33	.015	.023	.01	.08	1.09	.212	.23	.018
12A	.46	1.06	.71	.021	.024	.015	.09	1.18	.218	.24	.018

Table 7.2 Main Inclusion Types Found In Samples

No.	Common Types	Shape	Remarks
1B	$CaO.Al_2O_3.(Ca.Mn)S$ * $CaO.Al_2O_3$ Al_2O_3 MnS	Spherical Spherical Spherical Irregular	* Calcium aluminate and Calcium sulphide were intermixed.
1D	$CaO.Al_2O_3$ $CaO.Al_2O_3.(Mn.Ca)S$ * $CaO.Al_2O_3.CaS$ * (Ca,Mn)S	Spherical Spherical Spherical Elliptical	Some of the CaS contained small amount of Mn
2B	MnS $CaO.Al_2O_3$ $CaO.Al_2O_3.(Ca.Mn)S$ *	Irregular Spherical Irregular	$CaO.Al_2O_3.(Ca.Mn)S$ was not common, and Ca content was very small.
2D	$CaO.Al_2O_3$ $CaO.Al_2O_3.CaS$ *	Spherical Spherical	Calcium content was higher in $CaO.Al_2O_3CaS$.
3C	$CaO.Al_2O_3.SiO_2$ $CaO.Al_2O_3$ MnS	Spherical Spherical Irregular	

Table 7.2 (Continue)

Samples	Common Types	Shape	Remarks
4A	MnS Al_2O_3 $CaO.Al_2O_3$	Irregular Angular Spherical	
4B	MnS (Ca.Mn)S $CaO.Al_2O_3$	Irregular Elliptical Spherical	
4C	$CaO.Al_2O_3.CaS$ * $CaO.Al_2O_3.(Ca.Mn)S.MgO$ * $CaO.Al_2O_3$ $CaO.Al_2O_3.SiO_2$	Elliptical Spherical Spherical Spherical	
5A	$CaO.Al_2O_3.SiO_2$ $CaO.Al_2O_3$ MnS	Spherical Spherical Irregular	
6A	MnS (Ca.Mn)S $CaO.Al_2O_3$	Irregular Irregular Spherical	Ca content in (Ca.Mn)S was very small.
6B	(Ca.Mn)S $CaO.Al_2O_3.(Ca.Mn)S$ * $CaO.Al_2O_3$	Irregular Elliptical Spherical	
6C	$CaO.Al_2O_3.(Ca.Mn)S$ * $CaO.Al_2O_3.CaS$ * $CaO.Al_2O_3.(Ca.Mn)S.MgO$ * $CaO.Al_2O_3$ SiO_2	Spherical Spherical Spherical Spherical Angular	SiO_2 was not very common.

Table 7.2 (continue)

Samples	Common Types	Shape	Remarks
7A	CaS $CaO.Al_2O_3$ $CaO.Al_2O_3.CaS$ *	Elliptical Spherical Spherical	
9A	MnS Al_2O_3	Irregular Angular	
10A	MnS Al_2O_3 SiO_2	Irregular Angular Angular	
11A	$CaO.Al_2O_3$ $CaO.Al_2O_3.SiO_2.CaS$ $CaO.Al_2O_3.SiO_2.(Ca.Mn)S$ CaS SiO_2	Spherical Spherical Spherical Irregular Angular	

Some typical inclusion compositions were obtained as graphs of the X-ray spectra from the electron microscope energy dispersive X-ray analysis facility, and comparative measures of the quantities of the elements contained in these inclusions were given.

Ingots 10A and 11A were sent for forging, and the non-metallic inclusions were analyzed again after forging.

7.2.2 Results of Analysis of Non-Metallic Inclusions

Results of the scanning electron microscope analysis of non-metallic inclusions are shown in table 7.2. Only common types of inclusions are listed in the table.It was observed that the non-metallic inclusions in samples 9A and 10A were mainly MnS and Al_2O_3, since no CaSi cored wire was injected . Typical MnS and Al_2O_3 inclusions are shown in photos 7.1 and 7.2 respectively.

After a small amount of CaSi cored wire was added, Al_2O_3 was transformed to spherical $CaO.Al_2O_3$ or $CaO.Al_2O_3.SiO_2$ and $CaO.Al_2O_3$.(Ca.Mn)S inclusions. However some MnS inclusions remained in the steel, since the sulphur content

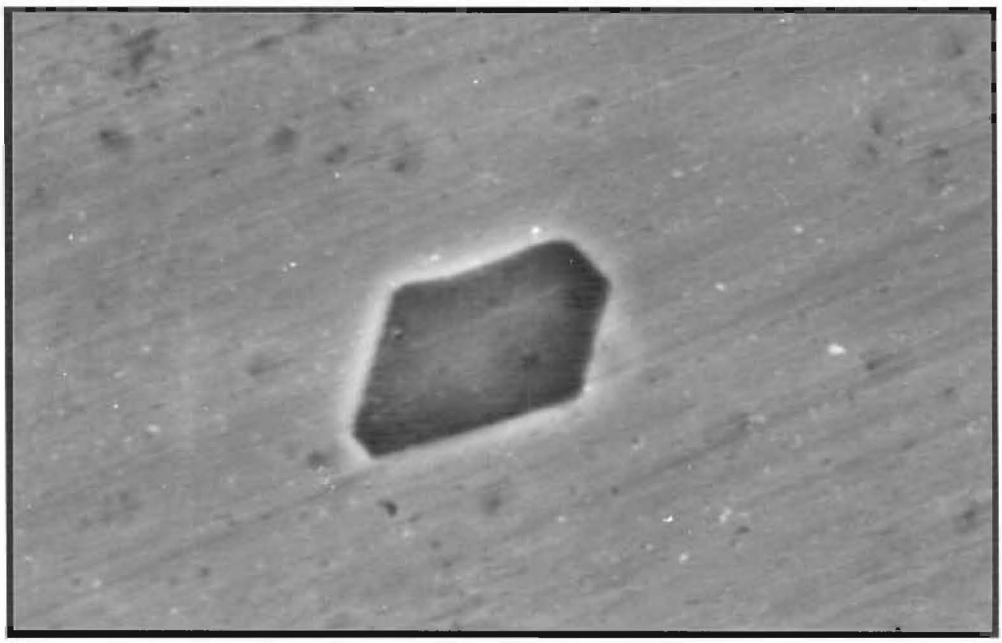

Photo 7.1 MnS inclusion in 10A before forging. 1μm

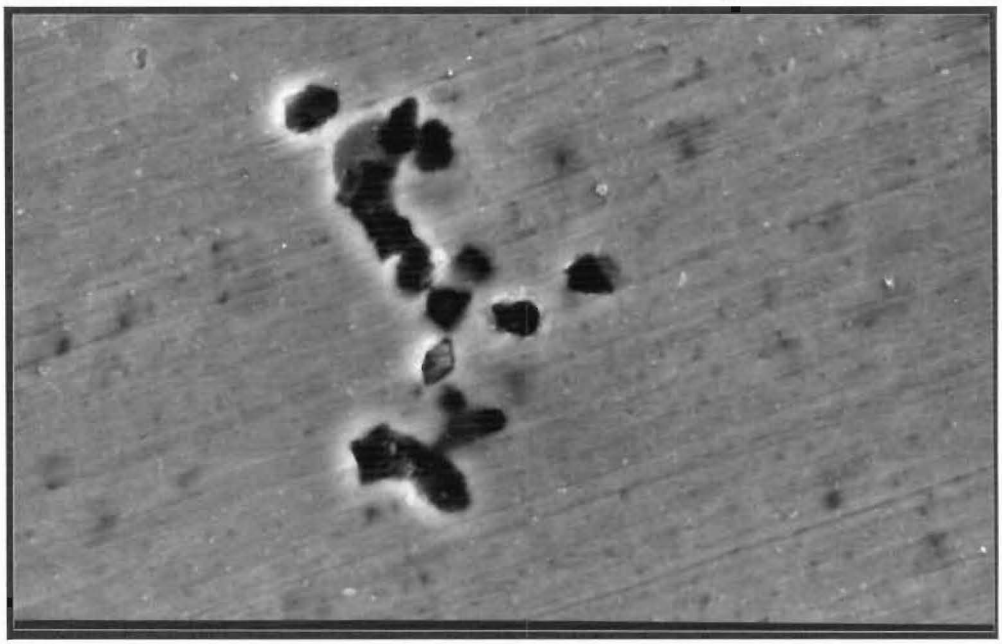

Photo 7.2 Typical alumina inclusion in 10A before forging. 1μm

was not very low. These types of inclusions were observed in samples 1B, 2B, 3C, 4B, 5A, and 6A. A typical spherical $CaO.Al_2O_3$ inclusions is shown in photo 7.3. With increasing of the amounts CaSi cored wire added, MnS was fully modified to (Ca.Mn)S or CaS, according to amount the of CaSi added and more oxy-sulphide inclusions were formed in the liquid steel. This situation was found in samples 1D, 4C, 6C, 7A,and 11A.

It was observed that samples 6C and 7A had significantly lower sulphur contents than the other samples.

7.3 Inclusions of Calcium Aluminate surrounded by Calcium Sulphides.

Inclusions of types $CaO.Al_2O_3.CaS$ or $CaO.Al_2O_3$(Ca.Mn)S were found in many samples, as shown in table 7.2. Since the size of these type of inclusion found were small, it was very difficult in most cases to distinguish calcium aluminate surrounded by calcium sulphide from calcium sulphides intermixed in calcium aluminate. However, some typical inclusions of calcium aluminate enveloped by CaS were found in sample 11A. This type of inclusion found in sample 11A is shown in photo 7.4, and figure 7.1 gives the composition of the centre-phase, and figure 7.2 gives the composition of the outer phase. It is shown that the centre-phase is mainly composed of $CaO\text{-}Al_2O_3$, and the outer phase is rich in CaS.

7.4 Control of Inclusion Shape and Composition by Calcium Addition

Inclusions in sample 10A analyzed by the scanning electron microscope were mainly irregularly shaped MnS and clusters of Al_2O_3. However after adding CaSi cored wire, oxide inclusions were transformed to globular $CaO.Al_2O_3$ type, and sulphide inclusions were mainly CaS and CaS intermixed in $CaO.Al_2O_3$, or deposited peripherally around them. These modified inclusions have different characteristic from unmodified inclusions.

Inclusion shapes in sample 10A and 11A are shown in photos 7.5 and 7.6

respectively, after the ingots were forged. It was observed that the MnS inclusions in sample 10A were elongated because of their high deformability index, but spherical $CaO.Al_2O_3$ and $CaO.Al_2O_3$,CaS types of inclusions retained their original shapes, which shows their deformability index is nearly zero.

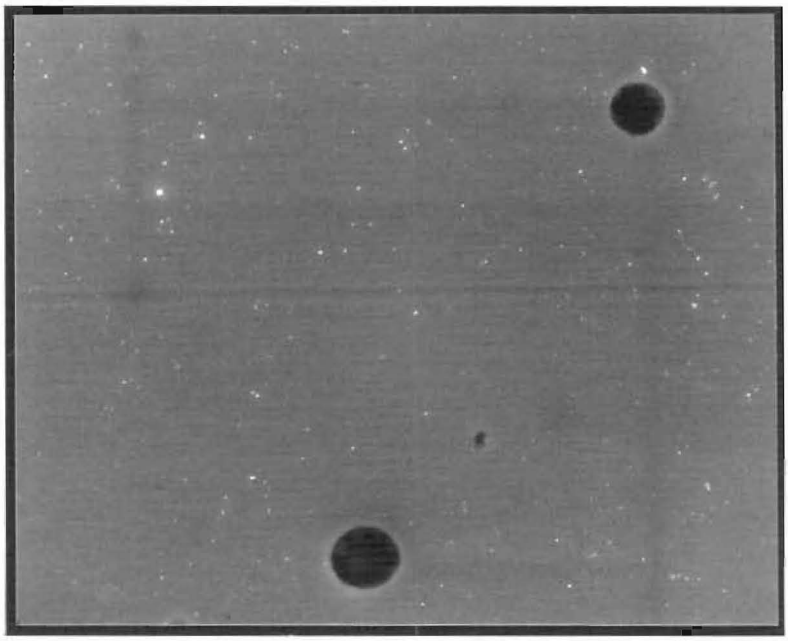

Photo 7.3 Typical spherical $CaO\text{-}Al_2O_3$ inclusions in 6B. 1μm

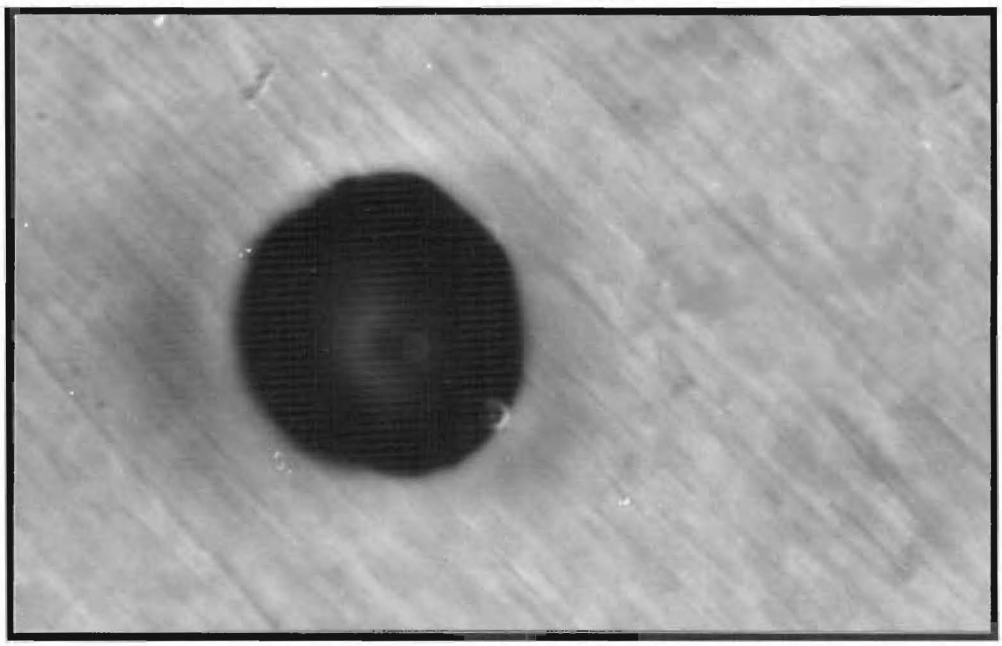

Photo 7.4 Duplex oxysulphide inclusion in 11A. 1μm

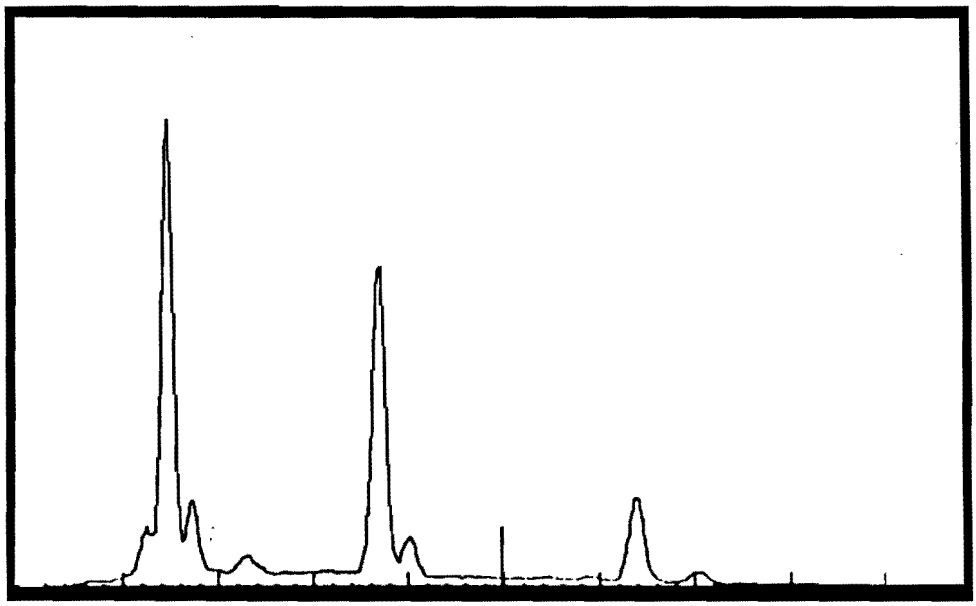

Figure 7.1 Composition of centre-phase of inclusion in photo 7-4.

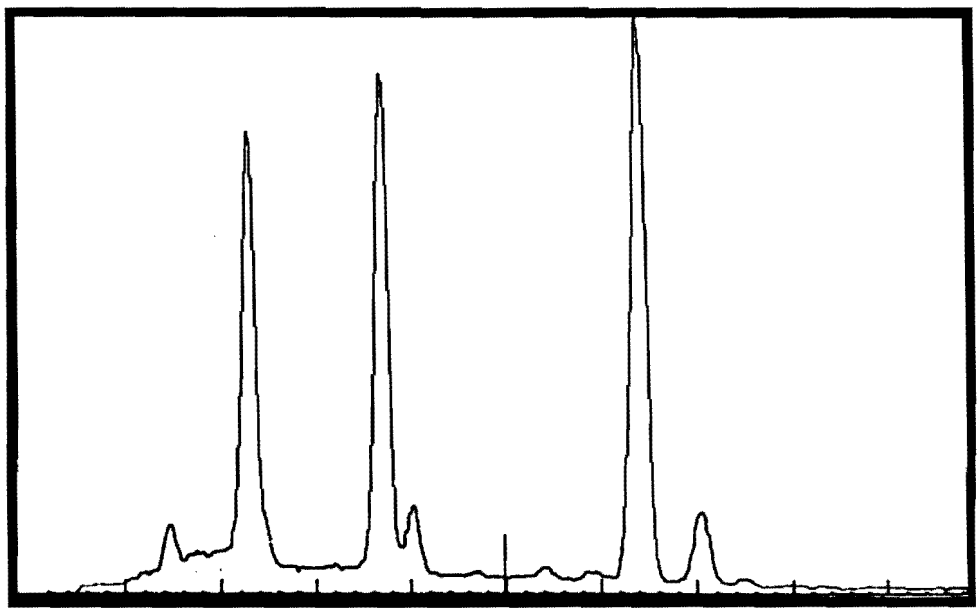

Figure 7.2 Composition of outer phase of inclusion in photo 7-4.

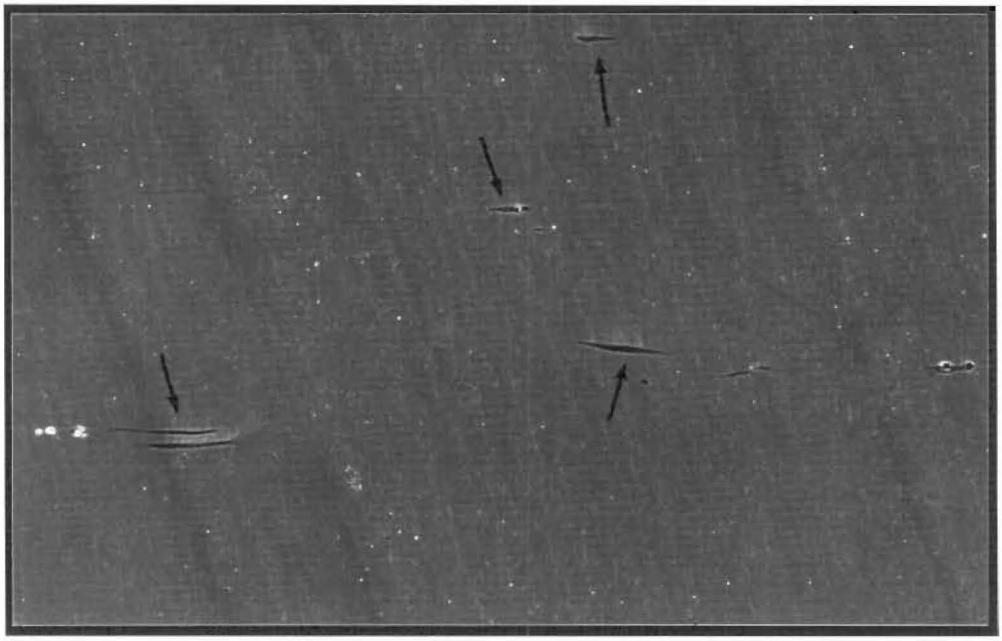

Photo 7.5 Inclusion shapes in sample 10A after forging. 1μm

Photo 7.6 Inclusion shapes in sample 11A after forging. 1μm

Some elongated elliptical inclusions of SiO_2 were found in both samples, indicating that SiO_2 was deformable. This deformable SiO_2 is probably cristobalite, which has a slight plasticity at steel hot-working temperatures, whereas other modifications of SiO_2 are brittle, with zero deformability index throughout the whole temperature range of interest[20].

CHAPTER 8

Fatigue Testing:
Experimental Procedure and Results

8.1 Introduction

Specimens for fatigue testing were produced from ingots 10A and 11A and were nitrided. Direct stress fatigue testing was carried out using an Amsler Vibrophore. S-N curves for materials 10A and 11A were plotted in order to compare their fatigue properties. The inclusions which caused fatigue crack initiation were analyzed using a scanning electron microscope with energy dispersive X-ray analysis in order to study (1) which types of inclusions were more detrimental to the fatigue properties of steel and (2) the effects of duplex oxysulphide inclusions on the fatigue properties of steel.

8.2 Experimental Procedure

8.2.1 Specimen Preparation

The ingots of initial size approximate 50×50mm were forged to 15mm diameter rod. The forging temperature was at about 1050°C.

The procedure for manufacture of the fatigue specimens is shown in figure 8.1.

After forging the rods were normalized at 875°C for about 20 minutes in order to refine the forged grain size, remove the differences in grain size found in forged sections, obtain a uniform structure and reduce distortion due to later quenching and tempering.

The rods were turned to 12mm diameter and hardened and tempered. They were heated to 860°C, held for 25 min followed by oil quenching, and tempering

at 630°C, for 60 minutes and cooled in air. A more ductile structure in the steel is obtained due to a high tempering temperature, so that after nitriding, superior mechanical properties of the steel can be obtained resulting from high hardness and strength in the case and good ductility in the core. The microstructure was tempered martensite which is form by the gradual breakdown of martensite during tempering at high temperature resulting in a uniform distribution of minute particles of carbide in a matrix of ferrite. The microstructures for specimens, 10A and 11A, are shown in photos 8.1 and 8.2 respectively. It is observed that the microstructures are almost identical.

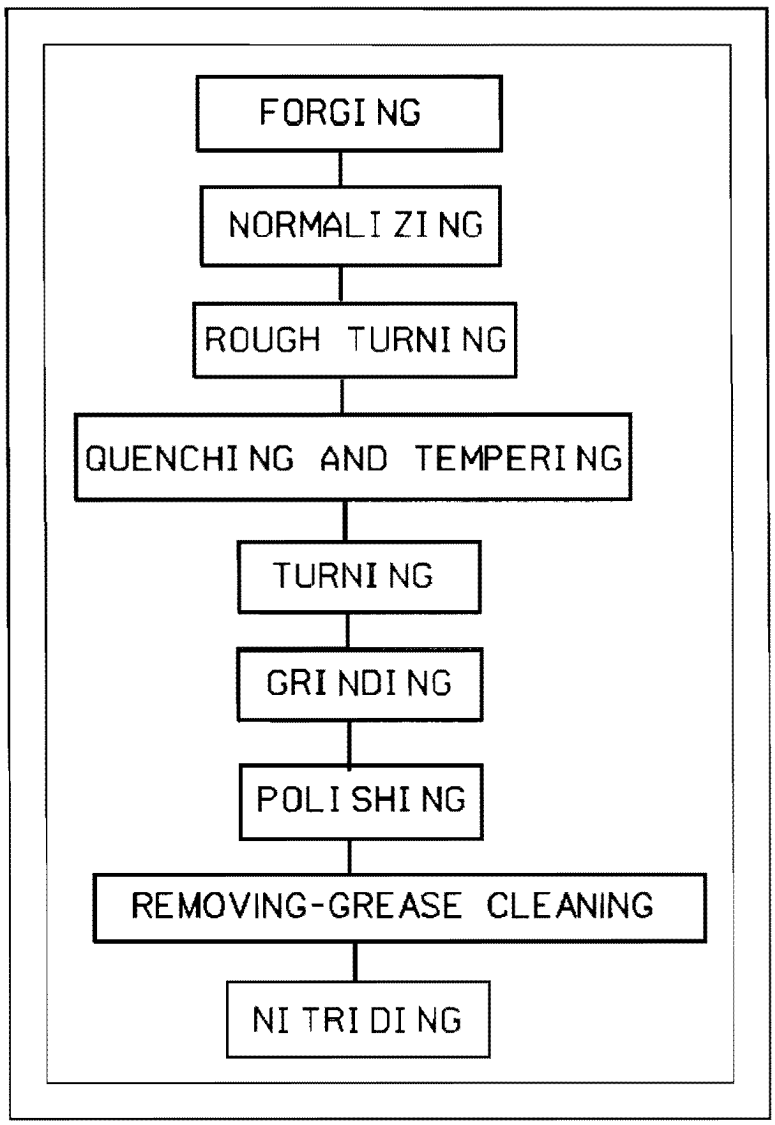

Figure 8.1 Procedure for fatigue specimens 10A and 11A.

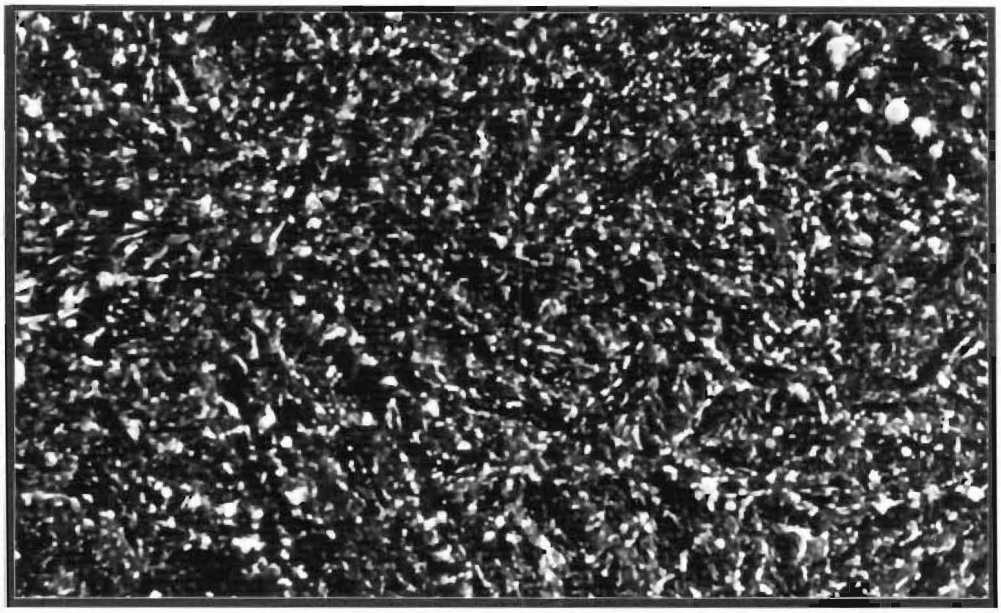

Photo 8.1 The microstructure for specimens 10A 1μm

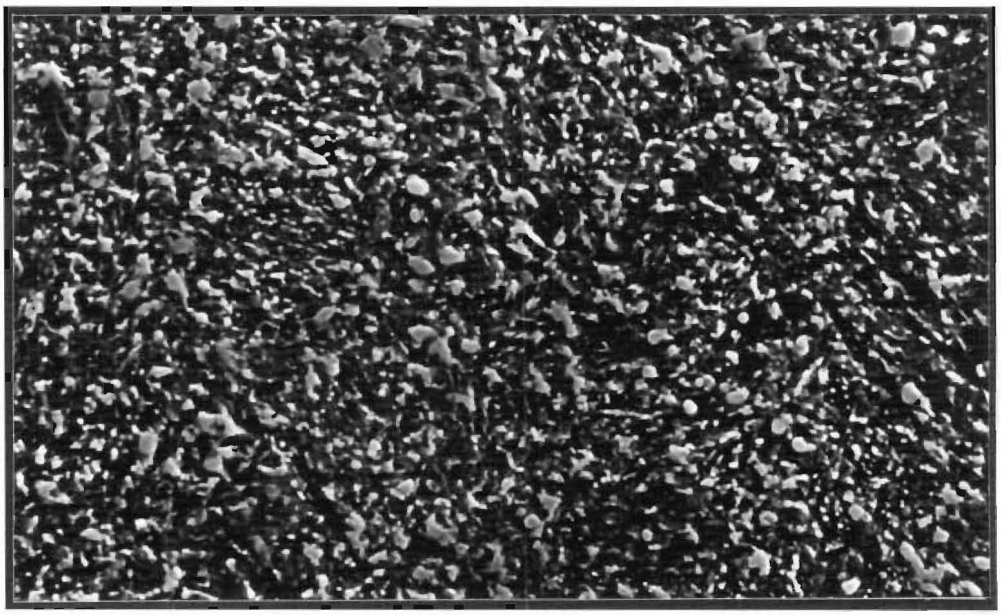

Photo 8.2 The microstructure for specimens 11A 1μm

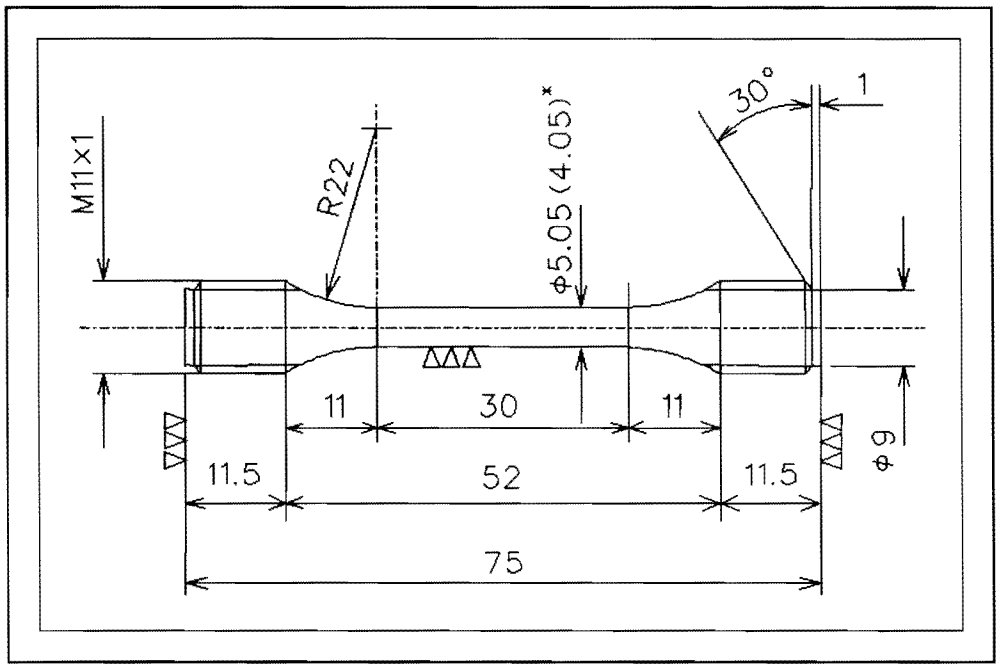

Figure 8.2 Dimensions of specimen and modified specimen for fatigue testing

During hardening and tempering, rods forged from ingots 10A and 11A were always kept at random positions in the furnace in order to balance any effect of temperature differences.

Specimens were turned and ground to the dimensions which are shown in figure 8.2. The test pieces were then polished before they were nitrided. The polishing was in a longitudinal direction using 800 grade waterproof silicon carbide paper and circumferential scratches were totally removed by final polishing.

The specimens were cleaned by ultrasonic cleaning in "turgin" agent after polishing, so that grease on the specimen surface, which is detrimental to nitriding, could be removed.

Specimens produced from 10A and 11A ingots were then nitrided at 500°C for 4 hours and they also were randomly placed in the furnace.

8.2.2 Fatigue Testing

Direct stress fatigue testing was carried out using an Amsler Vibrophore at a frequency of about 200 hertz. Since the 5mm diameter specimens broke in the threaded portion, these specimens were modified to 4mm diameter, of the dimensions shown in figure 8.2. This completely removed the nitrided case along the gauge length of the specimens. The specimens were polished and cleaned again and nitrided at 500°C for 16 hours.

A special specimen was made on to which four strain gauges were attached at 90° to each other so that the alignment of the direct stress machine could be checked. This specimen was inserted in the Amsler Vibrophore, increasing tensile loads were applied to it and the strains were recorded by the four strain gauges. The machine alignment was set as accurately as possible, so that the readings shown by the four gauges did not vary by more than 6.4% from one another.

Direct stress fatigue testing for the modified specimens was carried out using the Amsler Vibrophore.

8.2.3 Assessment of Non-Metallic Inclusions

The non-metallic inclusion assessment in specimens 10A and 11A was determined by a microscopic method according to ASTM standard E45: Method D, which is designed for application to steels with low inclusion contents.

[Method D is as follow: The samples are cut from the ingots and the polished surface should be parallel to the longitudinal axis of the product. The samples are ground and polished. Final polished surface is free of artifacts such as pitting, foreign material (for example, polishing media), and scratches. The entire surface of the polished sample is surveyed at a magnification of 100× with a field area on the sample of 0.50 mm^2 (a circle of 0.8mm diameter) and then each field of the sample is compared with the fields of plate III, which also have areas of 0.50mm^2. The inclusion rating shown at the left of Plate III for each inclusion type A, B, C and D (Type A is oxide inclusions, type B is sulphide inclusions, type C is silicate and type D is globular inclusions), that appears most like the field under observation, for both the thin and heavy series is recorded. This is done each

field containing inclusions equivalent to or greater than the base or 1/2 series. If some inclusions larger than these displayed on Plate III are found, they are recorded separately, and if the widths or diameter are greater than the limiting values shown on Plate III, these are also recorded separately.]

Nine samples each from 10A and 11A were produced, parallel to the forging direction. The polished surface of each sample was approximately 140mm^2 and the main aim for this test was to compare the inclusion contents of specimens from ingots 10A and 11A.

Each specimen was examined over the surface (140mm^2) at 100× magnification with a field area of 0.50mm^2. About 204 fields were observed for each specimen.The results for inclusion assessment in specimens 10A and 11A are shown in tables 8.1 and 8.2 respectively.

Table 8.1 Inclusion assessment in specimens 10A

	Average number of fields of nine specimens							
Inclusion Rating No.	Type-A		Type-B		Type-C		Type-D	
	Thin	Heavy	Thin	Heavy	Thin	Heavy	Thin	Heavy
0.5	77	7.5	41.5	18.3	3.6	0.5	8.9	0.6
1.0	29.4	2.4	26.4	4.6	1.1	0	2.0	0.1
1.5	9.5	0.8	9.1	2.0	0	0	0.3	0
2.0	1.1	0	5.6	0.1	0	0	0	0
2.5	0.1	0	0.8	0	0	0	0	0

Remark, Eleven fields 0.076mm long by about 0.025mm wide, three fields 0.178mm long by about 0.025mm wide and one field 0.305mm long by about 0.025mm wide of type-B; One field 0.508mm long by about 0.025mm wide and two fields 0.178mm long by about 0.025mm wide of type-C.

Table 8.2 Inclusion assessment in specimens 11A

	Average number of fields of nine specimens							
Inclusion Rating No.	Type-A		Type-B		Type-C		Type-D	
	Thin	Heavy	Thin	Heavy	Thin	Heavy	Thin	Heavy
0.5	0	0	7.8	0.4	8.0	0.9	60.3	28.9
1.0	0	0	3.9	0	1.4	0.3	40.5	4.3
1.5	0	0	1.1	0	0.2	0	11	0.4
2.0	0	0	0	0	0	0	0.9	0.1
2.5	0	0	0	0	0	0	0	0

Remark, Several type-D, globular,inclusions with about 0.025mm-0.038mm diameter were found in some fields; Six fields 0.178mm long by 0.025mm wide and one field 0.305mm long by 0.025mm wide of type-C, silicate inclusion.

It was observed that the incidence of type-A sulphide and type-B alumina inclusions were high in specimens 10A, and almost absent in specimens 11A. Conversely, the incidence of type-D globular inclusions was very low in specimens 10A, and much higher in specimens 11A.

The large inclusions which caused fatigue crack initiation in both specimens, 10A and 11A, were not found by the non-metallic inclusion assessment using this method. This probably indicates that (1) inclusions of this size are present in the steel in very small numbers; (2) the microscopic method used to determine the size, distribution and number of inclusion in the steel is not a complete metallographic study of the inclusions. The results obtained by a microscopic examination of the inclusions are a statistical sample, and may not show up inclusions which are present in small numbers.

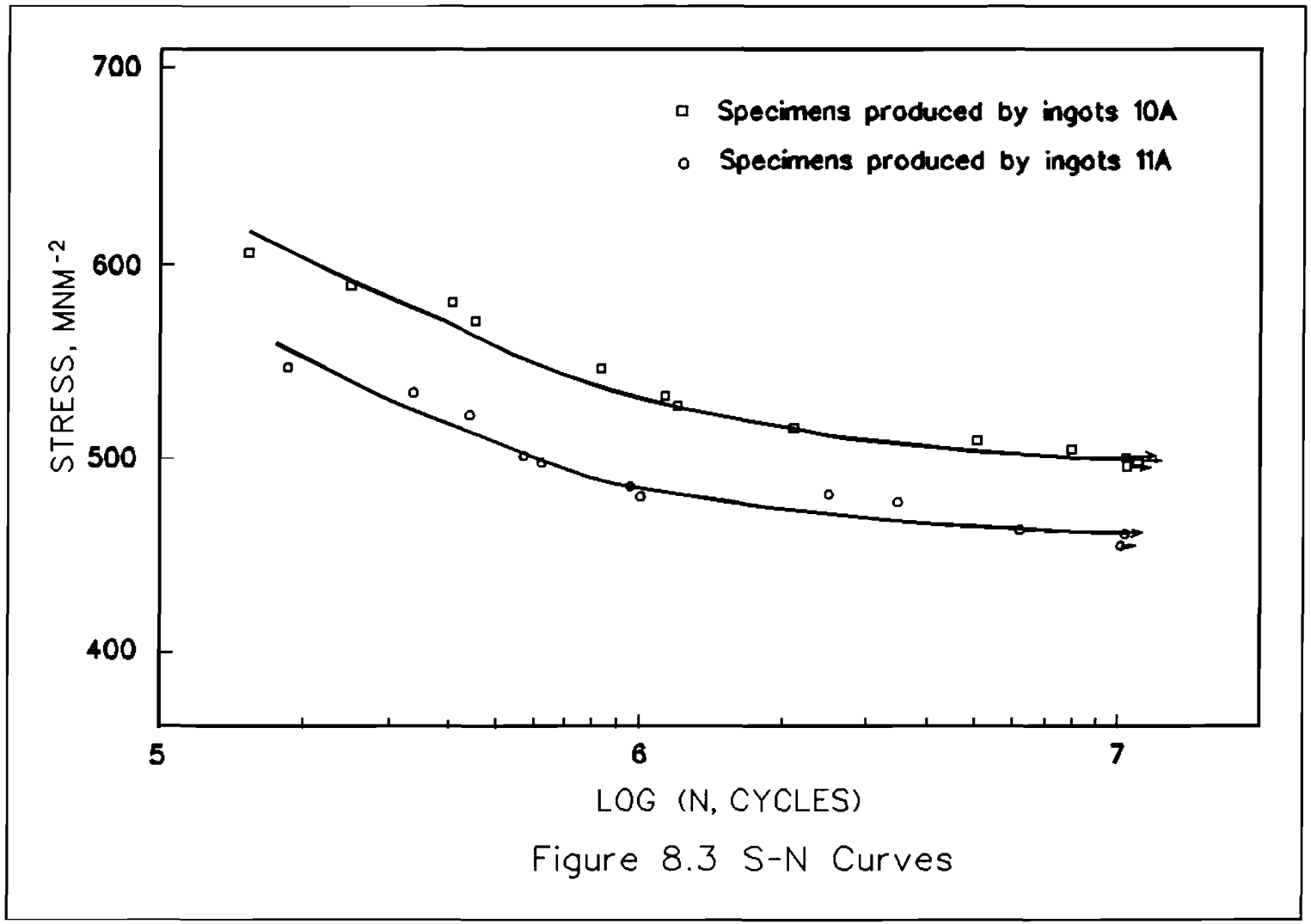

Figure 8.3 S-N Curves

8.3 Results

8.3.1 Fatigue Testing Results

The S-N curves obtained with zero applied mean stress are shown is fig. 8.3 for 4mm diameter nitrided specimens. Larger loads for higher stresses could not be applied due to fatigue test machine limitations, so that only lower stresses and higher cycles were plotted in the curves. The core hardness for all specimens were checked using a Vickers Pyramid Hardness Testing Machine after fatigue testing. Only those specimens with HV 309-317 were used in plotting the S-N curves.

8.3.2 Examination of Fracture Surfaces

Analysis of the fatigue fracture surfaces was carried out using the scanning electron microscope in the Mechanical Engineering Department.

Typical fatigue fracture surfaces for specimens 10A and 11A are shown in Photos 8.3 and 8.4 respectively. It is observed that the fatigue surfaces for both are nearly the same.

Analysis of all fracture surfaces showed that all fatigue cracks initiated from within the core and the fatigue crack zone is approximately circular. The final fracture had fibrous appearance, indicating final failure was by ductile fracture.

8.3.3 The Inclusions Which Caused Fatigue Crack Initiations

The fracture surfaces of all specimens were examined after fatigue testing by the scanning electron microscope and it was found that the fatigue cracks almost always initiated from a single non-metallic inclusion.

The compositions of inclusions which caused fatigue crack initiations in specimens 10A and 11A are shown in table 8.3.

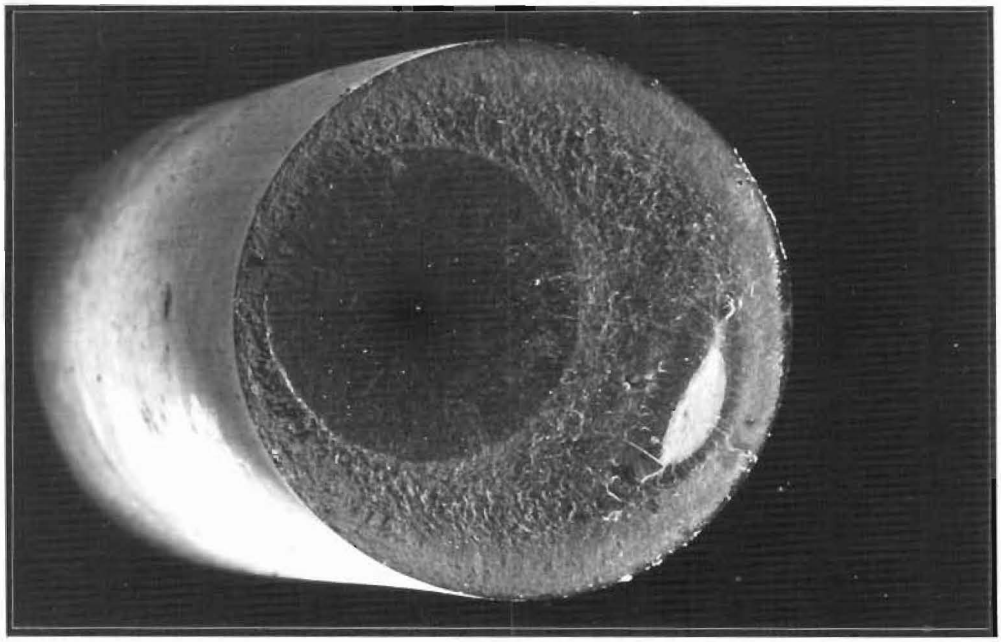

Photo 8.3 Typical fracture surface for specimens 10A. 1mm

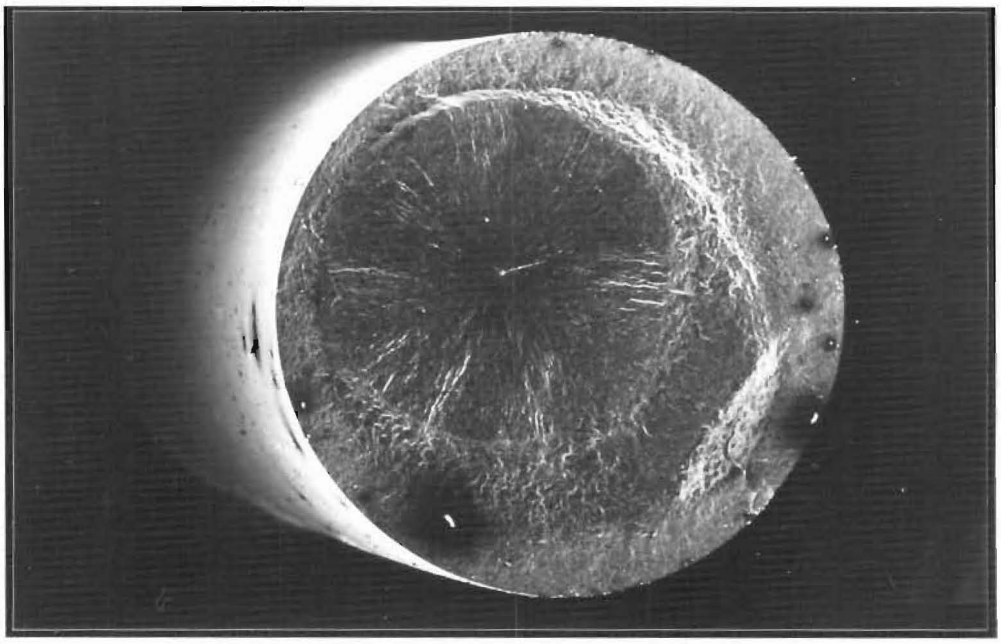

Photo 8.4 Typical fracture surface for specimens 11A. 1mm

Table 8.3 Composition of Inclusions from which fatigue cracks initiated

No.	Inclusion Composition	Remark
10A	Al_2O_3-SiO_2	very common
	Al_2O_3	very common
	Al_2O_3-SiO_2-MgO-MnO	
11A	CaO-Al_2O_3-SiO_2	very common
	CaO-Al_2O_3	very common
	CaO-Al_2O_3-SiO_2-MgO	

The inclusions which caused the fatigue crack initiations in specimens produced from ingots 10A mainly contained Al_2O_3 or Al_2O_3-SiO_2 and some contained a very small amount of MnO and MgO. Since the pure MnO phase is uncommon in steel[10], it probably existed as MnO-Al_2O_3, that is a Galaxite, which is a quite common inclusion type in steel. MgO can either form MgO or MgO-Al_2O_3 in steel. Kiessling[10] shows that Al_2O_3-SiO_2 can not dissolve MgO, therefore, MgO, and MgO in MgO-Al_2O_3, may deposit on the surface of Al_2O_3-SiO_2.

Some crack initiating inclusions which were nearly pure Al_2O_3 were found in the specimens. They formed a string, and each inclusion was angular in shape as shown in photo 8.5.

No sulphide inclusions were found among these inclusions and the sulphur content is almost negligible in the crack initiating inclusions in specimens 10A.

The inclusions which caused fatigue crack initiations in specimens produced from ingot 11A were mainly CaO-Al_2O_3 or CaO-Al_2O_3-SiO_2 type inclusions. A few of them also contained very small amount of MgO and MnO. The above-inclusions were generally larger than those which initiated cracks in specimens from ingots 10A and were of spherical shape, see photo 8.6. It was observed that most initiating inclusions debonded from the matrix, and some were also damaged, which is also shown in photo 8.6.

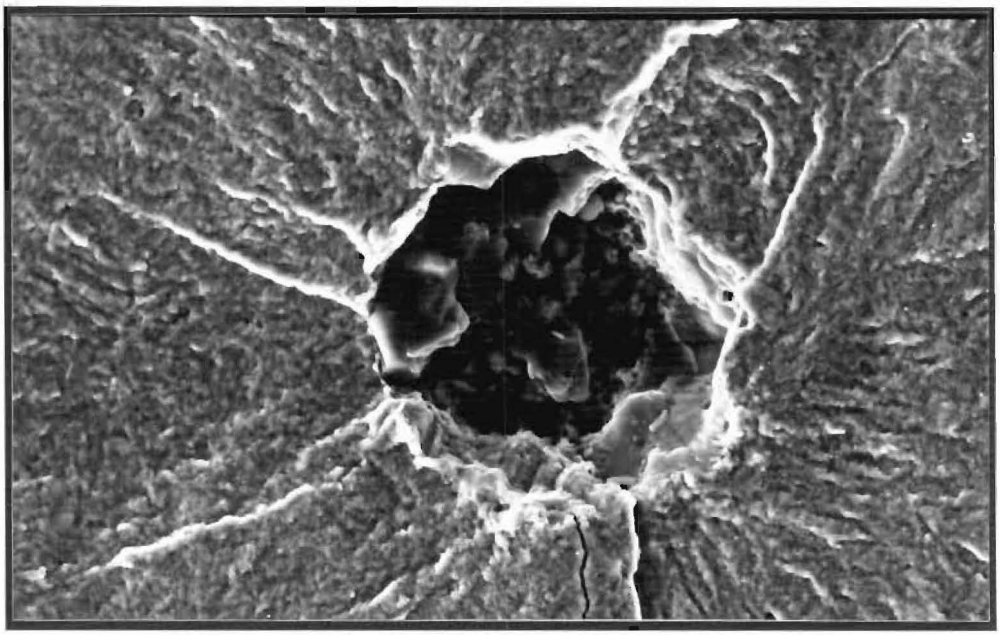

Photo 8.5 Typical initiating inclusion in 10A. 10μm

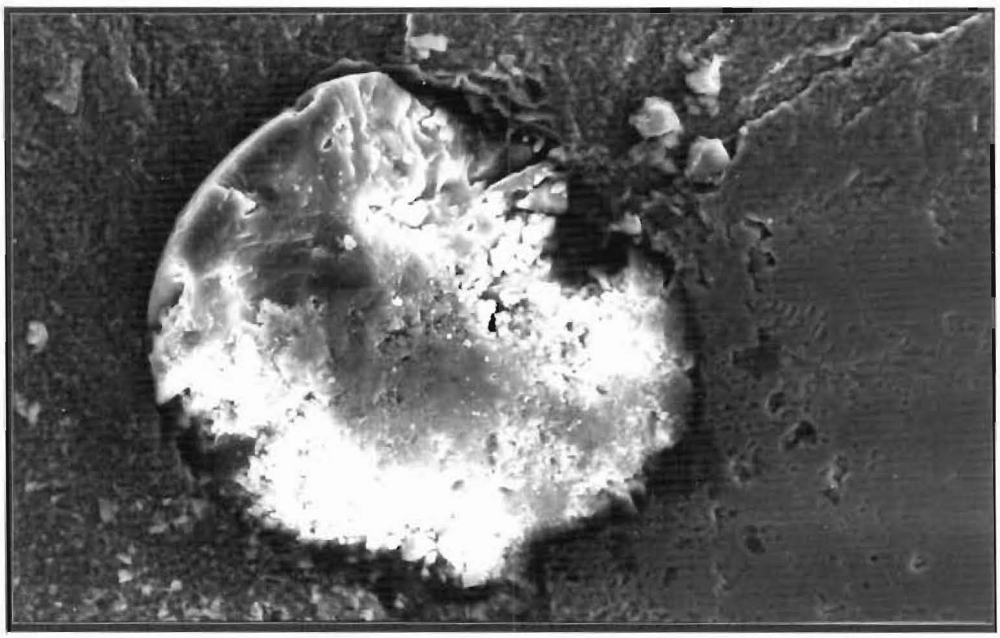

Photo 8.6 Typical initiating inclusion in 11A. 10μm

No inclusions with a peripheral sulphide layer were found to have caused fatigue crack initiation although a few initiating inclusions in specimens 11A contained a very small amount of sulphur.

The size distribution of initiating inclusions in 10A and 11A is shown in fig.8.4. It is observed that the size of initiating inclusions in 11A is significantly larger on average than in 10A. Mean sizes and standard deviations for initiating inclusions in 10A and 11A are 46.1μm, 13.6μm and 59.6μm, 12.8μm respectively.

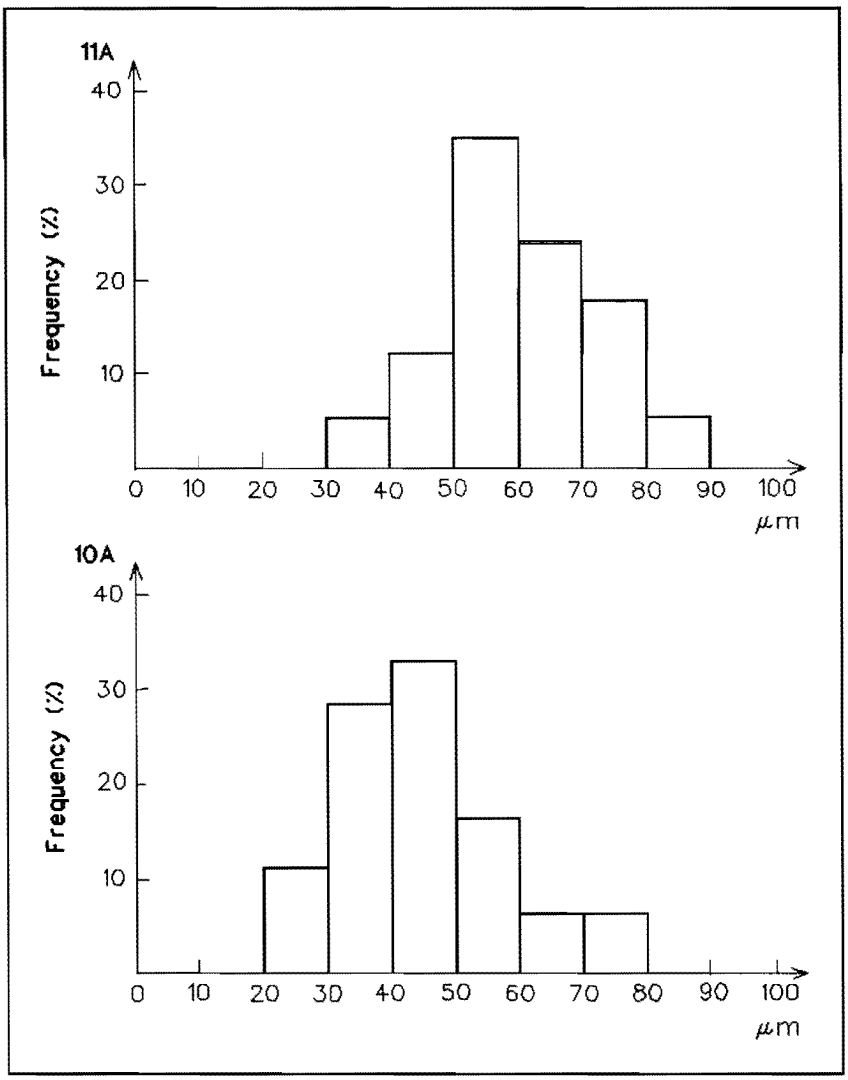

Figure 8.4 Frequency distribution of inclusion sizes for fatigue crack initiations in samples 10A and 11A

Analysis showed that some initiating inclusions in both types of specimens contained a very small amount of MgO. Since no MgO was added into the melts during steelmaking, MgO in the inclusions must have come from the refractory material, which is rich in MgO.

CHAPTER 9

Discussion

9.1 Influence of Melt Temperature on Calcium Injection Yield

Calcium injection yield is usually very low in the steelmaking process, especially in small furnaces. One effective method of increasing calcium injection yield in full scale practice is to inject the calcium alloy deeply into the melt, but this is impossible to realize in a small furnace.

Since desulphurization and modification of non-metallic inclusions are dominated by calcium, it is very important to investigate how calcium injection yield can be improved so that more calcium is used to modify non-metallic inclusions in the melt, rather than being lost by vaporization.

Several methods of adding CaSi were investigated in the small furnace, namely: (1) The use of different cored wire sheaths; (2) various calcium contents in CaSi were used; (3) the addition of CaSi at different temperatures.

No obvious effect on calcium injection yield of using different cored wire sheaths was observed, and the reaction between calcium and liquid steel was equally violent when CaSi cored wire with a thick or thin sheath was added into the melt.

It was also observed that, compared with adding CaSi with a low calcium content, the reaction between CaSi and molten steel was more violent when CaSi with a high calcium content was added into the liquid steel.

Addition of CaSi cored wire at different temperatures was investigated, and it was found that addition of CaSi at a lower temperature was favourable to

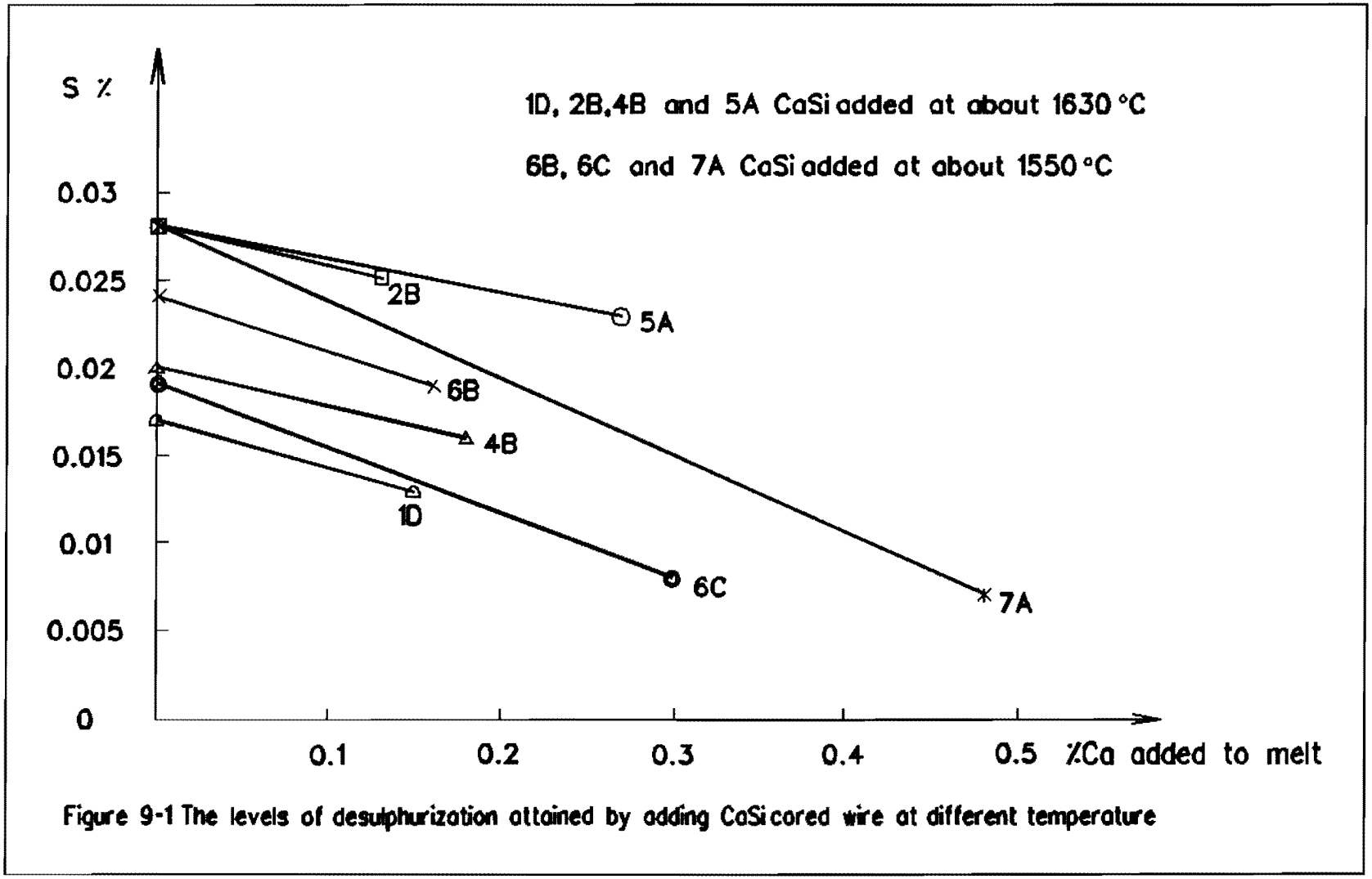

Figure 9-1 The levels of desulphurization attained by adding CaSi cored wire at different temperature

calcium injection yield in small furnaces, and it was also observed that the reaction with liquid steel was less violent, when CaSi cored wire was added into the melt at lower temperature than at higher temperature.

Because Pacific Steel was unable to analyze calcium in any samples, it is impossible to know directly which melt had the higher calcium injection yield according to the chemical compositions. However since the level of desulphurization in steel is mainly controlled by calcium added in the melt, the sulphur content in the samples can probably be used to estimate qualitatively the level of calcium injection yield. The levels of desulphurization attained by adding CaSi cored wire in some melts at different temperatures are graphed in figure 9.1. Calcium solubility is very low in liquid steel, and the very small amount calcium which diffuses into the liquid steel is almost instantaneously consumed by reaction with sulphur and non-metallic inclusions[56]. Plant data[31] also indicated that negligible calcium remains in liquid steel, after the addition of calcium is made. It is therefore supposed that the calcium content in liquid steel is zero before each addition of CaSi cored wire, although a very small amount calcium is present in the inclusions.

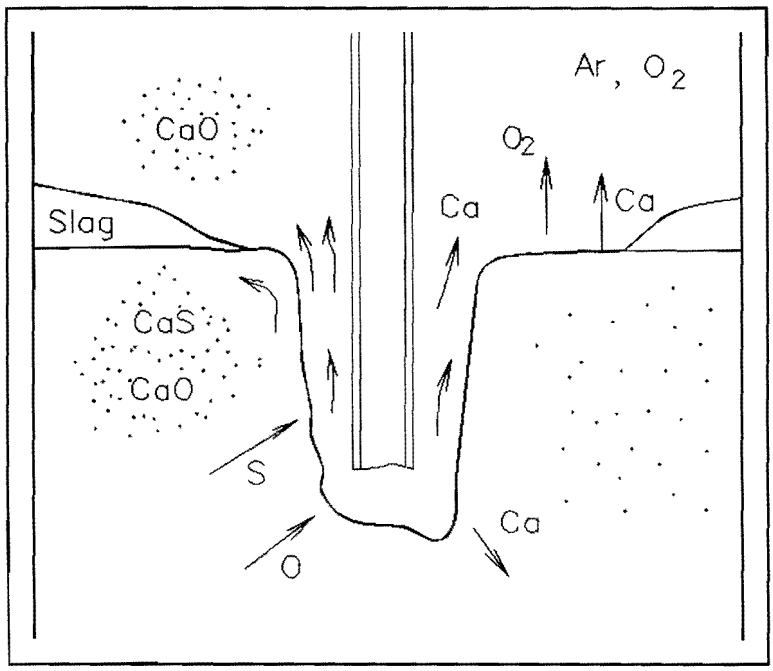

Figure 9.2 Calcium reaction mechanism in small furnace.

According to the calcium reaction mechanism for a small furnace proposed by Lu, et al[56] (whose diagram is presented as figure 9.2), a small amount of calcium will dissolve through the cavity interface (see fig.9.2) into the liquid steel, and only this calcium can be used to desulphurize and deoxidize, or modify non-metallic inclusions. Consequently, most of the calcium escapes into the freeboard region.

In the experiments, [O] content was thought to be very low in all melts except No.3 melt, because aluminium was added as a deoxidizer before adding CaSi. Thus it is considered that dissolved calcium in the liquid steel was mainly consumed in reaction with sulphur. Lu et al[56], when studying the relationship between calcium feed rate and the rate constant for calcium absorption, elimination and desulphurization, found that rate constants for calcium absorption and desulphurization are nearly equal, which is shown in figure 9.3. Thus, if the oxygen activity in liquid steel is low, calcium injection yield is proportional to E, where E can be expressed as

$$E=\frac{\%S-\%S_{initial}}{\%Ca_{added}} \qquad (9-1)$$

where E is level of desulphurization per unit weight of calcium added.

In figure 9.1, since E is higher when CaSi is added at lower temperature, calcium injection yield is thought to be higher at lower temperature.

This is probably attributable to the change of calcium vapour pressure with temperature. One of the main influences on calcium yield is calcium vapour pressure, and lower calcium vapour pressure is favourable to increased calcium injection yield in the steelmaking process.

The plot of vapour pressure for pure calcium versus temperature is shown in figure 9.4[103]. This indicates that calcium vapour pressure decreases with decreasing temperature. Calcium vapour pressure is approximately between 1.4 and 2.3 atmospheres at temperatures between 1550 and 1650^{O}C. At 1550^{O}C, the vapour pressure for pure calcium is about 1.4 atmosphere and the vaporization of calcium may be suppressed by the hydrostatic head at about 0.55 meter below

the liquid steel surface. On the other hand, it is reported[55] that the combination of calcium with silicon produces a lower vapour pressure than that of calcium alone in the liquid steel. Although data of vapour pressure of calcium combined with silicon has not been reported so far, its vapour pressure is at least less than 1.4 atmosphere at 1550°C.

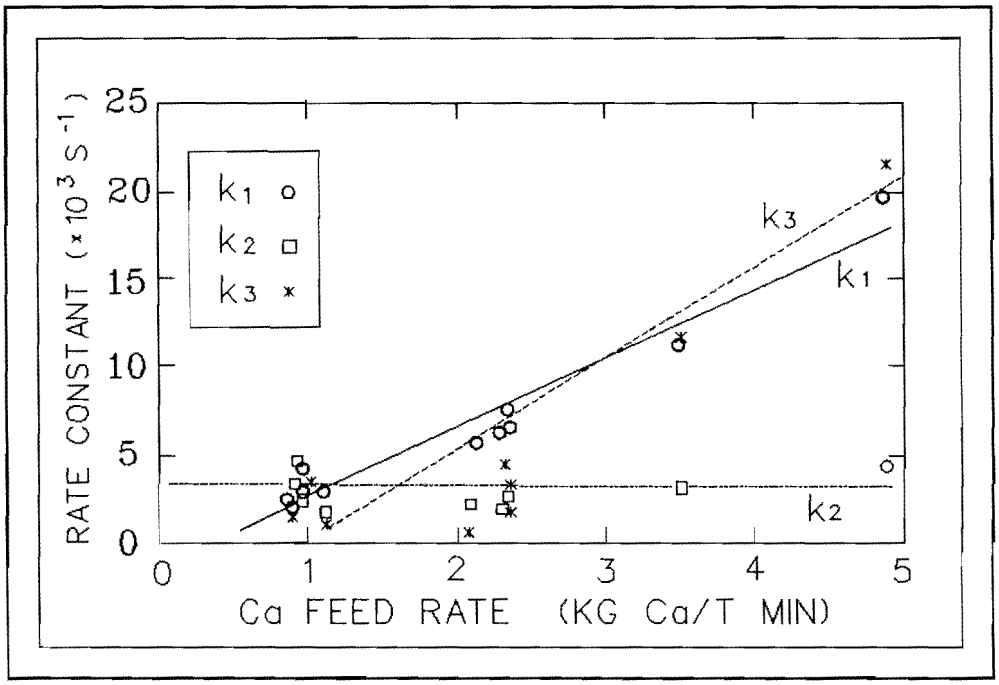

Figure 9.3 The apparent rate constants for calcium absorption, K_1, and calcium elimination, K_2, and desulphurization, K_3, as a function of the calcium feed rate.

It is considered that the vaporization of calcium at 1550°C can probably be suppressed by the hydrostatic head at the bottom of a small furnace. It was observed that the reaction was relatively gentle during CaSi cored wire injection at 1550°C in these experiments, which indicated that the vapour pressure of calcium combined with silicon at 1550°C is not high (near the ambient pressure).

Thus calcium injection yield can be improved at lower injection temperature rather than at higher temperature, and desulphurization and modification of non-metallic inclusions by adding CaSi at about 1550°C are more effectively achieved in a small furnace.

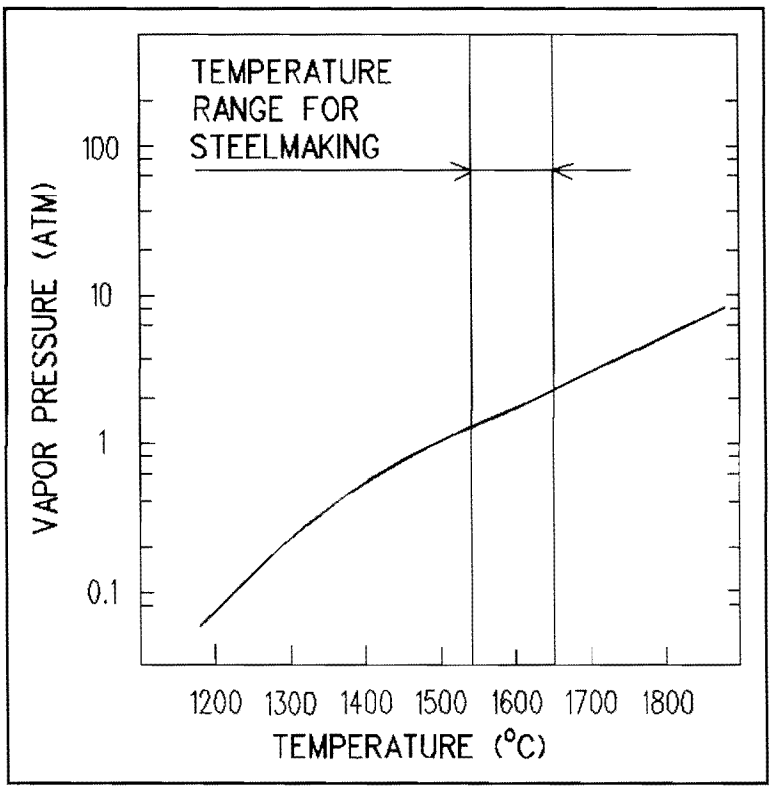

Figure 9.4 Vapour pressure of pure calcium

9.2 Desulphurization by Al_2O_3-CaO-SiO_2 System Slag

Desulphurization by Al_2O_3-CaO-SiO_2 basic slag was investigated in No.3 and No.4 melts. The sulphur content in 4A was 0.02%, see table 7.1, and if the initial sulphur content in the stock was 0.028% (the initial sulphur content was not measured, and the above-data is according to previous melt results). The basic slag Al_2O_3-CaO-SiO_2, removed 0.008%S. The slag melted slowly, and the reaction between liquid steel and slag lasted only about 20 min, as described in Chapter 6.

The general form of the desulphurizing equation is

$$(O^{-2}) + [S] \rightleftharpoons (S^{-2}) + [O] \qquad (9\text{-}2)$$

and a common way of expressing the sulphur capacity C'_s of a slag is

$$C'_s = a_{[o]}(\%S)/[\%S] \qquad (9\text{-}3)$$

Sulphide capacities in the CaO-Al_2O_3-SiO_2 system at 1650°C are shown in

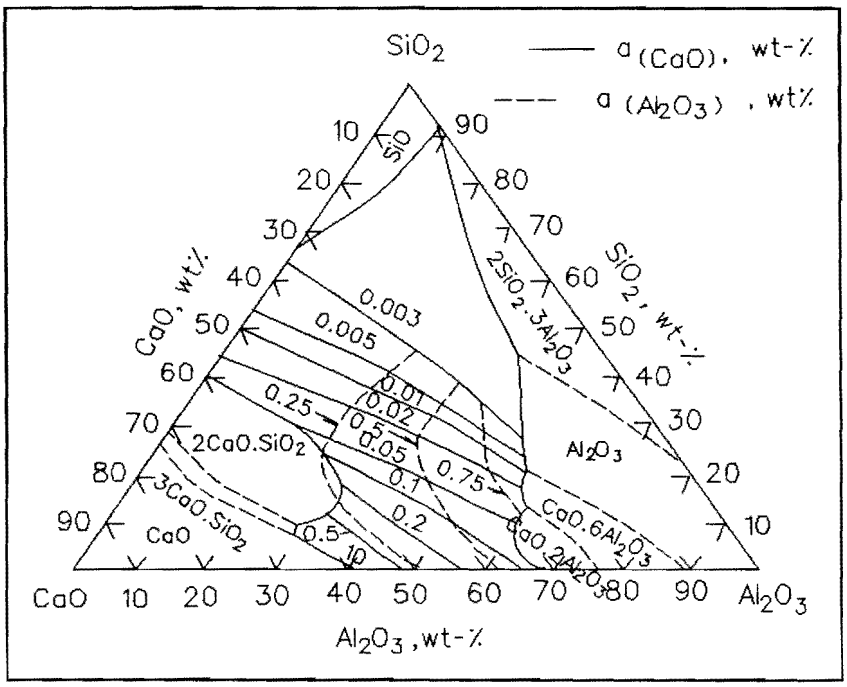

Figure 9.5 Activities of CaO a(CaO) and Al_2O_3 a(Al_2O_3) in Al_2O_3-CaO-SiO_2 system at 1600°C; activities in wt-%.

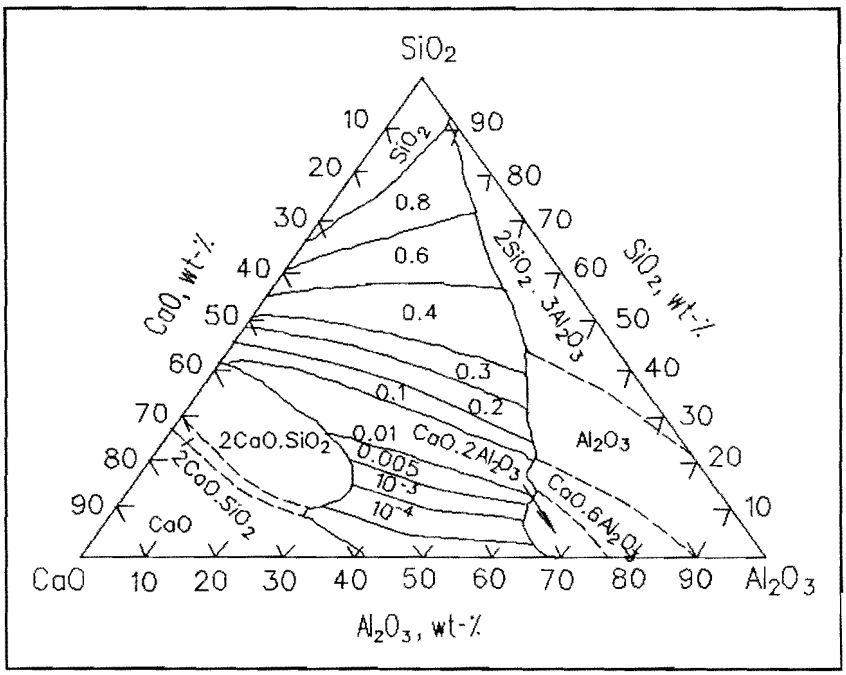

Figure 9.6 Activity of SiO_2 a(SiO_2) in Al_2O_3-CaO-SiO_2 system at 1600°C; a(SiO_2) values in wt-%.

fig.3.1. It is indicated, from equation (9-3), that for a given sulphide, the sulphur partition coefficient $L_s = (\%S)/[\%S]$ depends critically on the level of deoxidation of the liquid steel. In No.4 melt, some aluminium was added into the melt before the addition of materials slagged in order to decreased [O] activity. So [O] activity in the melt was probably very low, but was not measured.

Activities of $CaO_{a(CaO)}$ and $Al_2O_{3a(Al_2O_3)}$, and $SiO_{2a(SiO_2)}$ in Al_2O_3-CaO-SiO_2 ternary phase-diagrams are shown in fig 9-5 and 9-6[31] respectively, and it is evident that, if the activities of both alumina and silica are lower, higher capacities can be obtained.

In No.4 melt, the starting chemical composition of the slag is shown in table 6.6. Since both Al_2O_3 and SiO_2 contents are lower, the sulphide capacity of this slag should be higher. A small amount of MgO was added in this experiment in order to increase slag fluidity. Also the iron oxide content of the added slag was known to be very low.

The strong stirring caused by electromagnetic induction can improve slag-metal mixing, which is another prerequisite for effective desulphurization by Al_2O_3-CaO-SiO_2 slag. It was observed that the bath was stirred very intensely in the experiment, and it is supposed that good slag and metal mixing was achieved in No.4 melt.

Thus it is thought that desulphurization by Al_2O_3-CaO-SiO_2 basic slag is very effective in a small induction furnace, and very low sulphur content can be obtained, if the slag is completely melted and the holding time was more that 20 min. (Since the lining of the induction furnace was broken just before No.3 and No.4 melts, holding time after adding CaO, Al_2O_3, SiO_2 and MgO at 1650°C was limited to 20 min to prevent lining damage again).

9.3 Effect of Inclusions in Calcium Treated Steel on Fatigue Properties.

It is known that the level of detrimental effect of non-metallic inclusions on the fatigue properties of steels varies according to the types of inclusions.

Inclusions modified by calcium were reviewed in Chapter 3. According to the results of the experiments, Al_2O_3 inclusions will be first modified to calcium

aluminate or calcium alumina silicate inclusions after CaSi is added to the liquid steel. It was shown that most of alumina inclusions were modified to calcium aluminate by adding a small amount of CaSi, whereas some MnS inclusions still remained in the steel, see samples 1B, 4B and 6C in table 7.2. Another investigation[101] on the influence of calcium in modification of inclusions indicated that relatively low levels of calcium are needed for efficient alumina modification and figure 9.7 shows, that if the aluminium content is relatively low in liquid steel, only a small amount of calcium is required to modify alumina inclusions to globular calcium aluminate inclusions[85].

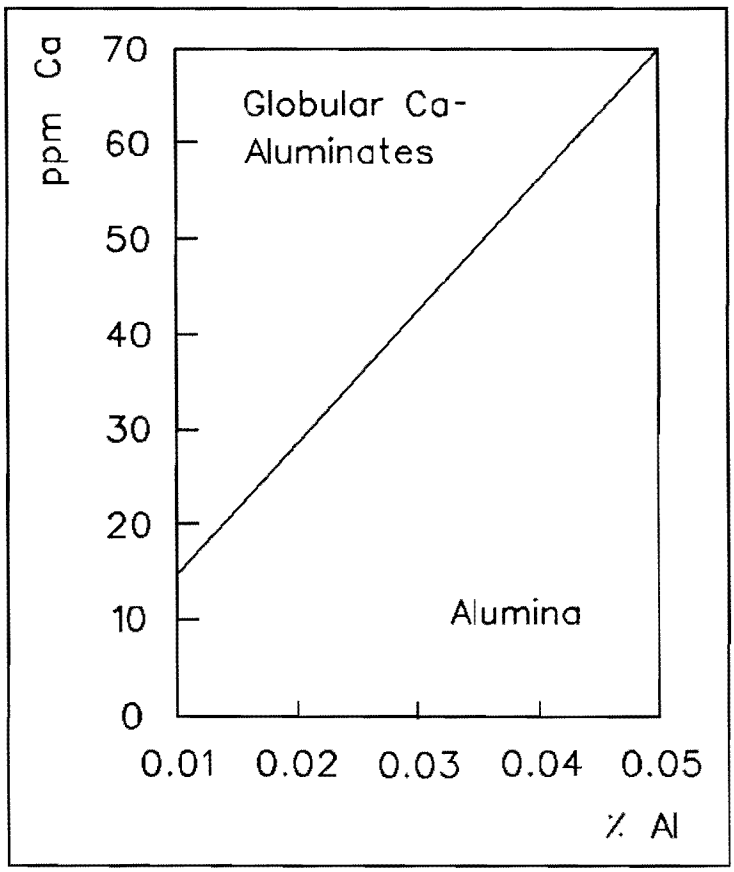

Figure 9.7 Influence of calcium on the composition of the inclusions.

Calcium aluminate inclusions remaining in liquid steel can form either duplex oxysulphide or remain as $xCaO.yAl_2O_3$ until solidification of the steel, although most of them will be removed from the liquid steel. Some duplex oxysulphide inclusions were found in ingots 11A, see figure 7.5 and 7.6. This indicates that some calcium aluminate inclusions in 11A were further modified to duplex oxysulphide inclusions. Also some calcium aluminate and calcium aluminium silicate inclusions still remained in the steel.

Analysis by the scanning electron microscope with energy dispersive X-ray analysis showed that all the inclusions which caused fatigue crack initiations in 11A were calcium aluminate and calcium alumina silicate inclusions. A typical inclusion which initiated fatigue cracking in 11A is shown in photo 9.1 and its composition was mainly calcium, aluminium and a small amount of silicon. It was observed that the inclusion was large (about 81μm diameter), debonded from the matrix and damaged. A small inclusion (about 5μm diameter) near the initiation area in the photo is also a globular calcium aluminate inclusion. It is considered that fatigue cracks often initiated from this type of inclusion because some of them are large and they have a low expansion coefficient which cause very deleterious tensile tessellated stresses around them.

Thus it is thought that calcium aluminate inclusions have a very deleterious influence on fatigue properties, and fatigue crack initiation is very often associated with this type of inclusion.

Analysis shows that most inclusion diameters which caused fatigue crack initiations in 11A are between 50-80 μm. This probably indicates that calcium aluminate inclusion easily undergo coalescence.

According to Stokes' law, the floating velocity of an inclusion should be as follows:

$$\upsilon = \frac{2}{9}\frac{gr^2}{\eta}(\rho_m - \rho_s) \qquad (9-4)$$

where, $\rho_m = 7.1\ g \cdot cm^{-3}$, $\rho_s = 3.02\ g \cdot cm^{-3}$[10] (since it is difficult to determine

the exact composition of calcium aluminate inclusion, a mean ρ_s for $CaO\text{-}Al_2O_3$ is used), gravitational constant g of 980 $cm \cdot s^{-2}$ and a liquid steel viscosity η of 0.065 poise at 1550°C[97].

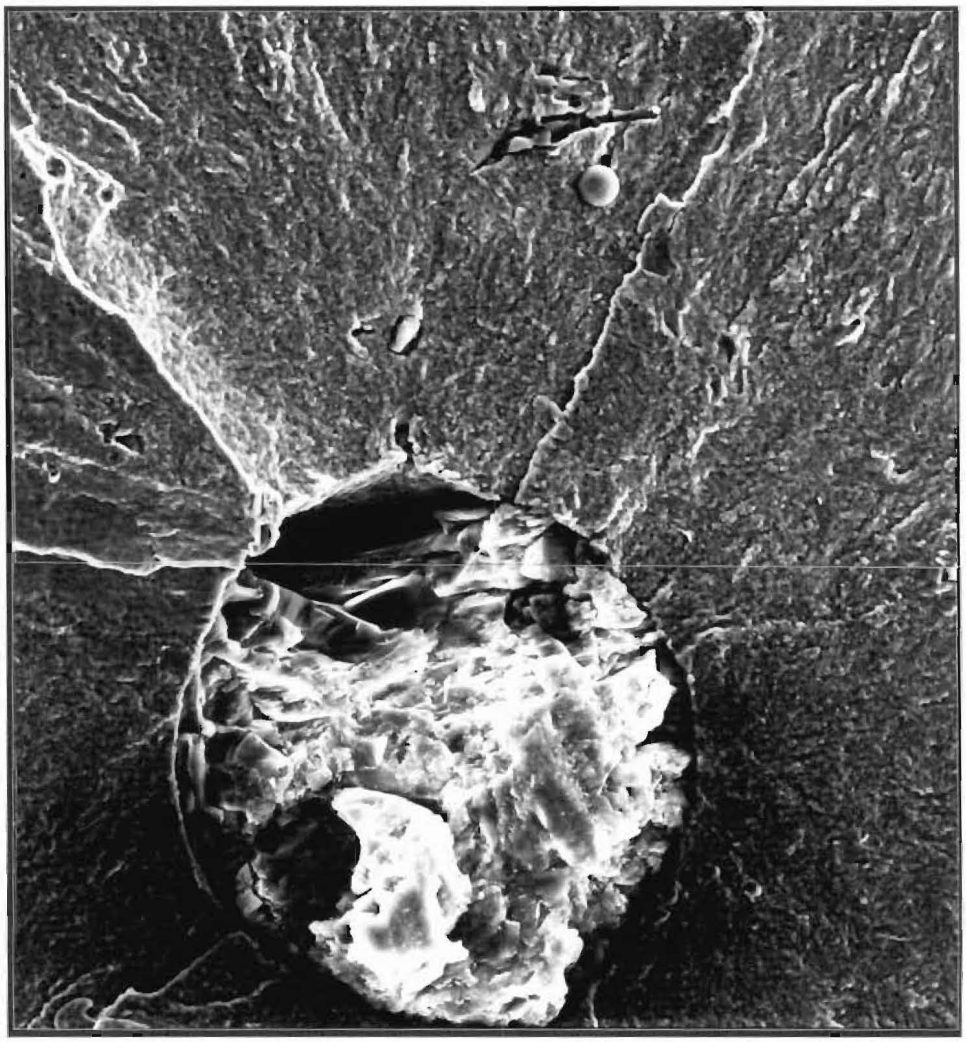

Photo 9.1 Typical calcium aluminate inclusion which initiated fatigue crack in 11A. 10μm

The floating velocity of an inclusion of 50 μm diameter is about 0.855 $cm \cdot s^{-1}$ according to equation (9-3).

Since the depth of the melt in the experiments is only about 15 cm, inclusions of this size should not exist in the liquid steel, if Stokes' law is strictly valid. However, most of the inclusions which caused fatigue crack initiation in ingot 11A are about 50 μm diameter, and some even more than 50 μm, indicating that the floating velocity of an inclusion doesn't strictly obey Stokes' low, and some other factors affect the floating of inclusions.

On the other hand, since the experiments were carried out using the induction furnace, the floating-up rate of inclusions should be increased, due to bath-stirring[40,95].

Some researchers[41,94] have shown that the rate of elimination for inclusions of different types is different. For example alumina inclusions easily precipitate in the bath and float out quickly from the melt[99,100].

Since some types of calcium aluminate inclusions are in the liquid state at steelmaking temperature, these inclusions can easily coalesce and grow to form large particles. The influence on inclusion size of different Al_2O_3:CaO ratios is shown in figure 9.8[104]. It indicates that particle size decreases with increasing Al_2O_3:CaO ratio in the calcium aluminates. A report by Tivelius[23] shows a similar result. It can be assumed that most of this type of inclusion is removed, but some large inclusions are still entrapped in the steel. The reason why large inclusions remain in the liquid steel is not known at present. Maybe they could have been late-forming reaction products which had not had a chance to escape from the steel before becoming entrapped at the rapidly-advancing ingot solidification front.

Since no duplex oxysulphide inclusions were found among inclusions which caused fatigue cracks, according to analysis (although they exist in 11A), it is inferred that this type of inclusion is less detrimental to fatigue properties of steel than calcium aluminate alone.

Analysis shows that only a few inclusions, which initiated fatigue cracks in specimens 11A, contained a very small amount of sulphur, although many oxysulphide inclusions in which calcium sulphide was intermixed were found in specimens 11A. This probably indicates that the detrimental effect caused by the inclusions on the fatigue properties of steel are decreased if the inclusions

contain a certain amount of sulphur.

The inclusions which initiated the fatigue cracks in 10A were mainly alumina, which were usually of small size. Alumina has a higher thermal expansion coefficient than calcium aluminate. Thus alumina inclusions are probably less harmful to fatigue properties than calcium aluminate inclusions.

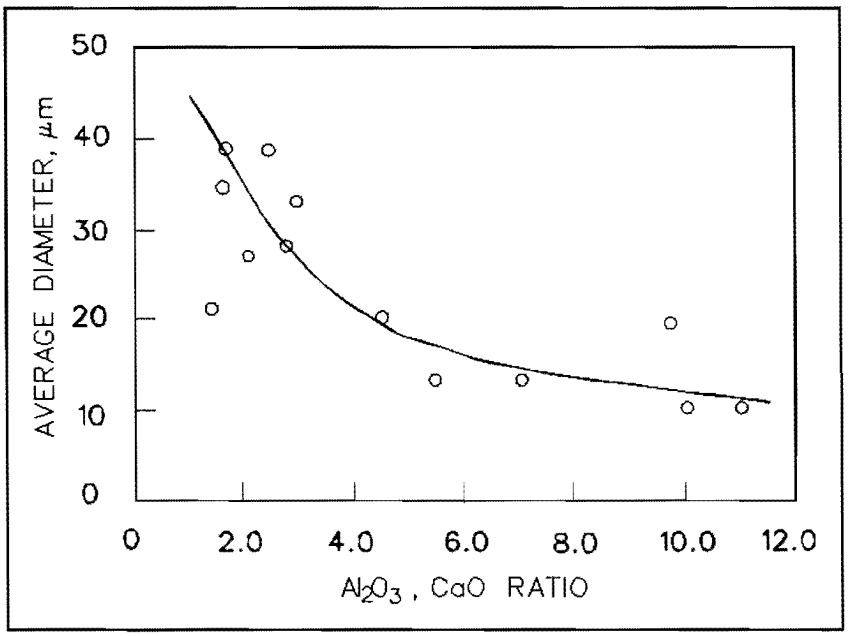

Figure 9.8 Relationship between size and Al_2O_3:CaO ratio of calcium aluminates.

According to the results, it can be considered that since large calcium aluminate or calcium alumina silicate inclusions were present in cast 11A, the fatigue cracks were more easily initiated from them in 11A than from the alumina inclusions in 10A.

9.4 The Role of Inclusions in Fatigue Crack Initiation

Since a high strength case with an associated compressive residual stress is obtained by nitriding, all fatigue cracks are initiated from the subsurface, whereas fatigue cracks in steel without case hardening are almost always initiated at the surface[3,4,81,82].

Analysis by the scanning electron microscope showed that nearly all fatigue cracks in specimens 10A and 11A initiated from inclusions in the core. Further analysis indicated that fatigue crack initiation in 11A always occurred at single inclusions and in 10A mainly occurred at single alumina inclusions for lifetimes of more than 5×10^5 cycles.

In nitrided steels there is a tensile residual stress acting on the core to balance the compressive residual stress in the case. In addition both calcium aluminate and alumina inclusions are surrounded by tensile tessellated stresses. These factors combine to produce crack initiation from inclusions in the core.

It was observed that all inclusions which caused fatigue crack initiation were debonded from the matrix at the fracture surface, and most of them were fatigue-damaged. Some inclusions were broken into two parts which existed in the separate halves of the specimens. The latter probably indicates that these inclusions were not completely debonded from the surrounding metal matrix, although they were debonded in the equatorial section (normal to the tensile axis).

Non-metallic inclusions in specimens 10A and 11A were analyzed by scanning electron microscope before fatigue testing and the results showed that these inclusions were completely bonded, whether non-metallic inclusions were calcium aluminate in 11A, or alumina in 10A. This indicates that debonding and inclusion damage were not because of forging but occurred as a result of the fatigue.

It can be inferred that since the inclusions were debonded from the matrix by high local stresses the tensile residual stress around them is partly or totally removed. Thus the inclusion behaves like a void, or a notch after it is debonded, and a high stress concentration around the debonded inclusion may cause fatigue crack initiation with further load cycling.

Since most of the inclusions were damaged or broken, it can be inferred that these inclusions have worse fatigue properties than the metal matrix or had undergone brittle fracture. Analysis by scanning electron microscope showed these inclusions were of $CaO\text{-}Al_2O_3$ and $CaO\text{-}Al_2O_3\text{-}SiO_2$ in specimens 11A.

It is considered that a fatigue crack must initiate from the region in which the inclusion and metal matrix are debonded, since all inclusions which caused

fatigue crack initiations were debonded in the fracture surface. In other words, fatigue crack initiation cannot occur in the region in which the inclusion and matrix are firmly bonded. Thus it is thought that the prerequisite for initiating fatigue cracks is that the inclusions are partly or completely debonded from the metal matrix. This is similar to Eid's proposal[82] that the prerequisite for fatigue crack initiation under high-cycle conditions is hole formation caused by progressive debonding.

Some inclusions were not damaged as fatigue cracks initiated from them, see photo 9.2. This indicates that undamaged inclusions can still cause fatigue crack initiation during fatigue service.

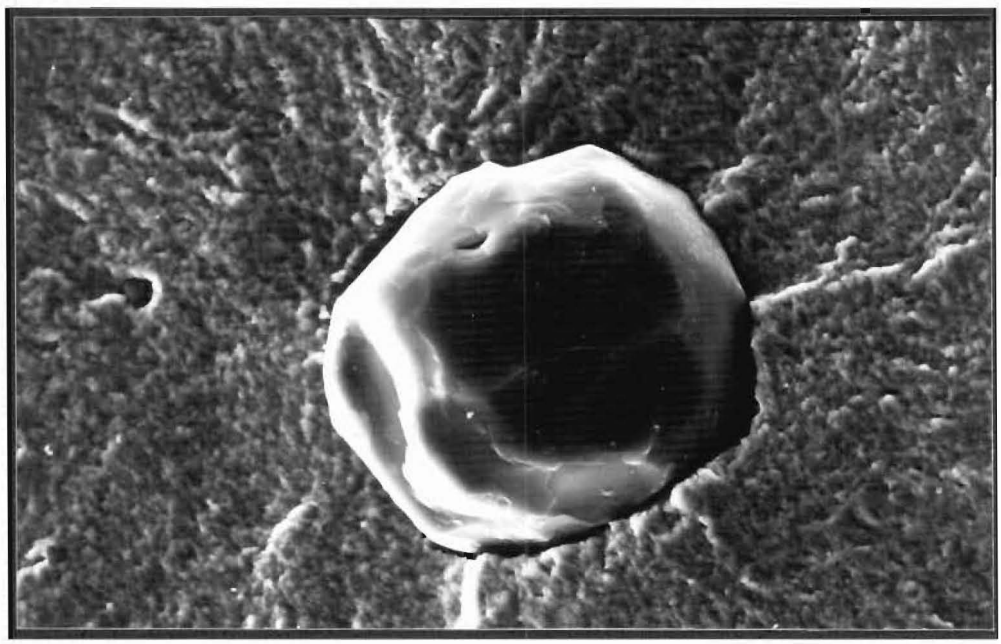

Photo 9.2 an undamaged inclusion which initiated fatigue crack in 11A. 10μm

Thus, it is considered that debonding of an inclusion from its matrix is a very important step although it is difficult to learn the details of crack nucleation at subsurface inclusions and inclusions within the core. Since calcium aluminate inclusions, which have associated high tensile residual stress fields, are present in specimens 11A, it can be inferred that inclusion debonding in specimens 11A

may occur at a lower applied stress amplitude than in specimens 10A. This probably leads to initiation of fatigue cracks at a lower stress amplitude and the observed lower fatigue strength of 11A.

No duplex oxysulphide inclusions or calcium sulphide intermixed with calcium aluminate inclusions were found among those inclusions which caused fatigue crack initiations. This probably indicates that the tendency for inclusions to debond from the matrix is reduced with increasing CaS or (Ca,Mn)S content in the inclusions. In other words, the probability of fatigue crack initiation at these inclusions will be decreased if a certain amount of CaS or (Ca,Mn)S is present in the inclusions.

9.5 Mechanism of Formation of Duplex Oxysulphide Inclusions in Calcium Treated Steel

The mechanism of formation of duplex oxysulphide inclusions is still not clear. Many reports[15,16,31,49,59,65,66,67,68] show that this type of inclusion is found in steel, especially after CaSi-injection. In the experiments, duplex inclusions were found in sample 11A after adding CaSi cored wire, but some large $CaO\text{-}Al_2O_3$, and $CaO\text{-}Al_2O_3\text{-}SiO_2$ inclusions were also present in the steel. These have a very deleterious effect on the fatigue properties of the steel, resulting in even worse fatigue properties of steel than in the case with no CaSi-injection, as shown in figure 8.1. Thus it is very important to know the mechanism of formation of duplex oxysulphide inclusions in liquid steel, if the fatigue properties of steel are to be further improved.

Several ideas about the formation of this type of inclusion were reviewed in Chapter 3. Some studies[21,68] show the oxide inclusions surrounded by CaS being formed during the solidification of steel. Since calcium sulphide is distributed relatively uniformly on the outer surface of calcium aluminate in steel, Takenouchi et al[68] assume that CaS deposited on the surface of oxide inclusions is probably formed by precipitation from within the CaS-containing inclusions.

Some workers [68,71] investigated the solubility of CaS in $CaO-Al_2O_3$, (shown in figure 3.1), and reported that the formation mechanism of peripheral CaS on the oxide surface is one of precipitation of CaS from the $CaO-Al_2O_3$ inclusions due to the solubility drop with reducing temperature.

According to their results, if the inclusion diameter is, for example, 20μm, the outer phase, precipitated by a temperature fall from 1550°C to 1450°C, is about 0.14μm skin of CaS, representing a 3.9% CaS content in $CaO-Al_2O_3$ inclusion before cooling.

However, the micrographs of duplex oxysulphide inclusions in many reports[5,12,13,15,68] show that the CaS-skin in duplex inclusions is not so thin. This probably indicates that the peripheral CaS does not only form by precipitation from within the CaS-containing inclusions. Therefore, it may be inferred that the deposition of small CaS inclusions, which are randomly distributed in liquid steel, and the reaction with sulphide on the surface of oxysulphide inclusion, are indispensable during the formation of duplex oxysulphide inclusions. In other words, it is inferred that the mechanism of formation of duplex oxysulphide inclusions is probably multiple.

Because the level of tensile tessellated stress reduction caused by the CaS outer phase mainly depends on the thickness of the CaS phase, then if the CaS-outer phase is, for example only 0.14μm, the beneficial influence of CaS on the stress-reduction must greatly decrease. The spherical duplex inclusion model is illustrated by figure 9.9[76]. It is thought that the sulphide shell, which has a high thermal expansion coefficient will resist transmission of stress to the matrix, from the oxide inclusion, which has a low thermal expansion coefficient.

Calculations of stress-reduction have been made by Brooksbank et al[76] for this duplex inclusion using the above-model, in which the sulphide forms a separate shell between the oxide and matrix. These indicated that, compared with a 20 μm diameter-$CaO.2Al_2O_3$ inclusion, the stress caused by a duplex oxysulphide inclusion decrease sharply, if a 16μm diameter, $CaO-2Al_2O_3$ inclusion is enveloped by a 2μm thick calcium sulphide shell as shown in figure 9.10. However, if the CaS outer phase is only 0.14μm thick and the inner phase,

$CaO.2Al_2O_3$, is 19.72μm diameter, calculation shows the stress-reduction caused by such a thin CaS case is very small , and may be almost neglected, as shown in figure 9.10 also(Calculation equation is shown in Appendix A.).

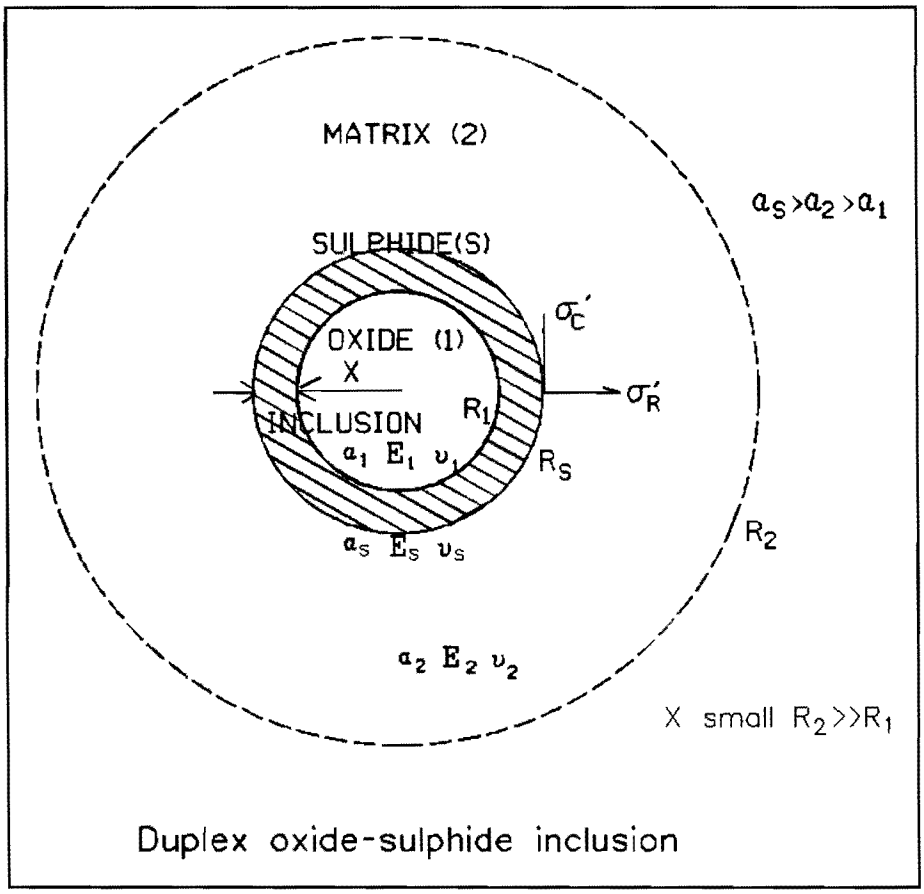

Figure 9.9 The spherical duplex oxysulphide inclusion model.

Therefore, according to the above calculation, the outer-phase, CaS or (Ca,Mn)S, must be sufficiently thick if the effects on fatigue properties of these duplex oxysulphide inclusions are to be less harmful or even harmless.

It can be considered that several factors may influence the formation of duplex oxysulphide inclusions in the liquid steel.

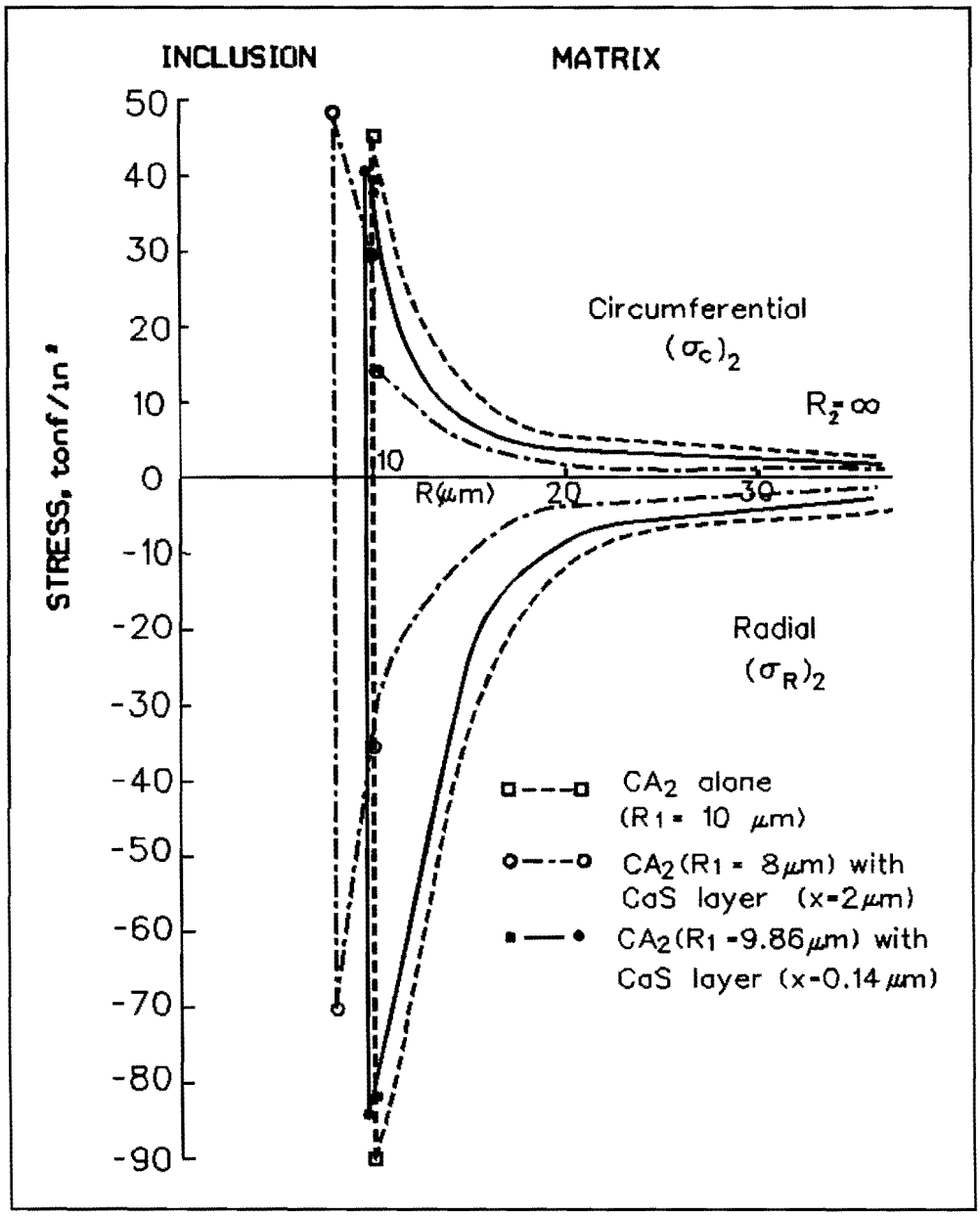

Figure 9.10 Effect of calcium sulphide envelopes on the stress around an inclusion of $CaO \cdot 2Al_2O_3$.

(1) Minute particle of CaS, randomly distributed in the liquid steel, may produce duplex oxysulphide inclusions by absorption on the surface of calcium aluminate inclusions which already exist in the liquid steel.

It is also inferred that some calcium aluminate inclusions which are entrapped

by early solidification may also form with a CaS rim, since some fine CaS particles are absorbed on their surface. However, in contrast to CaS, MnS usually forms during solidification[10,12,65], and, if calcium is absent or is present only in very small amounts in liquid steel, those calcium aluminate inclusions which are entrapped by early solidification may not form with a sulphide rim, since no minute particles of sulphide exist in the liquid steel. Thus duplex oxysulphide may only form during late-solidification in this situation.

(2) A relative low cooling rate is probably favourable to the formation of duplex oxysulphide inclusions, because more time is available for the precipitation of CaS dissolved in the $CaO\text{-}Al_2O_3$ inclusions. For this reason, it can be inferred that duplex oxysulphide inclusions form more easily in full-scale practice than in a small furnace.

In these experiments only 2.5kg or 3.5 kg ingots were cast, so that ingots were cooled very quickly and there was very little time for the precipitation of CaS from within calcium aluminate.

9.6 The deformability of Duplex Oxysulphide Inclusions

It is known that the calcium aluminate inclusions are very hard and undeformable. The results of these experiments also show that the spherical calcium aluminate inclusions in steel retain their shape during forging, see photo 7.6. (Ca,Mn)S is less deformable than MnS, but it can still be deformed in heavy forging.

The benefit of duplex oxysulphide inclusions is that the sulphide rim can reduce "Tessellated" stresses, which are very harmful to the fatigue properties of steel. However, if the thickness of the sulphide rim is reduced, or even totally removed in some places on the inclusion surface, especially in the equatorial region (normal to the forging direction), that is, rim deformation results from rolling or forging, the benefit of tessellated-stress reduction is lost.

It is assumed (1), that the sulphide rim is mainly (Ca,Mn)S, which has some deformability, and ,(2), that the thickness of the duplex inclusion outer layer is small. The deformations of duplex oxysulphide, and completely non-plastic $CaO\text{-}Al_2O_3$ inclusions, before and after rolling or forging, are shown in figure 9.11[92].

Since lengthening of the inclusions occurs mainly because of the interlocking bonds between the inclusions and the matrix, and the different plasticity of the steel and the inclusions tends to break the bonds, the breaking of the bonds will counteract the lengthening of the inclusions.

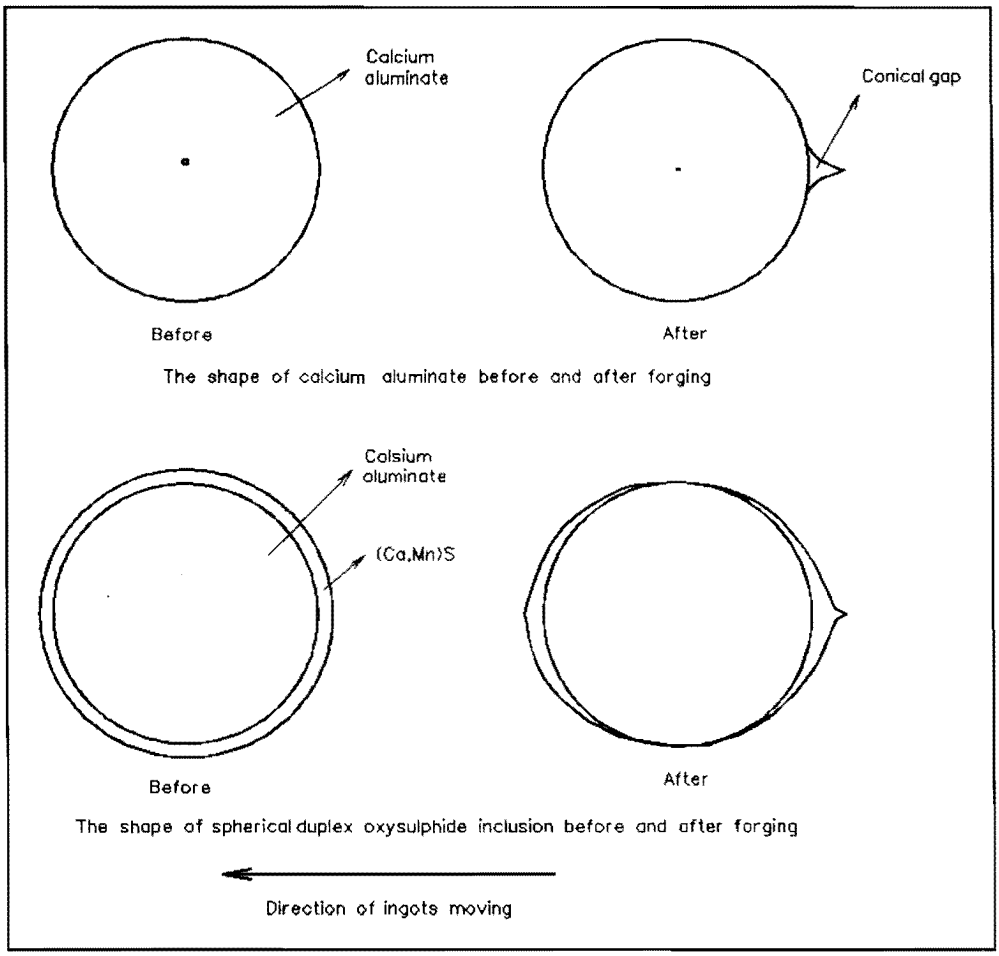

Figure 9.11 Deformation of oxide and duplex oxysulphide inclusion before and after forging

During the deformation of steel containing $CaO\text{-}Al_2O_3$ inclusions, total breaking of the bonds between the inclusion and the matrix takes place, since these inclusions are completely non-plastic. The inclusions retain their original shape, and conical gaps form after heavy rolling or forging.

During heavy forging or rolling of steel containing duplex oxysulphide inclusions, the central $CaO\text{-}Al_2O_3$ phases retains its spherical shape, and outer phase, (Ca,Mn)S may be slightly deformed. It could be inferred that the outer layer of an inclusion might lengthen in the direction of the metal flow, and the conical gap may be filled by this deformable (Ca,Mn)S phases. It is very difficult to determine the level of deformation of outer phases, (Ca,Mn)S, since the deformability of (Ca,Mn)S varies according to the calcium content in the (Ca,Mn)S phase. However, it can inferred that the outer phase, (Ca,Mn)S may lengthen and the thickness of the sulphide rim may be reduced, especially in the equatorial region (normal to forging or rolling direction), when steel is heavily rolled or forged.

Since the sulphide rim in duplex inclusions is not thick, if the thickness of the sulphide rim is further reduced by heavy rolling or forging, the benefit of "tessellated" stress reduction will decrease greatly, as already discussed in 9.5.

No obvious evidence was found in ingots 10A and 11A to show that conical gaps formed around inclusions during the forging. This may be because: (1), ingots 10A and 11A were not very heavily forged; (2), The conical gaps are more likely to form during the rolling rather than during the forging, and (3), although conical gaps form, they may be very narrow and very difficult to detect by a scanning electron microscope.

Some duplex oxysulphide inclusions in sample 11A after forging were analyzed by scanning electron microscope with energy dispersive X-ray analysis and one of them is shown in photo 9.3. Since the inclusion is small, it is very difficult to determine the change of sulphide rim thickness after forging. However, analysis shows that sulphur content was higher in area A than in other areas in photo 9.3. The compositions of area A and area B in photo 9.3 are shown in figure 9.12 and 9.13 respectively. This probably indicates that the sulphide rim was changed by forging, and the lengthened outer layer was concentrated in area A.

Since pure CaS is harder and less deformable than (Ca,Mn)S, if a pure CaS rim forms on the surface of an oxide inclusion, the reduction of sulphide rim thickness caused by forging or rolling may be much less than for (Ca,Mn)S. Thus the beneficial effect of duplex inclusions on reduction of "tessellated" stress may

still be retained after forging.

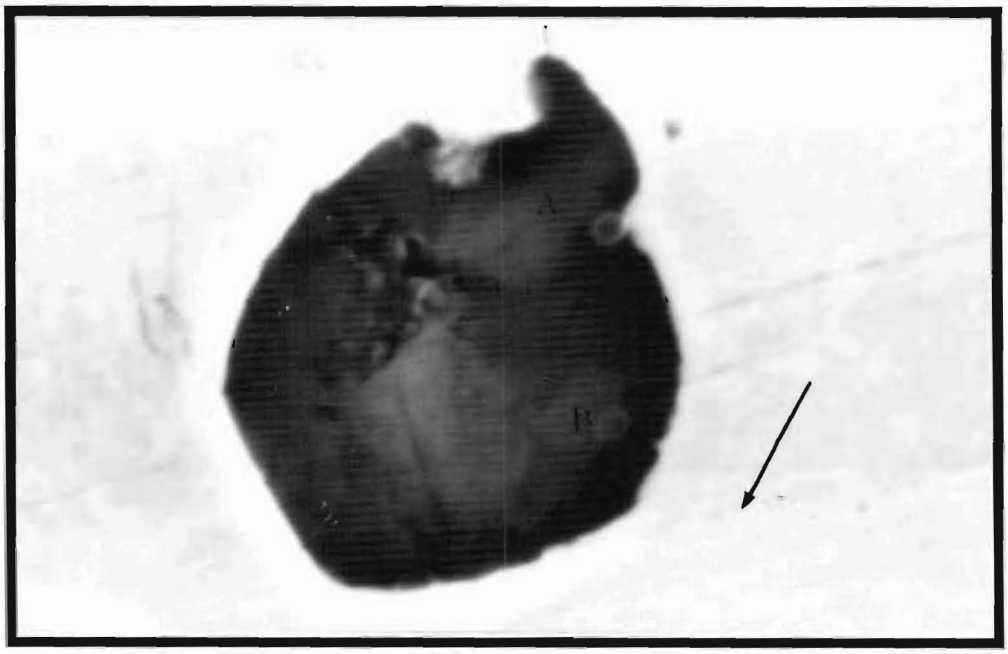

Photo 9.3 A duplex oxysulphide inclusion after forging. 1μm
Arrow shows the direction of forging.

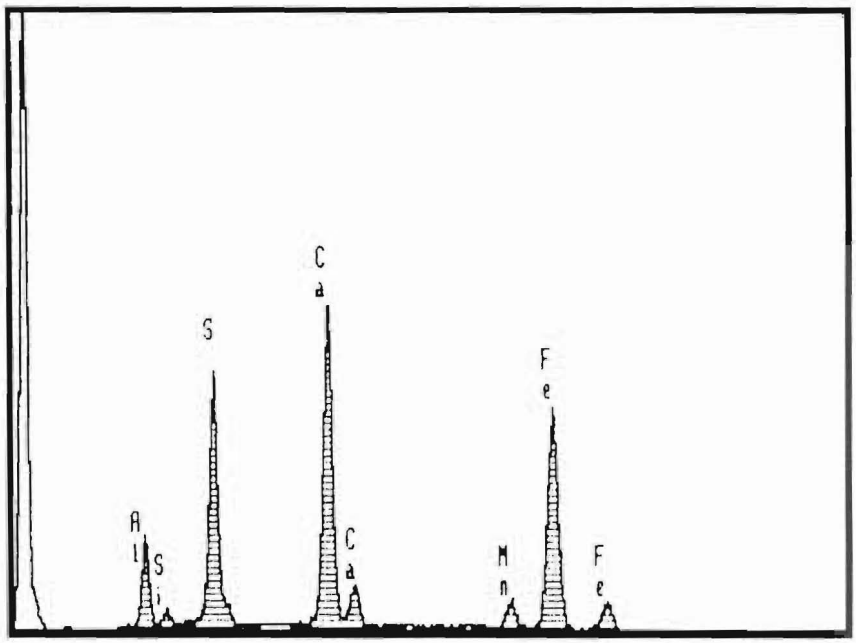

Figure 9.12 Composition of area A of inclusion in photo 9.3.

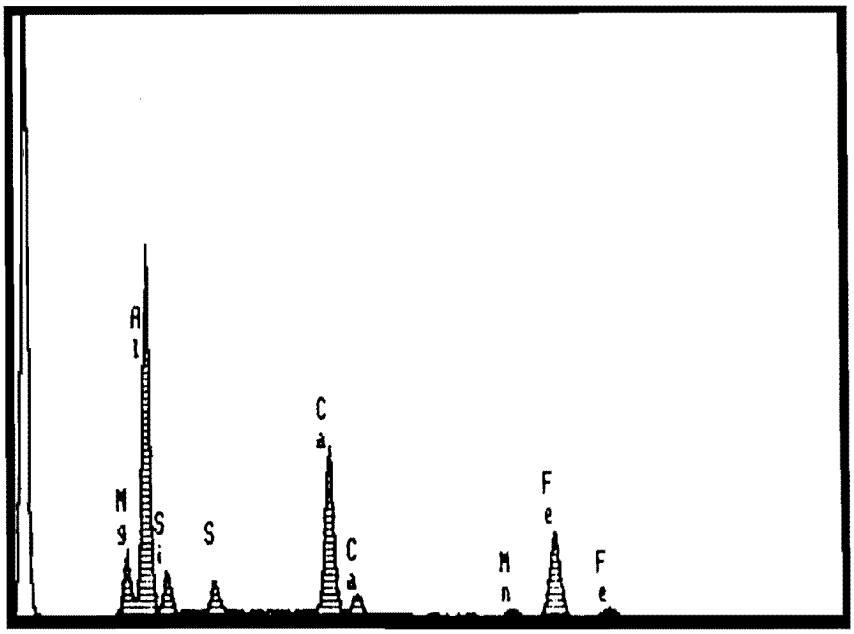

Figure 9.13 Composition of area B of inclusion in photo 9.3.

CHAPTER 10

Conclusions

1. Fatigue properties of nitrided steel can not be improved if calcium aluminate inclusions exist in the steel after CaSi is added, and may even be worsened.

Calcium aluminate and calcium aluminium silicate inclusions have a worse effect on the fatigue properties of steel than alumina inclusions.

It is believed that duplex oxysulphide inclusions are less harmful to fatigue properties of steel than calcium aluminate and/or calcium aluminium silicate alone in steel. It is very interesting to note that all inclusions which initiated fatigue cracks contained no, or negligible sulphur.

The results showed that some duplex oxysulphide inclusions formed in specimens 11A when CaSi was added. However, some calcium aluminate inclusions also remained in the steel, and these probably governed the fatigue properties of the steel whether duplex oxysulphide inclusions were present in the steel or not.

It is considered that calcium aluminate inclusions have a very deleterious influence on the fatigue properties, and fatigue crack initiation is always associated with this type of inclusion if they are present in steel.

It is inferred that the fatigue properties of steel can be improved if all calcium aluminate inclusions, especially large ones, are modified to duplex oxysulphide, or at least oxysulphide inclusions.

2. Fatigue cracks in nitrided steel always initiated from inclusions within the core. For the upper-end of the intermediate-cycle and high-cycle ranges fatigue crack initiation in calcium treated steel always occurred at a single spherical calcium aluminate or calcium aluminium silicate inclusions, and in non-calcium

treated steel mainly occurred at a single alumina inclusion.

The prerequisite for initiating fatigue cracks at the upper-end of the intermediate and high cycle range is that the inclusions are partly or completely debonded from the metal matrix. It was also shown that undamaged inclusions can still produce fatigue crack initiation during service.

3. Calcium injection yield can be improved by a lower injection temperature. Desulphurization and modification of non-metallic inclusions by the addition of CaSi at about 1550°C are effectively achieved in a small furnace.

THE LIBRARY
UNIVERSITY OF CANTERBURY
CHRISTCHURCH, N.Z.

References

[1] I.Jenkins; "Controlled Atmospheres for the Heat Treatment of Metal", London, 1946.

[2] A.Fry; "JISI", Vol.125, (1), 1932, pp191-212.

[3] J.M.Cowling and J.W.Martin; "Heat treatment '79'", Birmihgham, 22-24 May, 1979, The Metals Society/American Society for Metals.

[4] J.M.Cowling and J.W.Martin; "Metals Technology", August 1981, pp289-296.

[5] V.A.Tipnis, R.A.Joseph and J.H.Doubrava; "Metals Engineering Quarterly"; Vol.13,No.4,1973,pp39-47.

[6] R.F.Johnson and J.F.Sewell; "JISI", Vol.194, 1960, pp414-444.

[7] S.Enekes; "Production and Application of Clean Steels", Proc. Conf., pp215-220, June 1970, Balatonfured, Hungary.

[8] R.Kiessling; "Non-Metallic Inclusions in Steel", The Institute of Metal, London, 1989.

[9] R.Tricot; "Production And Application of Clean Steels", Proc. Conf., pp199-204, June 1970, Balatonfured, Hungary.

[10] R.Kiessling; "Non-Metallic Inclusions in Steel", The Metal Society, London, 1978.

[11] L.E.K.Holappa; "International Metals Reviews", 1982, vol.27 No.2, pp53-76.

[12] F.B.Pickering; "Inclusions", The Institute of Metallurgists, 1979, pp29-46.

[13] L.Tolnay, G. Karoly and P.Tardy; "Clean Steels", Proc. Conf., pp296-302, June 1986, Hungary.

[14] R.Kiessling; "Sulphide Inclusions in Steel", Proc. Int. Symposium, 7-8 Nov.1974, pp104-122.

[15] S.K.Saxena; "Ironmaking and Steelmaking", 1982, vol.19, No.2, pp50-57.

[16] S.K.Saxena; "Swedish Symposium on Non-Metallic Inclusions in Steel", pp69-90, 27-29, April 1981.

[17] J.R.Hiam; "Sulphide Inclusions in Steel", Proc. Int. Symposium", 7-8 Nov. 1974, pp212-229.

[18] W.J.MCG. Tegart and A.Gttins; "Suphide Inclusions in Steel", Proc. Int. Symposium", 7-8 Nov. 1074, pp198-211.

[19] P.Dewsnap; "Iron and Steelmaker", August 1982, pp15-17.

[20] R.E.Lismer and F.B.Pickering; "JISI", 1952, Vol.170, pp48.

[21] W.J.M.Satter and F.B.Pickering; "JISI", 1969, Vol.207 pp992.

[23] B.Tivelius, T.Sohlgren, E.Sjoman and R.Kallstrom; Swedish Symposium on Non-Metallic Inclusions in Steel, pp116-125, 27-29, April 1981.

[24] D.L.Davidson and J.Lankford; "International Materials Reviews", Vol.37, 1992, pp45-74.

[25] T.J.Baker and J.A.Charles; "JISI", 1972, Vol.210, pp702.

[26] K.Thelning; "Steel and Its Heat Treatment", Butterworths, London and Boston.

[27] M.Volmer and A.Weber; Z. Phys. Chem., 1925, Vol.119, pp277.

[28] F.C.Collins and J.P.Leineweber; J. Phys. Chem., 1965, Vol.60, pp389-394.

[29] M.Kahlweit; Z. Phys. Chem., 1960, Vol.25, pp1-25.

[30] A.Nicholson and T.Gladman; "Ironmaking and Steelmaking", 1986, Vol.13, No.2,pp53.

[31] A.Nicholson, D.J.Howarth and J.Turton; "Ironmaking and Steelmaking", 1983, Vol.10, No.1, pp31.

[32] R.Kiessling; Swedish Symposium on Non-metallic Inclusions in Steel, 27-29 April 1981, pp7-18.

[33] R.Lagneborg; "Swedish Symposium on Non-Metallic Inclusions in Steel", Stockholm, Sweden, 1981, pp285-352.

[34] S.Linder; "Scan. J. Metall.", 1974, Vol.3, pp137.

[35] L.Lindskog and H.Sandberg; "Scan. J. Metall.", 1973, Vol.2 pp71.

[36] M.Ichinoe, H.Mori, H.Kajiok and I.Kokubo; "Production and Application of Clean Steels", Int. Conf., 1970, Hungary, pp137-167.

[37] E.T.Turkdogan; "JISI", 1966, pp914.

[38].M.L.Turpin and J.F.Elliott; JISI, 1966, pp217.

[39] Y.Miyashita; "Transaction ISIJ", Vol.7, 1969, pp1.

[40] Takaho Kawawa and M.Ohkubo; "Transaction ISIJ", Vol.8, 1968,pp203.

[41] N.Sano, S.Shiomi and Y.Matsushita; "Trans. ISIJ", Vol.7, 1967, pp244-253.

[42] A.L.Gueussier, E.V. Vachinery, J.L.Tranchcant and R.Szezesny; "Iron and Steel Engineer", October 1983, pp35-41.

[43] D.Turnbull and J.Fisher; J. Chem. Phys., 1949, Vol.17, pp71.

[44] K.Senda; "Trans. ISIJ", Vol.7, 1967, pp134.

[45] Y.Kojima, K.Takahashi, H.Sakao and K.Sano; "Trans. ISIJ", Vol.7, 1969, pp172.

[46] T.Higahi, T.Suzumoto and T.Kishida; "Trans. ISIJ", Vol.9, 1969, pp127.

[47] V.I.Yavoiskiy; "Trans. ISIJ", Vol.15, 1975. pp493.

[48] R.K.Iyengar and W.O.Philbrook; "Meta. Trans.A", Vol.3 July 1972, pp1823-1827.

[49] I.N.Golikov; "Production and Application of Clean Steels", Int. Conf., June 1970, Hungary.

[50] G.Pomey and B.Trentini; "Production and Application of Clean Steels", Int. Conf., June 1970, Hungary, pp1.

[51] E.Grethem and L.Philippe; "Production and Application of Clean Steels", Int. Conf., June 1970, Hungary, pp29.

[52] R.G.Ward and K.A.Salmon; "JISI", December 1960, pp393.

[53] G.J.Hassall, D.P.Jackaman and R.J.Hawkins; "Ironmaking and Steelmaking", 1991, Vol.18, No.5 pp359.

[54] E.T.Turkdogan; Proc. of the First Int. Calcium Treatment Symposium, 1988, Glasgow, Scotland, pp3-13.

[55] F.Pellicani, B.Durand and A.Gueussier; Proc. of the First Int. Calcium Treatment Symposium, 1988, Glasgow, Scotland, pp14-22

[56] D.Lu, G.A.Irons and W.K.LU; Proc. of the First Int. Calcium Treatment Symposium, 1988, Glasgow, Scotland, pp23-30.

[57] L.Nerryson, K.E.Obery and F.J.Weiss; Iron and Steel Engineer, 1980, Vol.57, (2), pp41-43.

[58] S.Gustafsson and P.O.Mellberg; Swedish Symposium on Non-Metallic Inclusions in Steel, 1981, Stockholm, Sweden, pp35-68.

[59] A.Rozman, P.Bracum, V.Presern and M.Kmetic; Proc. of The First Int. Calcium Treatment Symposium, 1988, pp53-60.

[60] G.J.W.Kor; Proc. of the First Int. Calcium Treatment Symposium, 1988, Glasgow, Scotland, pp39-44.

[61] K.Kaneko; "J.Iron Steel Inst. Jan.", 1977, Vol.63, pp1244-1251.

[62] S.Kobayyashi, Y.Omori and K.Sambongi; "Trans. ISIJ", Vol.14, 1971, pp260-269.

[63] T.Ototani, Y.Kataura and T.Degawa; "Trans. ISIJ", Vol.16, 1976, pp275-282.

[64] C.Galellier, H.Gaye and M.Nadit; Proc. of the First Int. Calcium Treatment Symposium, June 1980, pp31-38.

[65].Lauri.Holappa; Swedish Symposium on Non-Metallic Inclusions in Steel, 27-29 April 1981, pp19-34.

[66] S.Kitamura, K.Miyamura and I.Fukvoka; "Trans. ISIJ", Vol.27, 1987, pp344-350.

[67] D-Z.Lu, G.A Irons and W-K.Lu; "Ironmaking and Steelmaking", 1991, Vol.18, No.5, pp342-346.

[68] T.Takenouchi and K.Swzuki; "Trans ISIJ", Vol.18, 1978, pp344-351.

[69] O.Haida, T.Emi, G.Kasai, M.Naito and S.Moriwaki; "J.Iron steel Inst. of Jan.", 1980, Vol.66, pp354.

[70] H.M.Pielet and D.Bhattacharya; "Metal. trans.", 1984, 15B, pp547-562.

[71] B.Oztur and E.T.Turkdogan; "Metal. Trans.", 1984, pp299.

[72] P.V.Riboud and C.Gatellier; "Ironmaking and Steelmaking", 1985, Vol.12, No.2 pp79-86.

[73] A.Mitchell and F.Reyes-Carmona; "Clean Steel", Proc. Conf., June 1986, Balatonfured, Hungary, pp320-334.

[74] G.R.Speich and W.A.Spitzig; "Metall. Trans.A", 1982, 13A, pp2239-2257.

[75] A.Herbert, C.Temson, G.K.Notmam, D.Morris and S.Knowles; "Ironmaking and Steelmaking", 1987, Vol.14, No.1, pp10-16.

[76] D.Brooksbank and K.W.Andrews; "JISI", June 1970, pp582-586.

[77] D.Brooksbank and K.W.Andrews; "JISI", June 1972, pp246-255.

[78] W.A.Wood; "Fracture", The Proceeding of the First Tewksbury Symposium, 1965, pp62-78.

[79] J.T.Barnby and F.M.Peace; "Acta. Metall.", 1971, Vol.19, pp1351.

[80] J.Lankford; "Engineering Fracture Mechanics", 1977, Vol.9, pp617-624.

[81] J.Lankford and F.N.Kusenberger; "Metall. Trans.", Vol.4, Feb. 1973, pp553-559.

[82] N.M.A.Eid and P.E.Thomason; "Acta. Metall.", Vol.27, pp1239-1249.

[83] G. Harkegard; "Engineering Fracture Mechanics", 1974, Vol.6, pp795-805.

[84] K.Tanaka and T.Mura; "Metall. Trans.A", Vol.13, Jan. 1982, pp117-123.

[85] G.M.Faulning et al.; "Iron and Steelmaker", February 1980, pp14-27.

[86] D.Brooksbank and K.W.Andrews; "JISI", Vol.206, June 1968, pp595-599.

[87] D.Brooksbank and K.W.Andrews; "JISI", Vol.207, 1967, pp474.

[88] D.Brooksbank and K.W.Andrews; "JISI", Vol.208, 1970, pp495.

[89] H.C.Child; "Surface Hardening of Steel", Engineering Design Guides 37, Oxford University Press, 1980.

[90] W.E.Puckworth; "Metallurgia", 1964, Vol.69, pp53.

[91] G.Harkegard; "Eng. Fracture Mechanics", 1974, Vol.6, pp795-805.

[92] S.Rudrik; "JISI", 1966, Vol.204, pp374-376.

[93] T.Ototani and Y.Kalaura; "Trans.ISIJ", 1972, Vol.12 pp334-342.

[94] D.V.Wilson; "Acta Metallurgica", 1965, Vol.13 pp807-814.

[95] B. Berg, G.Carlsson and M.Bramming; "Scand. J. Metallurgy", Vol.14, 1985, pp299-305.

[96] "Fatigue Design Handbook", Society of Automotive Engineers, PA, USA.

[97] R.N.Barfield and J.A.Kitchener; "JISI", 1955, Vol.180, pp324.

[98] George Krauss; "Steel: Heat Treatment and Processing Principles".

[99] A.Kohn, M.Wanin, J.Arnoult, R.Jhomas and L.Backer; "Production and Application of Clean Steels", Int. Conf., Hungary, 1970, pp92-98.

[100] F.H.Wochlbier and G.W.P.Pengstorff; "J. Met.", May 1967, Vol.19, pp50-53.

[101] P.Verschueren and S.Paridaens; "Clean Steel 3", Proc. Conf., pp217-225 June 1986.

[102] Tzu-Ye Shih and Toru Araki; "Trans. ISIJ", 1973, Vol.13, pp11-19.

[103] J.J.Debarbadillo; "Sulfide Inclusions in Steel", Proc. Int. Symposium, 7-8 Nov. 1974, pp70-99.

[104] F.B.Pickering; "Production and Application of Clean Steel", Int. Conf., 23-26 June 1970, Hungary, pp75-91.

[105] R.Kiessling; "J. Metals", 1969, Vol.21, No.10, pp48.

[106] W.E.Duckworth; "Metallurgia", 1969, Vol.69, pp53.

APPENDIX

Equations For Stresses Around Duplex Oxide-Sulphide Inclusion

1. Notation

E = Young's modulus.

ν = Poisson's ratio.

T = temperature change (increase is positive).

R_1 = radius of oxide core.

R_2 = radius of matrix.

R_s = outer radius of sulphide envelope.

$d = R_1/R_2$ (small).

$h = R_1/R_s$ (which approaches unity).

X = thickness of sulphide layer ($= R_s - R_1$)

P_A' = pressure in the oxide core.

Subscript: 1 refers to the oxide core;

s refers to the sulphide layer;

2 refers to the matrix.

$k = E/(1 = 2\nu)$

$g = 2E/(1 = \nu)$

α = mean linear coefficient of thermal expansion over the given temperature range.

σ_R' = radial stress at matrix/inclusion interface in the matrix.

σ_C' = circumferential stress at matrix/inclusion interface in the matrix.

σ_R = radial stress.

σ_C = circumferential stress.

2 Stresses Around Duplex Oxide-Sulphide Inclusions

Calculations have been made for the duplex inclusion using the spherical model shown in figure 9-9 in which the sulphide forms a separate shell between the oxide and matrix[76].

2.1 Stresses in Oxide Inclusions ($0 \le R \le R_1$)

$$P_A' = \frac{\left(\frac{h^3-d^3}{\frac{d^3}{k_2}+\frac{h^3}{g_2}}\right)\cdot[(\alpha_2-\alpha_s)\cdot T\cdot(1+\frac{g_s}{k_s})+(\alpha_s-\alpha_1)\cdot T\cdot(h^3+\frac{g_s}{k_s})]+[(1-h^3)g_s\cdot(\alpha_s-\alpha_1)\cdot T]}{\left(\frac{h^3-d^3}{\frac{d^3}{k_2}+\frac{h^3}{g_2}}\right)[h^3(\frac{1}{k_1}-\frac{1}{k_s})+\frac{1}{k_s}(1+\frac{g_s}{k_1})]+[(1+\frac{g_s}{k_1})-h^3\cdot g_s\cdot(\frac{1}{k_1}-\frac{1}{k_s})]}$$

(A-1)

2.2 Stresses in the Sulphide Layer ($R_1 \le R \le R_s$)

$$(\sigma_R)_s = P_A' + \frac{g_s}{(1+\frac{g_s}{k_s})}[P_A'\cdot(\frac{1}{k_1}-\frac{1}{k_s})+T\cdot(\alpha_1-\alpha_s)](1-\frac{R_1^3}{R^3}) \qquad (A\text{-}2)$$

$$(\sigma_R)_s = \sigma_R' \ (\text{at } R=R_s)$$

$$(\sigma_C)_s = P_A' + \frac{g_s}{(1+\frac{g_s}{k_s})}[P_A'\cdot(\frac{1}{k_1}-\frac{1}{k_s})+T\cdot(\alpha_1-\alpha_s)](1+\frac{1}{2}\frac{R_1^3}{R^3}) \qquad (A\text{-}3)$$

2.3 Stresses in the Matrix ($R_s \leq R \leq R_2$)

$$(\sigma_R)_s = \frac{\sigma_R'}{[1-(\frac{d}{h})^2]}[\frac{R_s^3}{R^3} - (\frac{d}{h})^3] \qquad (A\text{-}4)$$

where $\sigma_R' = [(\sigma_R)_s]$ at $R = R_s$

$$(\sigma_C)_s = \frac{-\sigma_R'}{[1-(\frac{d}{h})^3]}[\frac{1}{2}\frac{R_S^3}{R^3} + (\frac{d}{h})^3] \qquad (A\text{-}5)$$